Genetically targeted anatomical and behavioral characterization of the cornu ammonis 2 (CA2) subfield of the mouse hippocampus

Frederick L. Hitti

Submitted in partial fulfillment of the

requirements for the degree of

Doctor of Philosophy

under the Executive Committee

of the Graduate School of Arts and Sciences

COLUMBIA UNIVERSITY

2014

ABSTRACT

Genetically targeted anatomical and behavioral characterization of the cornu ammonis 2 (CA2) subfield of the mouse hippocampus

Frederick L. Hitti

The hippocampus is critical for storing declarative memory, our repository of knowledge of who, what, where, and when. Mnemonic information is processed and encoded in the hippocampus through several parallel routes, most notably the trisynaptic pathway, in which information proceeds from entorhinal cortex (EC) to dentate gyrus (DG) to CA3 and then to CA1, the main hippocampal output. Absent from this pathway is the CA2 subfield, a relatively small area interposed between CA3 and CA1 that has recently been shown to mediate a powerful disynaptic circuit linking EC input with CA1 output. Usually ignored or grouped together with CA3, CA2 has generally escaped exploration presumably due to its relatively small size and somewhat ill-defined borders.

A few studies have proposed an important role for the CA2 subfield of the hippocampus, however, the relevance of this subfield in a behaving animal has not been explored. The function of a particular brain region may be inferred by examining the effects of a lesion of that area. Indeed, the hippocampus's role in learning and memory was elucidated following the bilateral medial temporal lobe ablation of Henry Molaison (patient H.M.). Similarly, a lesion of CA2 could be used to infer its role in learning, memory, and disease.

Due to the relatively small size of CA2, physical or chemical lesions are not precise enough to ablate this region without collateral damage. To overcome this limitation, I generated a CA2-specific transgenic mouse line to enable genetic targeting of this subfield. I used this mouse line to map CA2 connectivity and explore its behavioral role. Using monosynaptic rabies tracing, CA2 axon tracing, and electrophysiology, I confirmed the disynaptic pathway and presence of septal and subcortical inputs to CA2. Genetically targeted inactivation of CA2 caused a remarkably profound loss of social memory, with no change in sociability. This impairment was not the result of a general loss of hippocampal function as CA2-inactivation did not impact performance on several other hippocampal-dependent tasks, including spatial and contextual memory. These behavioral and anatomical results thus reveal CA2 as a hub of sociocognitive processing and implicate its dysfunction in social endophenotypes of psychiatric diseases such as schizophrenia and autism.

Table of Contents

List of Figures and Tables

Acknowledgements

I thank T.R. Reardon for providing the rabies virus and Justine Kupferman and Franklin Lema for experimental assistance. I thank Christine Denny, Zoe Donaldson, Jayeeta Basu, and Marco Russo for helpful discussions. I thank the NIMH for awarding me a Ruth L. Kirschstein F30 NRSA grant to fund my work.

I thank my thesis committee members, René Hen, Josh Gordon, Nate Sawtell, and Richard Tsien for their guidance.

I would especially like to thank my mentor, Steven Siegelbaum, for providing a great environment to work in, invaluable advice and tutelage, and constant support. I first experienced Steve's effectiveness as an instructor during his pharmacology lectures in medical school. It was during his instruction of the ion channels graduate course, however, that I fully realized his brilliance and unmatched teaching ability. To this day, the ion channels course remains the best class I've ever taken. This is due in large part, if not entirely, on Steve's instruction throughout the course. Thank you for sparking (or shall I say reaffirming) my interest in neurobiology, and thank you for taking me on as a student in your lab. The experience has been rewarding, enjoyable, and unforgettable.

I dedicate this work to my parents whose love, support,

and guidance have made my success possible.

Chapter 1

Introduction

The hippocampal formation is a brain region that is critical for various forms of learning and memory (Squire, 1992). It consists of three parts: the dentate gyrus (DG), the hippocampus proper, and the subiculum. According to current classification schemes based on initial studies by Lorente de Nó, the hippocampus proper is further subdivided into the CA3, CA2, and CA1 subregions, with CA1 providing the major hippocampal output. One of the most fundamental challenges in determining the neural mechanisms by which the hippocampal formation encodes memories is to characterize the nature of the hippocampal circuit and how it processes and ultimately stores the sensory information it receives.

To date, most studies have focused on how information is processed by the hippocampal formation through the classic trisynaptic pathway (Amaral and Witter, 1989). In this excitatory pathway, neurons in layer 2 of the entorhinal cortex (EC) synapse onto DG granule cells, which in turn synapse on to CA3 neurons by way of the mossy fibers (mf). CA3 then projects to CA1 through the Schaffer collaterals (sc), CA1 projects to the subiculum (S), and the subiculum projects back to the deep layers of the EC, thereby completing the cortico-hippocampal loop (Figure 1.1).

Conspicuously absent from this circuit is the CA2 subfield. Usually ignored (van Strien et al., 2009) or grouped together with CA3 (Amaral and Witter, 1989), CA2 has generally escaped exploration presumably due to its relatively small size and somewhat ill-defined borders. Nonetheless, several lines of evidence suggest that it may play a unique role in the hippocampal circuit.

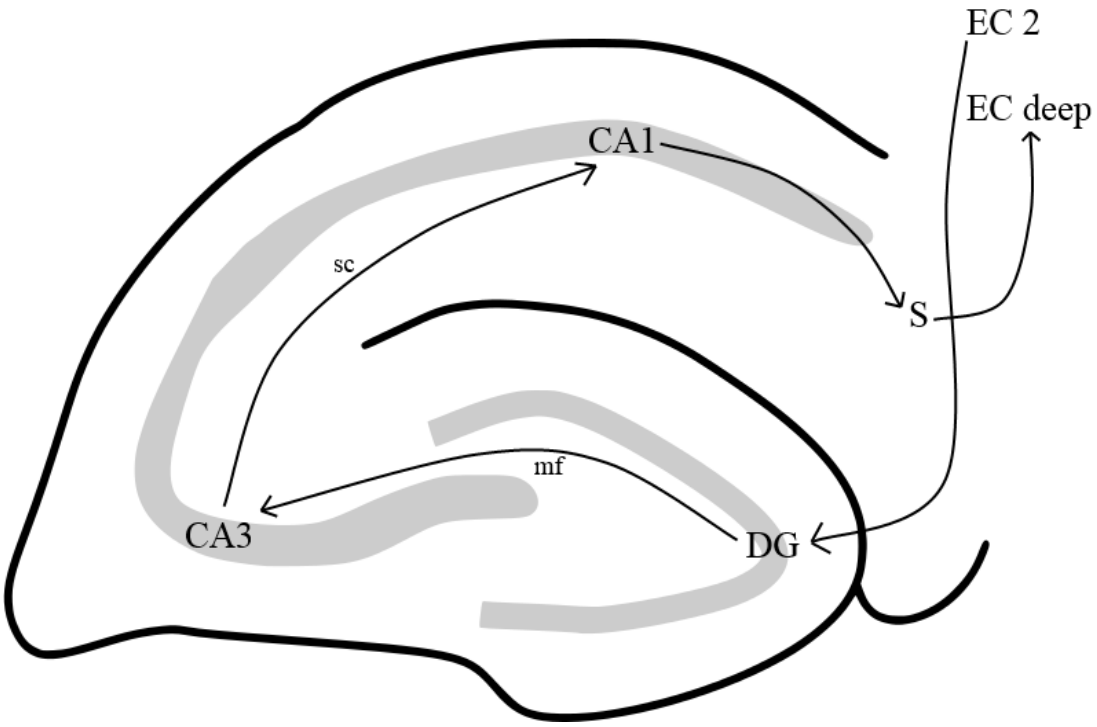

Figure 1.1: The trisynaptic circuit. The components of the main hippocampal circuit are illustrated in this diagrammatic representation of the hippocampus.

1.1 Is CA2 truly distinct from CA1 and CA3?

Characterization of hippocampal anatomy dates back to studies done by Ramón y Cajal in the late 19th century (Ramón y Cajal, 1893). Cajal divided the CA region into two parts, "la región inferior y la región superior del asta de Ammon" (the lower and upper blades of Ammon's horn). Lorente de Nó, a student of Cajal, was the first to divide the CA region into four parts, CA1-4, with CA1 and CA2 corresponding to Cajal's lower blade and CA3 and CA4 corresponding to Cajal's upper blade (Lorente de Nó, 1934). This classification system provided the nomenclature for hippocampal subfield anatomy currently used today (Figure 1.2, left), although CA4 is no longer considered a separate region.

Lorente de Nó characterized the cells of the hippocampus in several species, including mouse, primate, and human. He found that the fields of the CA region were remarkably conserved throughout these species. The CA1-4 fields were defined as separate regions due to differences in both the cytoarchitecture and the connectivity of the pyramidal cells located within these fields. Using these criteria, he was able to clearly delineate a separate class of neurons located between CA1 and CA3.

Unlike CA1 neurons, the dendrites of CA2 and CA3 pyramidal cells do not ramify within the stratum radiatum (SR). The somas of CA2 and CA3 pyramidal neurons are also much larger than the somas of CA1 pyramidal neurons. CA2 differs from CA3 in several important ways. First, while CA3 neurons are famous for their thick Schaffer collateral axons that project to CA1, CA2 neurons never send out Schaffer collaterals. The axons of CA2 are most prominent in the stratum oriens (SO) and SR. Second, CA2 cells do not possess the conspicuous "thorny excrescences" of CA3 cells (Figure 1.2, right). Third, along with the absence of these thorns, CA2 neurons receive little mossy fiber input from the DG granule cells. Fourth, the apical

dendrite of CA2 neurons splits into two branches very close to the soma whereas the apical dendrite of CA3 neurons splits only after passing through the stratum lucidum.

The anatomical differences described by Lorente de Nó are not the only indicators that CA2 is indeed unique and separate from CA1 and CA3. Examination of the expression patterns of various genes within the hippocampus demonstrates that many genes are expressed in CA2 but not in CA1 or CA3. Defining a neuronal population should include consideration of a variety of elements including, but not limited to, anatomy, gene expression, electrophysiological properties, and connectivity (Luo et al., 2008). CA2 differs from CA1 and CA3 in all of these respects (Lorente de Nó, 1934; Lein et al., 2005; Chevaleyre and Siegelbaum, 2010).

CA1, CA2, and CA3 pyramidal neurons each possess a unique electrophysiological profile. Indeed, these characteristics alone are suitable for differentiation of CA2 from CA1 and CA3 (Table 1.1; Chevaleyre and Siegelbaum, 2010). Compared to CA1 neurons, CA2 neurons have a lower input resistance, higher capacitance, lower resting potential, lower action potential (AP) amplitude, shorter AP duration, and less sag (decreased I_h current). Furthermore, CA2 neurons have a lower input resistance, increased capacitance, and shorter AP duration compared to CA3 pyramidal neurons.

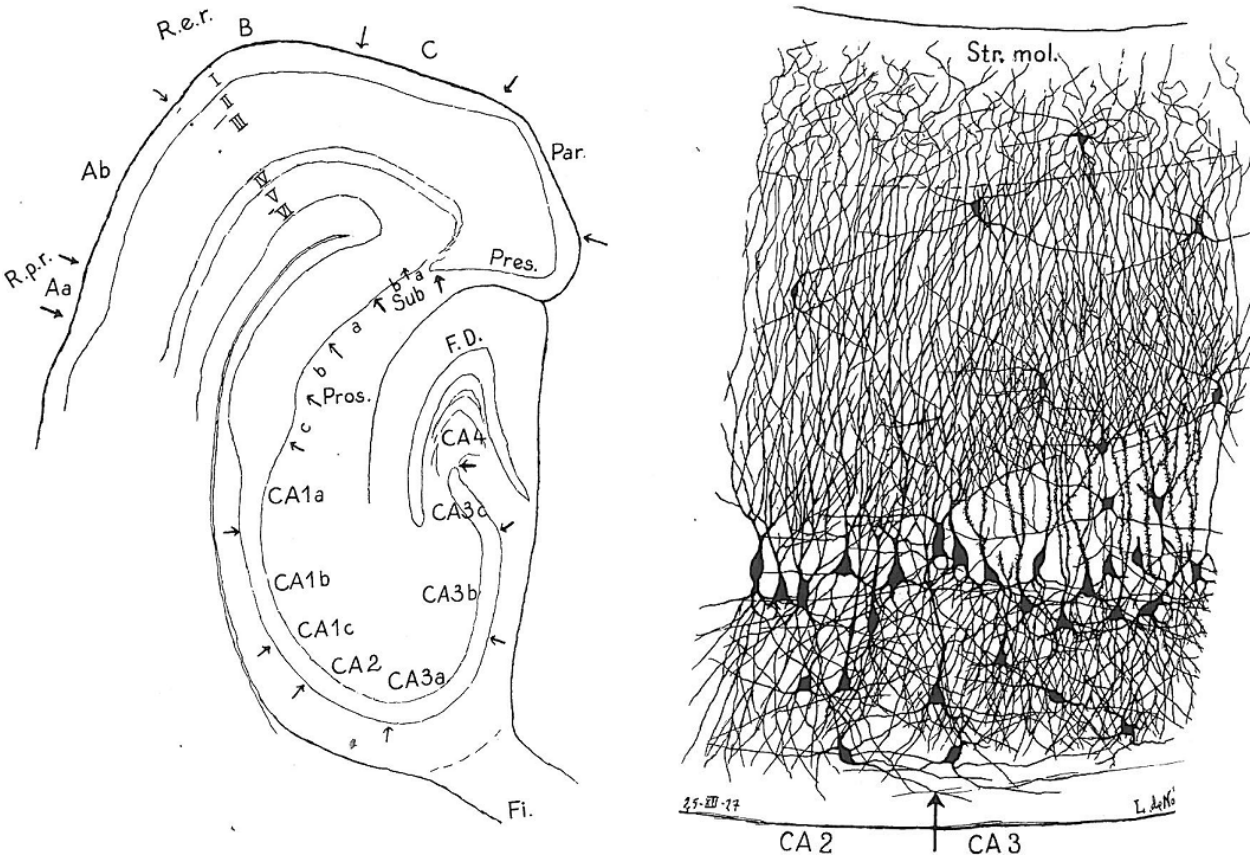

Figure 1.2: The hippocampal subfields. Left panel, Drawing of a horizontal section through the entorhinal cortex and hippocampus. Right panel, Drawing of a Golgi-Cox stain demonstrating the cytoarchitectural differences between CA2 and CA3. The CA3 "thorny excrescences" (arrowhead) are lacking in CA2. (Reproduced from Lorente de Nó, 1934.)

	Input Resistance (MΩ)	Capacitance (pF)	Resting Potential (mV)	AP Amplitude (mV)	AP Duration (ms)	Sag (mV)
CA1	107 ± 10.7	170.1 ± 11.4	71.9 ± 1.2	95.3 ± 1.8	0.99 ± 0.03	8.4 ± 0.3
CA2	76.2 ± 11.1	305.3 ± 20.8	75.3 ± 1.0	84.8 ± 1.6	0.78 ± 0.02	4.1 ± 0.2
CA3	107.5 ± 28.1	150.1 ± 26.1	74.4 ± 0.8	84.4 ± 4.4	0.95 ± 0.03	4.3 ± 0.4

Table 1.1: Electrophysiological properties of hippocampal pyramidal neurons. The properties of pyramidal neurons in the CA1, CA2, and CA3 subfields were measured with whole-cell recordings in acute hippocampal slices. CA2 neurons differ from both CA1 and CA3 neurons in input resistance, capacitance, and action potential (AP) duration. (Adapted from Chevaleyre and Siegelbaum, 2010).

Differences in gene expression between CA2 and CA1/CA3 have been also documented in the literature (Figure 1.3). These differences include enriched or restricted expression of *Cacng5* (Fukaya et al., 2005), STEP (Boulanger et al., 1995), TREK-1 (Talley et al., 2001), adenosine A1 receptors (Ochiishi et al., 1999), calbindin (Leranth and Ribak, 1991), chromogranin A (Munoz, 2004), RGS-14 (Lee et al., 2010), α-actinin-2 (Wyszynski et al., 1998), NT-3 and *pcp-4* (Zhao et al., 2001), FGF-2 (Gómez-Pinilla et al., 1994), *Tiam1* and *Mapk3* (Lein et al., 2004). The molecular profile of CA2 is unmistakably distinct from that of the other CA subfields.

Along with genetic, anatomic, and functional differences between CA2 and CA1/CA3, the CA2 subfield has also been implicated in various disease processes including temporal lobe epilepsy (Wittner et al., 2009; Andrioli et al., 2007), schizophrenia, and mood disorders (Benes and Todtenkopf, 1999; Benes et al., 1998). Temporal lobe epilepsy is often associated with hippocampal sclerosis, which is characterized by neuronal cell loss in the CA region. The pyramidal cells of CA2 are resistant to this cell death (Table 1.2; Andrioli et al., 2007). Similarly, CA2 neurons exhibit increased survival following ischemic insults (Sadowski et al., 1999). Studies from resected human hippocampi have demonstrated that the surviving CA2 cells are capable of generating epileptiform activity independent of the subiculum (Wittner et al., 2009). In patients with schizophrenia and bipolar disorder, loss of parvalbumin-positive interneurons located in the pyramidal layer of CA2 has been documented (Table 1.3; Benes et al., 1998).

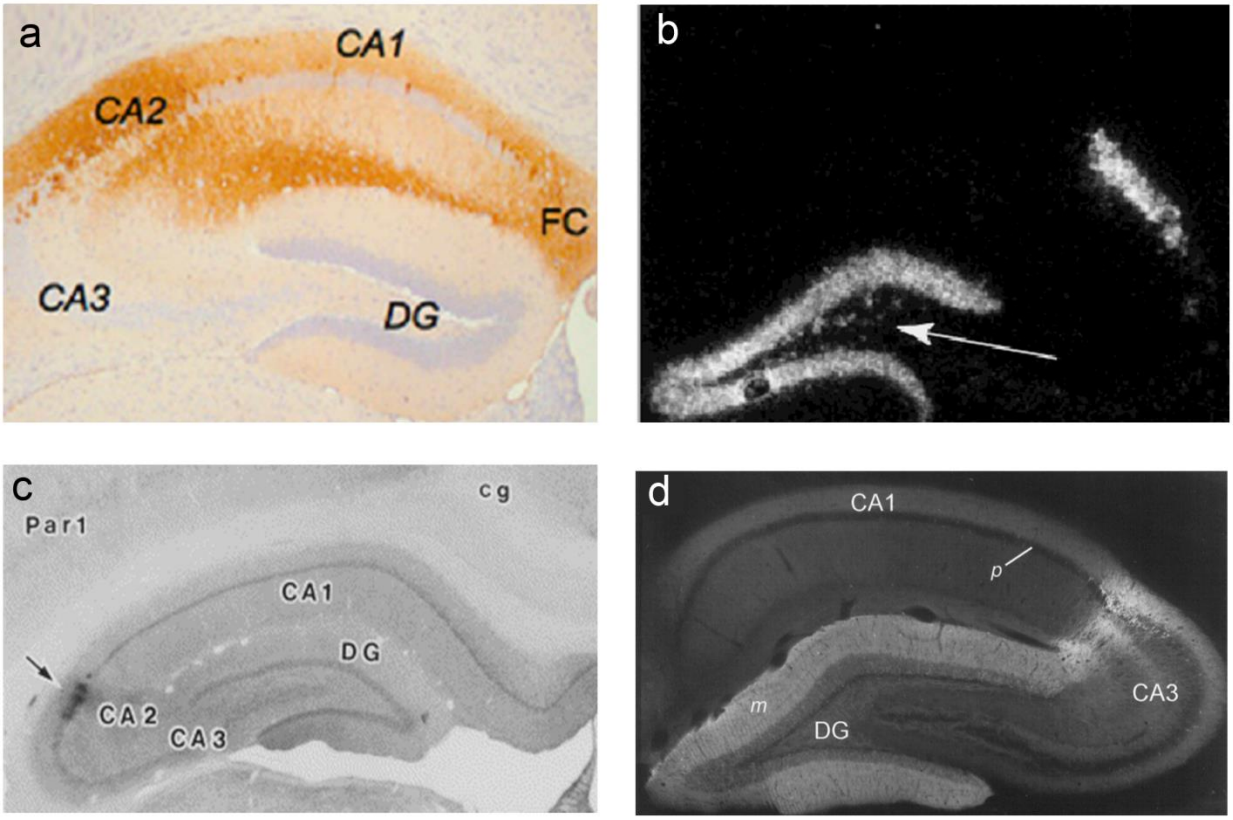

Figure 1.3: Molecular markers of CA2. Many genes are expressed exclusively, with respect to the hippocampus, in CA2. **a,** RGS14 protein expression in the mouse brain is largely restricted to CA2 (Adapted from Lee et al., 2010). **b,** *In situ* hybridization showing *Pcp-4* mRNA expression in CA2 and DG (Adapted from Zhao et al., 2001). **c,** CA2 neurons strongly express the adenosine A1 receptor (Adapted from Ochiishi et al., 1999). **d,** The α-actinin-2 protein is enriched in CA2 neurons (Adapted from Wyszynski et al., 1998).

Neuron Density (neurons/mm^3)	Non-sclerotic	Sclerotic	P
DG (polymorphic)	6433±386	3907±283	< 0.01
CA4	9511±565	7240±489	< 0.01
CA3	17468±785	9726±748	< 0.01
CA2	18700±946	16457±648	N.S.
CA1	11151±374	5227±289	< 0.01

Table 1.2: CA2 neuron density in hippocampal sclerosis. CA2 neurons are resistant to the cell death seen in hippocampal sclerosis (Adapted from Andrioli et al., 2007).

	CA1	CA2	CA3	CA4
Control	18.7 ± 1.8	9.3 ± 1.2	19.9 ± 2.6	16.9 ± 2.7
Schizophrenic	17.6 ± 3.3	18.4 ± 3.9	21.9 ± 3.3	24.5 ± 7.4
Manic depressive	25.3 ± 5.2	19.1 ± 4.8	37.9 ± 11.4	23.6 ± 7.8

Table 1.3: Ratio of pyramidal to non-pyramidal neurons in schizophrenic and manic depressive brains. The ratio of pyramidal neurons (PNs) to non-pyramidal neurons (NPs) is increased in the CA2 subfield of brains obtained from schizophrenic and manic depressive patients suggesting a selective loss of parvalbumin-positive interneurons in CA2. (Adapted from Benes et al., 1998).

1.2 Reexamining the circuitry of the hippocampus

Circuit analysis of the hippocampus has focused on the trisynaptic pathway and the direct perforant path input to CA1 from layer 3 of the EC. Several studies, most notably (Chevaleyre and Siegelbaum, 2010), have demonstrated that CA1 receives input from not only CA3 and layer 3 EC, but also from CA2. Optical imaging with a voltage-sensitive dye following mossy fiber stimulation revealed an increased signal in CA3 then CA2 and finally in CA1, giving evidence for a CA3 → CA2 → CA1 circuit (Sekino et al., 1997). In addition to this circuit, Bartesaghi and colleagues postulated an EC → CA2 → CA1 circuit based on recordings of extracellular field potentials in CA2 following stimulation to the dorsal psalterium (Figure 1.4, Bartesaghi and Gessi, 2004). Furthermore, their data also suggested that CA2 and the DG were more effectively driven by the EC compared to CA3 and CA1 (Bartesaghi et al., 2006).

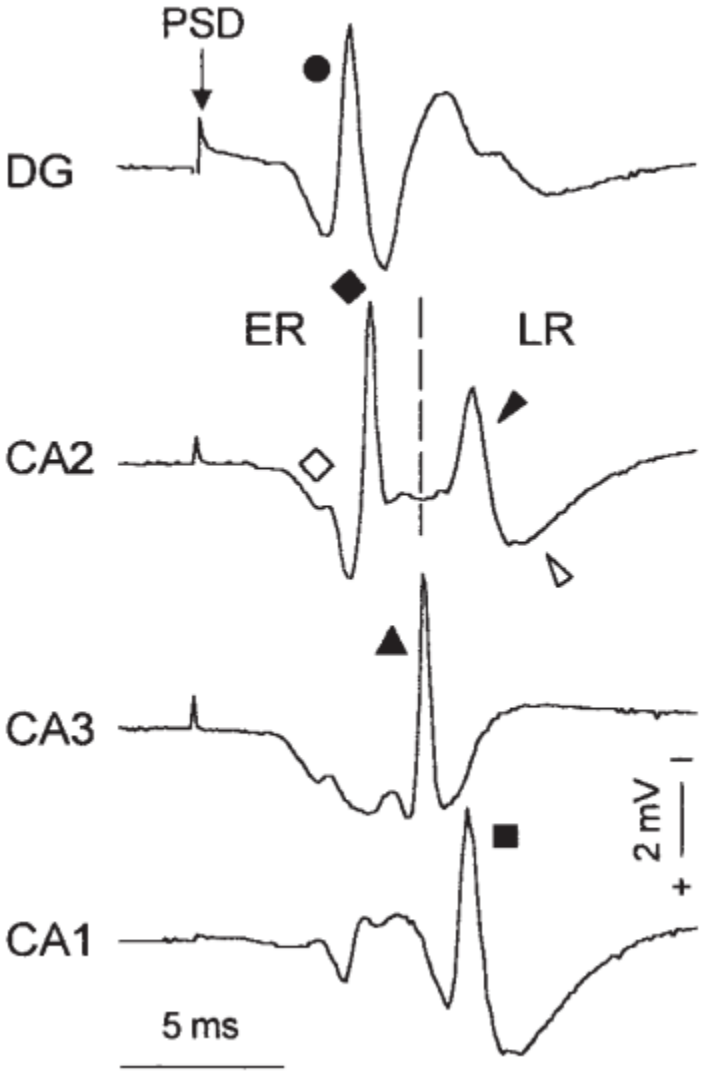

Figure 1.4: Responses evoked in field CA2 by stimulation of the dorsal hippocampal commissure. An early response (ER) and late response (LR) are observed in CA2 following stimulation of the dorsal psalterium. The latency and current source-density (CSD) analysis (not shown) of the early response suggests that it is a result of EC perforant path input onto CA2. The late response is likely a result of CA3 input to CA2. (Adapted from Bartesaghi and Gessi, 2004).

To further examine CA2's contribution to the hippocampal circuit, recent studies in the Siegelbaum lab have employed whole-cell recordings from acute hippocampal slices (Chevaleyre and Siegelbaum, 2010). They demonstrated that the CA2 subfield plays an important role in forming a di-synaptic circuit between the EC and CA1, confirming the findings of Bartesaghi and colleagues. Robust excitatory postsynaptic potentials (EPSPs) were measured in CA2 neurons following stimulation of layer 2 EC axons with the stimulating electrode placed in the molecular layer of the DG (Figure 1.5). Furthermore, these responses were greater in CA2 pyramidal neurons compared to the responses measured in CA3 neurons. Since these inputs are targeted to the distal dendrites of CA2 neurons, this suggests that CA2 neurons have unique dendritic integration properties that allow for robust responses to distal input (Piskorowski and Chevaleyre, 2012). Several mechanisms, that are not mutually exclusive, could support robust distal input as measured in the cell soma. CA2 neurons may receive a greater number of PP inputs or express a greater number of glutamate receptors in the distal dendritic compartment compared to CA3 neurons. Alternatively (or additionally), the dendrites of CA2 neurons may possess passive properties that enhance propagation of distal EPSPs to the soma. Finally the active properties of CA2 dendrites may enable them to amplify distal EPSPs by generating dendritic spikes that propagate to the soma.

In addition to strong excitation by their EC inputs, CA2 neurons make strong connections with CA1 neurons. This was elegantly demonstrated by paired whole-cell recordings (Figure 1.6; Chevaleyre and Siegelbaum, 2010). Previous paired recordings between CA3 and CA1 neurons showed two peaks in the excitatory postsynaptic current (EPSC) amplitude histogram. One peak was centered at 0 pA, and represents failures of a presynaptic action potential to elicit a postsynaptic response, presumably due to a failure to release glutamate. The second peak, at

around -4 pA, represents trials where the presynaptic action potential succeeded in eliciting a postsynaptic response. The finding that there was only a single peak of successes, whose amplitude was similar to that of a miniature excitatory synaptic current suggested that a single CA3 neuron makes only a single synapse with a given postsynaptic CA1 neuron, and that synapse releases at most a single quantum of transmitter (Bolshakov and Siegelbaum, 1995). In contrast, Chevaleyre and Siegelbaum (2010) found that the EPSC amplitude histogram determined with paired CA2 and CA1 recordings showed up to 6 peaks, a peak of failure and 5 peaks in the distribution of successes. This suggests that CA2 neurons either make multiple synapses with a single CA1 neuron or that multiple quanta are released from one site. Both possibilities would result in more effective transmission between CA2 and CA1 compared to transmission between CA3 and CA1. Although fewer in number than CA1 or CA3 neurons, CA2 neurons certainly appear to play an integral role in the hippocampal circuit.

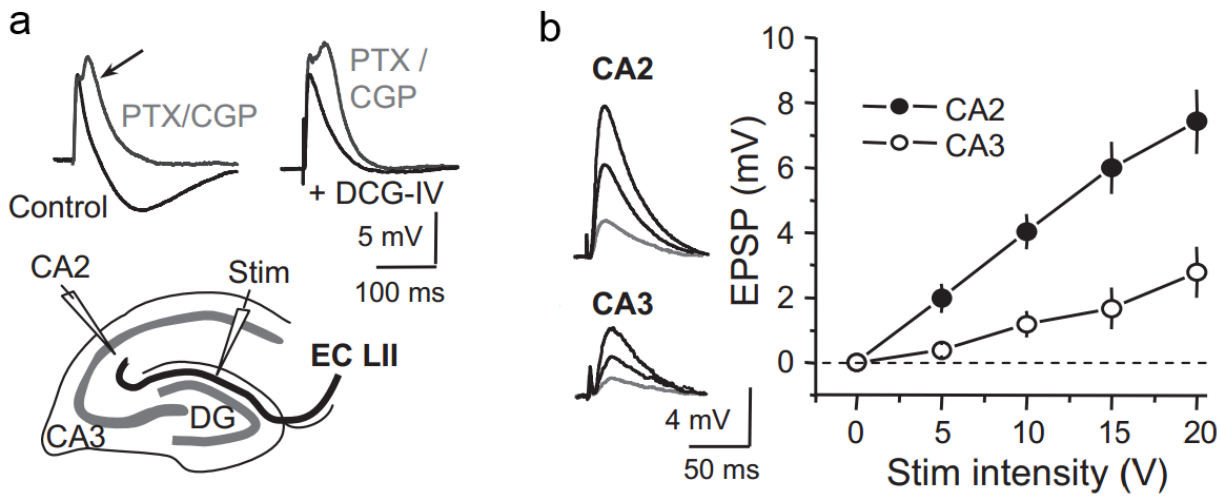

Figure 1.5: CA2 receives input from layer 2 of the entorhinal cortex. a, Whole-cell recordings of CA2 neurons revealed robust EPSPs in response to stimulation of layer 2 entorhinal axons with a stimulation electrode placed in the middle molecular layer of the DG. With inhibition blocked (PTX/CGP) a polysynaptic response was observed (arrow), presumably due to activation of CA2 from input from the EC L2 → CA3 → CA2 pathway. When mossy fiber transmission was blocked with DCG-IV, the polysynaptic response was abolished. **b,** The EPSPs in response to stimulation of layer 2 EC axons were significantly greater in CA2 pyramidal neurons compared to CA3 pyramidal neurons. (Adapted from Chevaleyre and Siegelbaum, 2010).

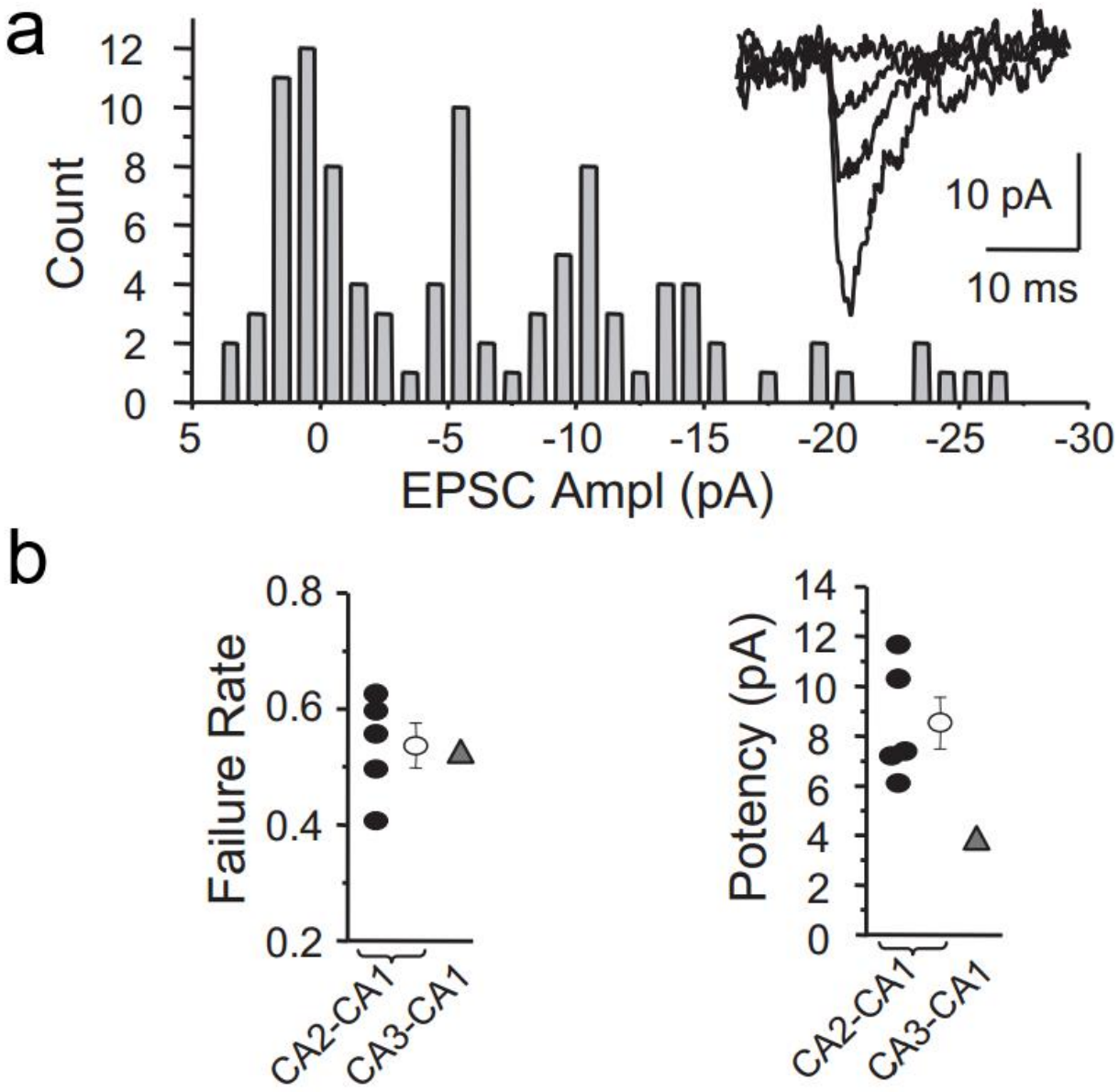

Figure 1.6: Paired recordings reveal strong connections between CA2 and CA1 neurons. a, Histogram of excitatory postsynaptic current (EPSC) amplitudes measured in a CA1 neuron after firing an action potential in a connected presynaptic CA2 neuron. The histogram reveals 5 peaks, indicating either multiquantal release from one synapse or coordinated release at multiple synapses onto the same postsynaptic target. Inset, example traces. **b,** While the EPSC failure rate of CA2 → CA1 synapses was similar to the failure rate for CA3 → CA1 synapses, the potency of the CA2 → CA1 EPSCs was much greater than the potency of the CA3 → CA1 EPSCs suggesting that the CA2 → CA1 connection is stronger than the CA3 → connection. (Adapted from Chevaleyre and Siegelbaum, 2010).

1.3 The role of the hippocampal formation and its subregions in learning and memory

Memory is commonly subdivided into two categories, declarative (explicit) memory and non-declarative (implicit) memory. Non-declarative memory includes priming and procedural learning (habits and skills). These are memories that do not involve the conscious recollection of information. Conversely, declarative memory involves conscious recollection of facts (semantic memory) or events (episodic memory). Studies done in rodents and primates have demonstrated that the hippocampus is essential for declarative memory and dispensable for implicit memory (Squire, 1992). More recent studies have focused on determining whether specific subregions of the hippocampal formation play specific and selective roles in memory formation, consolidation and recall.

The function of a particular brain region may be inferred by examining the effects of a lesion of that area. Indeed, the hippocampus's role in declarative memory was elucidated following the bilateral medial temporal lobe ablation of Henry Molaison (patient H.M.) (Squire, 1992). Much more precise lesions are required to determine the function of individual components of the hippocampal circuit. The mouse is an excellent model system for making precise, genetic lesions because of the relative ease of transgenesis. Additionally, many behavioral tests are available for the study of hippocampal-dependent learning and memory. Hence, the mouse is ideal for the study of genetic lesions of the hippocampus.

Declarative memory includes spatial, contextual, and social memory. Spatial memory includes a representation or map of an animal's environment and locations of objects within that environment. This form of memory is essential for the navigation of animals through their environment. The hippocampus has received much attention as a brain region critical for spatial

memory particularly following the discovery of "place cells" (cells that fire at specific locations in an animal's environment) throughout the hippocampus (Bird and Burgess, 2008). Contextual memory, similar to spatial memory, encodes information about an animal's environment. While spatial memory is often considered as the repository of a map of an animal's environment for navigation, contextual memory is more often described as the binding of multimodal sensory information (olfactory, visual, auditory) that could be used to identify the context in which a salient event may have occurred (Chun and Phelps, 1999). Lastly, social memory is defined as the memory of individual conspecifics. This form of memory has also been shown to be mediated by the hippocampus (Kogan et al., 2000).

These types of memory can be readily assayed in mice. Spatial memory in rodents is most commonly assayed with the Morris water maze test (Morris et al., 1982; Squire 1992). In this test, a mouse learns to use distal cues to navigate to a hidden platform. Contextual memory is often assayed with contextual fear conditioning (Gewirtz et al., 2000; Squire 1992). In this task, a mouse is given a brief electrical shock in a chamber. Subsequently, the mouse learns to associate that context (the conditioning chamber) with an aversive, fearful stimulus (shock). Mice demonstrate freezing behavior (lack of all movement save for respiration) upon recognition of the conditioned context. Hence, contextual memory is assessed as time spent freezing. Finally, social memory, the ability of a subject to remember other individuals, can be assayed by the 3-chamber and direct interaction tests. In the three-chamber test (DeVito et al., 2009), social memory is assessed by the increased time a subject mouse spends interacting with a novel unrelated mouse present in one chamber compared to the time it spends interacting with a familiar co-housed littermate present in another chamber. In the direct interaction test (Kogan et al., 2000), a subject mouse is first exposed to an unfamiliar mouse in trial 1. After a 1h inter-trial

interval (ITI), the subject mouse is exposed either to a second unfamiliar mouse or re-exposed to the same mouse encountered in trial 1. When a novel mouse is introduced in trial 2, mice will exhibit similar social interaction times for the two trials. However, when subjects are re-exposed to the stimulus mouse initially encountered during trial 1, mice with intact social memory will spend less time exploring the stimulus animal in the second trial. Hippocampal lesion studies have demonstrated that the hippocampus is essential for spatial, contextual, and social memory as assayed by the aforementioned tests (Morris et al., 1982; Gewirtz et al., 2000; Kogan et al., 2000; Squire 1992).

The CA1 subfield is the main output of the hippocampus (Figure 1.1; van Strien et al., 2009). Therefore, specific genetic lesions of CA1 are expected to produce a phenocopy of a traditional hippocampal ablation. Indeed, knockout of the NMDA receptor, which is thought to be essential for synaptic plasticity and learning, in CA1 resulted in a loss of spatial memory as assayed by the Morris water maze task (Tsien et al., 1996). Furthermore, later experiments with these knockout mice demonstrated that the knockouts were also deficient in various non-spatial hippocampal-dependent learning and memory tasks including contextual fear conditioning and social transmission of food preference (Rampon et al., 2000). These experiments support the role of CA1 as the major output subfield of the hippocampus, because the knockout mice demonstrated deficits in all of the hippocampal-dependent tasks tested. Hence, disruption of CA1 plasticity did, in fact, phenocopy traditional hippocampal ablation.

CA3 is a critical component of the trisynaptic pathway (Figure 1.1; van Strien et al., 2009) and provides input to CA1. Ablation of output from CA3 to CA1, by the selective expression of tetanus neurotoxin (TeNT) in these neurons, has been performed by the Tonegawa lab (Nakashiba et al., 2008). Surprisingly, they found no deficit in Morris water maze

performance in the lesioned animals. In contrast, a loss of contextual fear memory, another hippocampal-dependent task, was observed in the lesioned animals (Figure 1.7). Fear memory was assayed by measuring the amount of time the mouse spent freezing, which is defined as the absence of all movement except respiration. The greater the freezing levels, the more robust the fear memory. The CA3-inactivated group had significantly decreased levels of freezing compared to the control group (Figure 1.7). Additionally, CA1 place fields were larger in the lesioned animals only in a novel context. In familiar environments, the place fields in CA1 of the lesioned group matched those of the control group. These selective deficits were surprising because CA3 is an integral component of the trisynaptic circuit. The authors suggested that the perforant path input to CA1 (EC layer 3 → CA1) compensated for the absence of CA3 input. However, *in vitro* studies have demonstrated that the perforant path input to CA1 produces a weak effect at the soma (Chevaleyre and Siegelbaum, 2010; Golding et al., 2002). In light of recent findings from the Siegelbaum lab, the parallel disynaptic circuit mediated by CA2 seems like a more likely candidate for this compensation. In this thesis I use genetic ablation of CA2 to address this hypothesis.

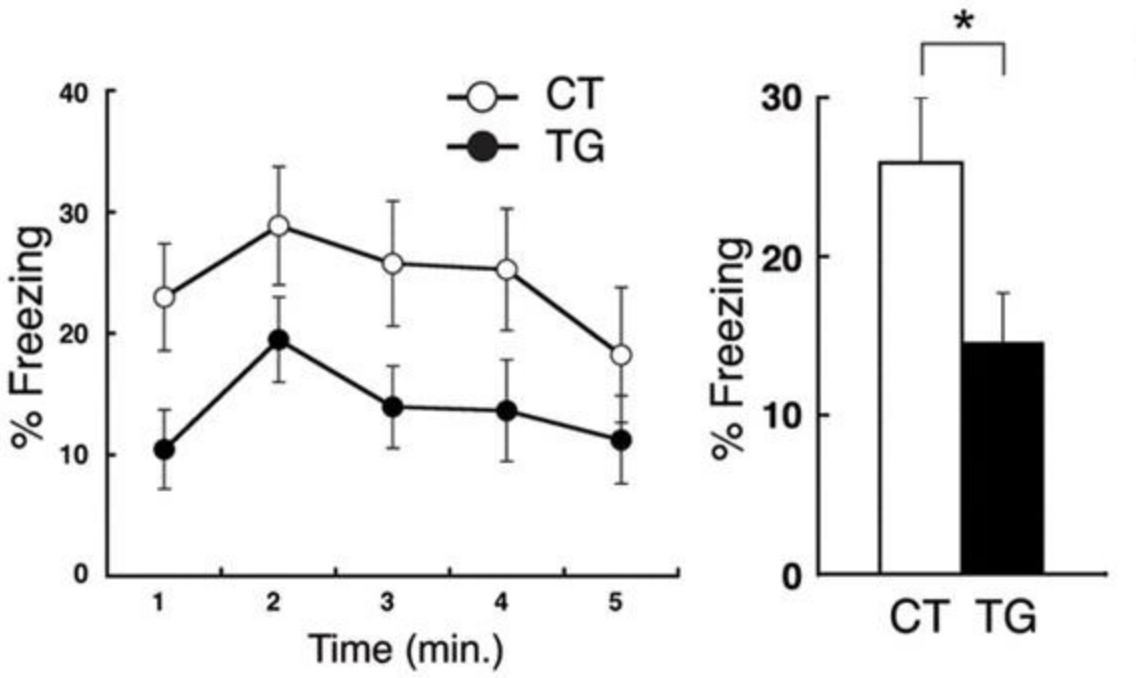

Figure 1.7: CA3 inactivation abolishes contextual fear memory. Left, percent freezing during the 5 minute memory retrieval session plotted as 1 minute bins. The transgenic (TG) CA3-inactivated group displayed significantly lower levels of freezing than the control group (CT) throughout the entire session. Right, freezing levels averaged over the 5 minute session. The CA3-inactivated group (TG) spent significantly less time freezing than the control (CT) group.

The dentate gyrus (DG) is a unique region of the hippocampus that exhibits adult neurogenesis. Hence, new neurons are generated and incorporated into the hippocampal circuit in adulthood in this subregion (Altman and Das, 1965; Eriksson et al., 1998). To study the function of the DG in learning and memory, old granule cells (those born before adulthood) were inactivated by the expression of TeNT in these neurons (Nakashiba et al., 2012), and young granule cells (those born during adulthood) were ablated by x-ray irradiation. Nakashiba and colleagues found that the old granule cells were essential for efficient pattern completion (the ability to recall a memory based on incomplete information) while the young granule cells were required for pattern separation, or the distinction between two similar contexts. This was surprising because DG had long been hypothesized to mediate pattern separation while CA3 had been proposed to mediate pattern completion. The authors have suggested that the old granule cells recruit pre-existing CA3 attractor states, while the young granule cells aid in the generation of novel CA3 attractor states.

In addition to CA1, CA3 and DG, genetic inactivation of layer III of entorhinal cortex (EC3) has also been performed (Suh et al., 2011). EC3 projects to the distal dendrites of CA1. In this study, the authors found that these inputs were essential for temporal associational memory as assayed by trace fear conditioning. In this task, mice are presented with a tone, and then following a short delay (trace interval), a shock is delivered. Without the trace interval, this form of learning is simple auditory fear conditioning that is dependent on the amygdala and not the hippocampus. With a trace interval interposed between the conditioned stimulus (CS) tone and the unconditioned stimulus (US) shock, the task becomes hippocampal dependent. Hence, the hippocampus is required to bind events that are not contiguous in time. Interestingly, while CA3-inactivation abolishes contextual fear memory (Figure 1.7), it does not impair trace fear

conditioning. Therefore, temporal associational memory is likely mediated by the direct EC inputs to CA1.

1.4 The anatomy and function of CA2

Although there have been no studies that directly address the role of CA2 in hippocampal-dependent learning and memory, clues as to its potential role have come from an analysis of CA2 circuitry and molecular characteristics. Previous studies have investigated the circuitry of CA2 (Cui et al., 2013; Haglund et al., 1984; Kiss et al., 2000; Magloczky et al., 1994; Vertes 1992; Vertes et al., 1999) using dyes and chemical tracers. These studies have shown that CA2 receives input from both subcortical and cortical nuclei including layer 2 of the entorhinal cortex, paraventricular nucleus (PVN) of the hypothalamus, the medial septum, the vertical and horizontal limbs of the nucleus of diagonal band of Broca (NDB), the supramammillary nucleus (SUM), and the median raphe nucleus (MRN).

The major output of CA2 is to CA1 (Cui et al., 2013; Chevaleyre and Siegelbaum, 2010). CA2's axons ramify in stratum oriens (so) and stratum radiatum (sr) (Figure 1.8). Previous work has also identified several extrahippocampal targets of CA2. Cui and colleagues observed outputs to SUM, medial and lateral triangular septum nuclei and the vertical and horizontal limbs of the diagonal band of Broca.

Furthermore, a recent study using genetically targeted rabies tracing has demonstrated output of CA2 to EC2 (Rowland et al., 2013). CA1 provides the major output of the hippocampus to the deep layers of the EC (Figure 1.1). The finding of a connection between CA2 and EC2 is particularly intriguing because such a connection would provide for an alternate route of hippocampal information output.

One hint as to the function of CA2 comes from the observation that CA2 neurons express high levels of the vasopressin 1b receptor (AVPR1B) for the hormone arginine-vasopressin, which has been implicated in social behavior (Young et al., 2006). *Avpr1b* knockout mice have been generated and the behavioral effects of loss of this receptor have been studied (Wersinger et al., 2002; DeVito et al., 2009). Whole-brain knockout of the vasopressin 1b receptor resulted in reduced aggression, impaired social recognition, and impaired detection of temporal order (Wersinger et al., 2002; DeVito et al., 2009). While these studies suggested an important role of CA2 in mediating social behavior, they could not definitively assign these functions to CA2 because even though AVPR1B is heavily expressed in CA2, its expression is not limited to this subregion (Young et al., 2006). Furthermore, the reduced aggression phenotype has not been observed in animals with hippocampal ablations, thus pointing to an extra-hippocampal explanation for some of these findings.

RGS14 is another protein that is heavily expressed in CA2 (Lee et al., 2010). Knockout of this protein resulted in increased long term potentiation (LTP), an electrophysiological correlate of learning, in CA2 neurons. Moreover, knockout of RGS14 resulted in quicker learning of the Morris water maze task (Lee et al., 2010). These results indicate that RGS14 may serve to limit plasticity in CA2, and that CA2 may be involved in spatial learning and memory. However, like the AVPR1B knockout described above, the RGS14 knockout resulted in loss of the protein throughout the entire brain. Hence, the phenotype observed may have resulted from a loss of RGS14 in areas outside of the hippocampus.

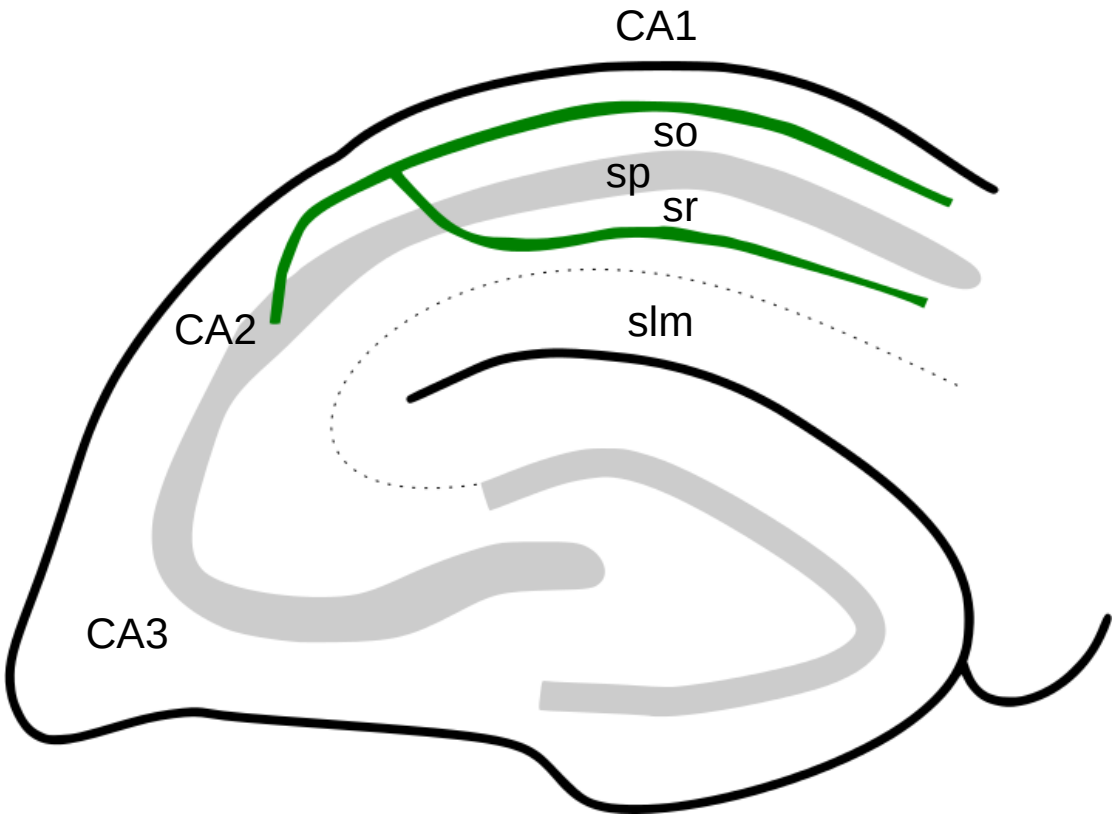

Figure 1.8: Output of CA2. A schematic of the hippocampus with CA2's axons drawn in green. The major projection of CA2 is to CA1. The axons of CA2 largely ramify in stratum oriens (so) and stratum radiatum (sr). Stratum pyramidale (sp) and stratum lacunosum moleculare (slm) are also demarked for reference.

1.5 Aims of the thesis

In this chapter, I have introduced the hippocampus, its anatomy, and one of its substituents, the CA2 subfield. In Chapter 2, I detail the generation of a transgenic mouse line that allows genetic targeting of this subfield. Genes that are endogenously expressed exclusively in CA2, with respect to the hippocampus, will be described. Details of the transgenic Cre construct and targeting strategy will be outlined. Lastly, demonstration of the CA2-specificity of the line will be illustrated through the use of Cre-dependent vectors.

Chapter 3 addresses the use of the CA2-Cre mouse line for genetically targeted anatomical investigation of this area. A Cre-dependent vector that carried the enhanced yellow fluorescent protein (eYFP) gene was used to express eYFP in the axons of CA2 to illuminate the output areas of CA2. To characterize the inputs to CA2, a modified rabies virus was injected into the hippocampus of the CA2-Cre mice. The rabies virus was transcomplemented with a Cre-dependent Adeno-associated virus (AAV) vector. This strategy resulted in monosynaptic, retrograde labeling of the inputs to the Cre-positive CA2 cells.

To study the *in vivo* relevance of CA2, a genetic inactivation of this region was performed as further detailed in Chapter 4. Briefly, a Cre-dependent viral vector was used to express tetanus neurotoxin (TeNT) in CA2, thus abolishing CA2 output. A battery of behavioral tests were conducted on the CA2-inactivated mice to determine the *in vivo* role of this subfield. I demonstrate the critical role of this subfield for mediating social memory.

I draw conclusions from the findings presented in this work in Chapter 5 and describe potential future directions. The final chapter details the methods used to obtain the data described in Chapters 2-4.

Chapter 2

Generation of a CA2-specific transgenic mouse line

2.1 Introduction

The mouse is an excellent model system for genetic manipulation because its genome has been fully sequenced (Mouse Genome Sequencing Consortium et al., 2002), a large number of cDNAs have been published (Kawai et al., 2001), and a vast array of bacterial artificial chromosome (BAC) libraries are available (Osoegawa et al., 2000). With the use of cell type-specific promoters, expression or deletion of virtually any gene may be directed to selected cell populations (Utomo et al., 1999).

A very versatile tool for cell type-specific gene ablation or expression is a transgenic mouse line that expresses Cre recombinase under the control of a restricted promoter (Utomo et al., 1999). Cre recombinase is an enzyme that mediates site-specific recombination between 34 bp loxP sites. Depending on the orientation of the loxP sites, a genome segment may be excised or inverted. Therefore, Cre-mediated deletion of a gene would entail crossing a Cre line with another line that contains a floxed (flanking loxP sites) target gene. The converse, selective expression of a gene, would require a floxed stop cassette upstream of the gene. A newer, less leaky method for Cre-dependent expression of a gene is the flip-excision (FLEx) system (Schnütgen et al., 2003). In this system, two sets of incompatible loxP sites flank an inverted open reading frame (ORF). Cre will first flip the ORF using one set of loxP sites and then use the second set of loxP sites to excise two of the four loxP sites. The result is stable placement of the

ORF in the correct orientation in Cre-positive cells alone. The ORF will remain inverted in Cre-negative cells (Figure 2.1).

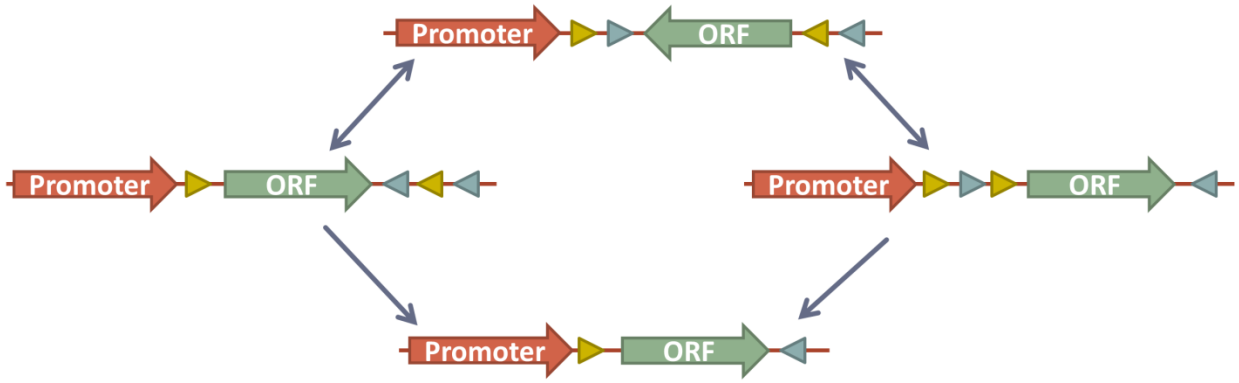

Figure 2.1: The FLEx system for Cre-dependent expression of genes. The inverse open reading frame (ORF) is flanked by incompatible loxP sites (yellow and teal triangles). In the first, reversible step the ORF is flipped in the correct orientation by Cre-mediated recombination at the yellow loxP sites (left) or at the teal loxP sites (right). Cre then either flips the construct back or excises two of the loxP sites. The result is placement of the ORF in the correct orientation only in Cre-positive neurons.

2.2 Genes expressed selectively in CA2

Creating a cell type-specific Cre mouse line first involves the identification of an endogenous gene that is expressed selectively in the cell population wished to be studied. The advent of the BGEM atlas (Magdaleno et al., 2006) and the Allen brain atlas (Lein et al., 2007) has greatly facilitated this process. These atlases detail the mRNA expression of nearly every gene in the mouse genome. Using these atlases and the available literature, I identified several genes that were expressed exclusively in CA2 with respect to the hippocampus. This list of candidate genes was pared down by selecting only those genes that produced faithful expression in the GENSAT brain atlas (Gong et al., 2003). The GENSAT project creates and characterizes mouse lines that express eGFP under the control of a BAC. For reasons that will be elaborated below, I have chosen to generate a BAC transgenic Cre line. Consequently, ensuring that a BAC containing the candidate gene could recapitulate the endogenous pattern of expression was of paramount importance. The candidate genes that met the aforementioned criteria were *Amigo2* (Figure 2.2) and *Cacng5*, also known as the γ-5 TARP (Figure 2.3).

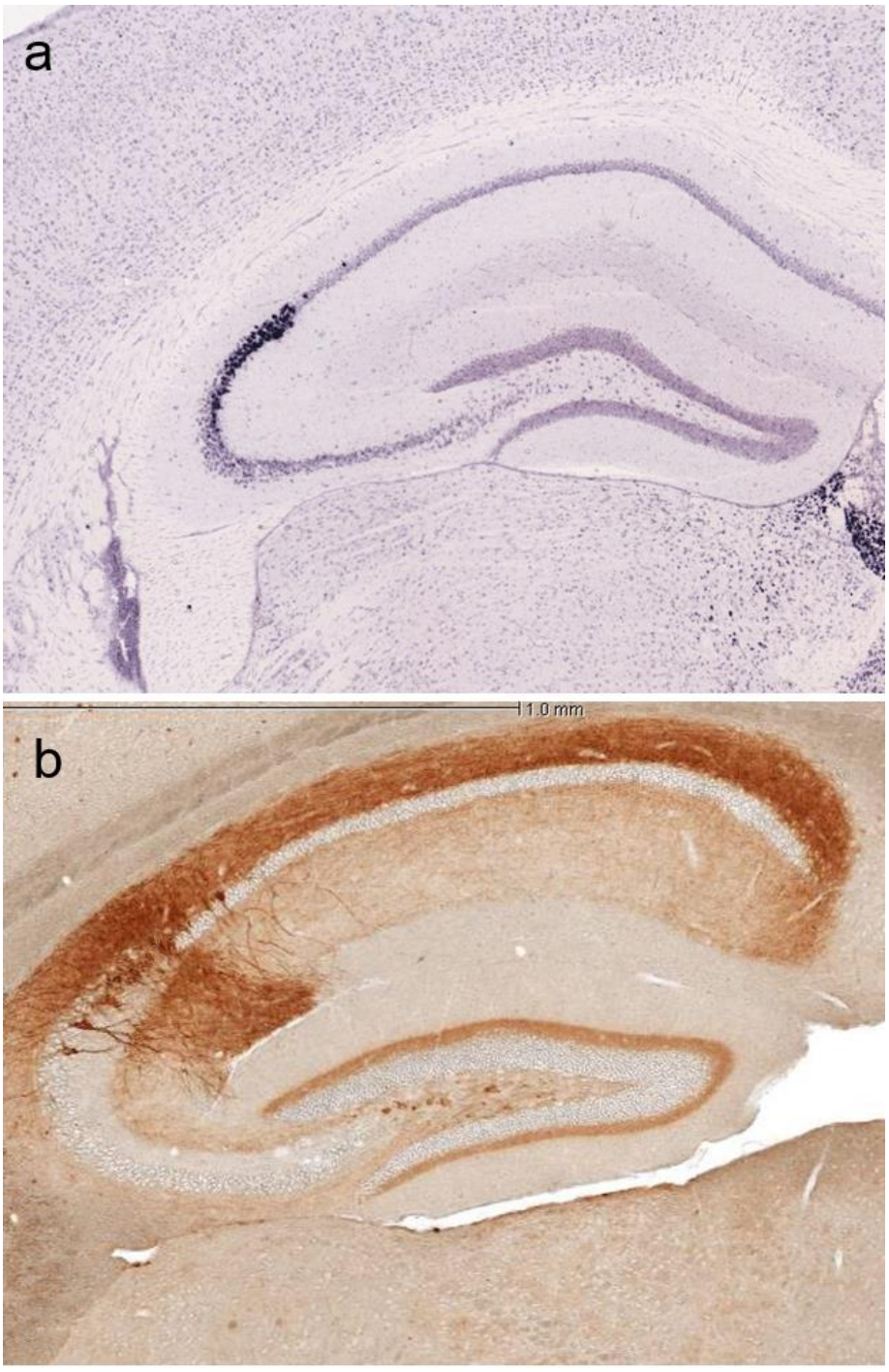

Figure 2.2: *Amigo2* expression in the mouse brain. a, *In situ* hybridization demonstrating CA2-specific expression of *Amigo2* mRNA. (Adapted from Lein, 2007). **b,** GFP expression driven by an Amigo2-GFP BAC transgenic mouse is largely restricted to CA2. There is also faint expression in mossy cells located in the hilus of the DG. (Adapted from Heintz, 2003).

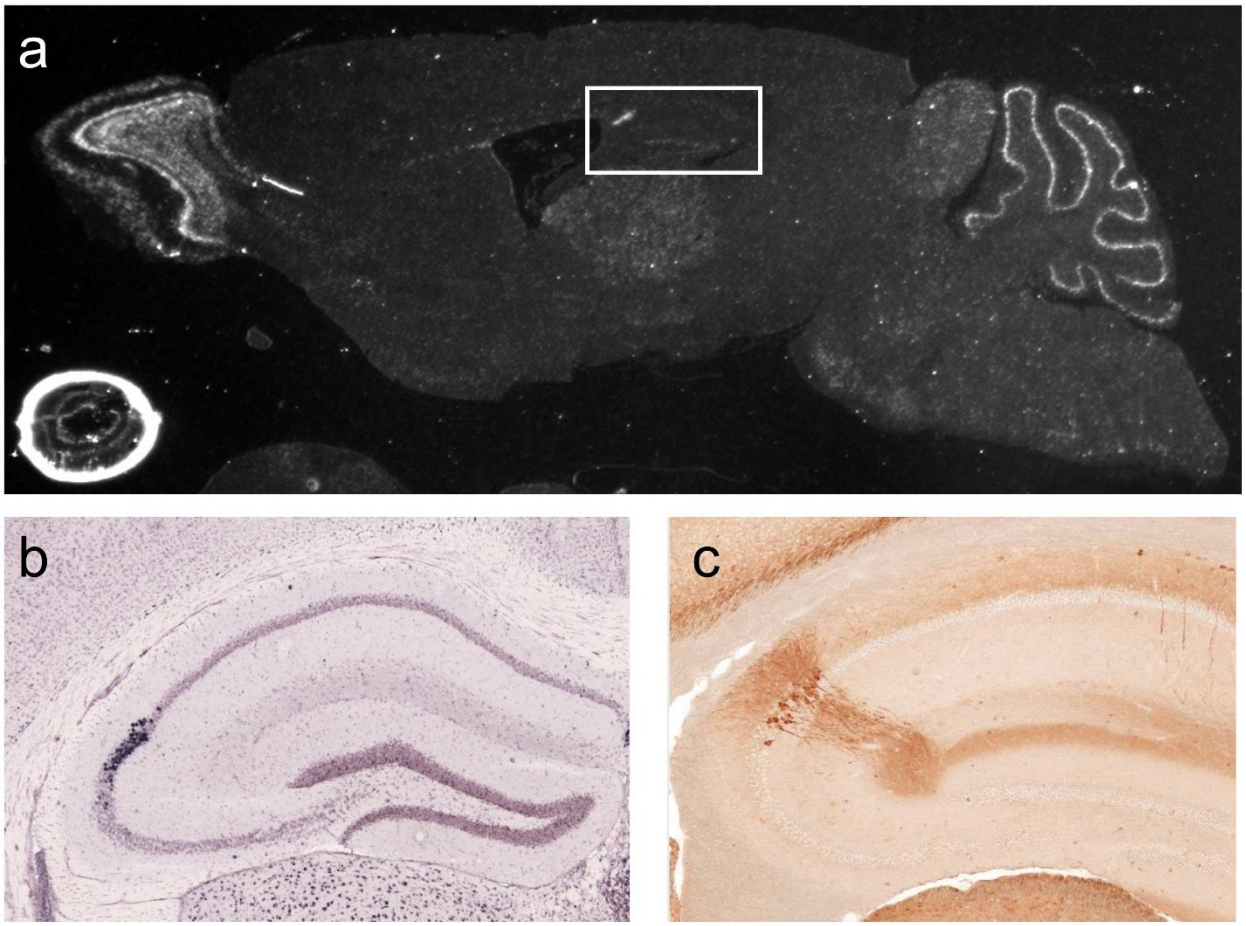

Figure 2.3: *Cacng5* expression in the mouse brain. a, *In situ* hybridization from the BGEM atlas demonstrating CA2-specific expression of *Cacng5* mRNA. The white box indicates the location of the hippocampus (Adapted from Magdaleno et al, 2006). **b,** *In situ* hybridization from the Allen Brain Atlas demonstrating expression of *Cacng5* restricted to CA2. (Adapted from Lein, 2007). **c,** GFP expression driven by a Cacng5-GFP BAC transgenic mouse is largely restricted to CA2. (Adapted from Heintz, 2003).

2.3 BAC transgenesis

Generation of a cell type-specific Cre mouse line may be accomplished in one of three ways: traditional transgenic, BAC transgenic, and targeted mutation. Both the traditional transgenic and BAC transgenic approaches involve the production of a DNA construct that is injected into the pronuclei of embryos that are then implanted into pseudopregnant females. The DNA integrates randomly into the genome, and as such, it is prone to insertional effects. (The DNA surrounding the integration site may alter expression of the transgene.) Targeted mutations involve the generation of a DNA construct, followed by recombination in embryonic stem (ES) cells, which are then injected into blastocysts to produce chimeric mice. These chimeras must then be bred to produce transgenic founders. Generating a mouse line with a targeted mutation is much more time consuming than generating a traditional or BAC transgenic line. The advantage of a targeted mutation is that it is the most effective means of recapitulating the expression of an endogenous gene. While a BAC transgenic does not work as reliably as a targeted mutation, it is much more effective than a traditional transgenic. Traditional transgenic approaches use constructs that are relatively small (~10 kb), so the promoter they use to drive transgene expression is approximately several kb. Finding these promoters is usually an empirical process that is unreliable. BAC constructs, on the other hand, are much larger (~200 kb). They are less prone to insertional effects because they contain more of a "buffer" region surrounding the integration site. Furthermore, their large size allows for, in the majority of cases, inclusion of an entire gene. As a result, the transgene can be driven by not just a promoter, but by all of the regulatory elements of the gene including putative enhancers and repressors. The BAC transgenic approach is therefore a good compromise between expression fidelity and cost.

The large size of BACs makes traditional cloning techniques impossible. To create the BAC constructs, I used the galK selection system in conjunction with λ Red-mediated homologous recombination (Figure 2.4; Warming et al., 2005).

I chose this method because the galK cassette permits both positive and negative selection. This enables seamless changes (no selection cassettes left behind) to be made to the BAC. A PCR product was generated that contained, in order, homology arm 1, the Cre ORF, HSV polyA, and homology arm 2. The homology arms were selected so that the Cre ORF would be inserted precisely at the start codon of the candidate gene contained on the BAC.

The modified BACs were then sequenced and a SpeI restriction digest was done to confirm that no intramolecular rearrangements had occurred (Figure 2.5). 3 recombinants (shown in lanes 4, 5, and 12) matched the expected digest pattern. The digest patterns of these recombinants were identical to the digest pattern of the unmodified BAC (shown in lane 2), except for the band marked with the arrow. This part of the BAC contained the recombination site, and thus the band appears higher on the gel for the recombinants (marked with arrows) due to the addition of the Cre-HSV-polyA cassette. The Amigo2-Cre and Cacng5-Cre BAC constructs were injected into embryos and implanted into pseudopregnant females by the transgenic mouse core facility at the Irving Cancer Research Center at Columbia.

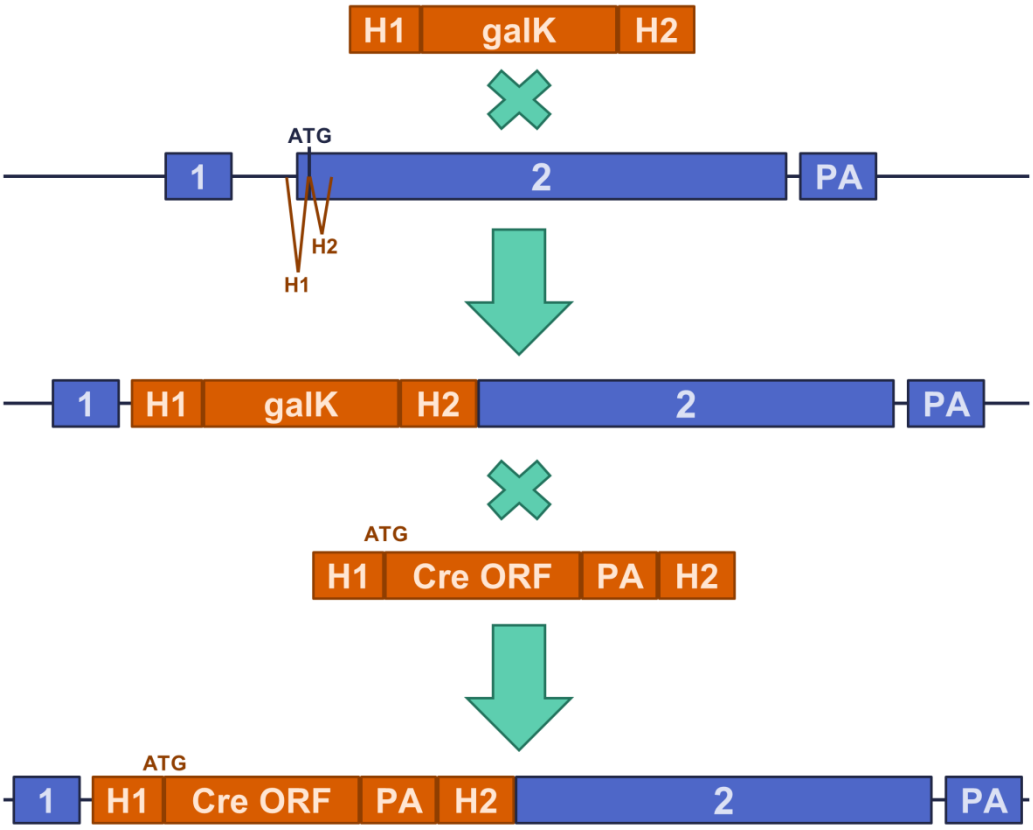

Figure 2.4: Recombineering strategy to create the BAC construct. Generation of CA2-Cre mouse line. λ Red-mediated homologous recombination with galK positive and negative selection was used to make seamless changes to the bacterial artificial chromosome (BAC). PCR cassettes shown in orange, and *Amigo2* locus shown in blue. The PCR cassette contained two homology arms (H1, 58nt; H2, 62nt) that flanked the galactose kinase (galK) cassette. The homology arms flanked the *Amigo2* start codon. Recombination followed by positive selection was used to obtain the galK integrate. Recombination of the modified BAC with a PCR cassette containing the Cre open reading frame (ORF) and polyA (PA) flanked by the same homology arms yielded the final BAC used to generate the transgenic lines.

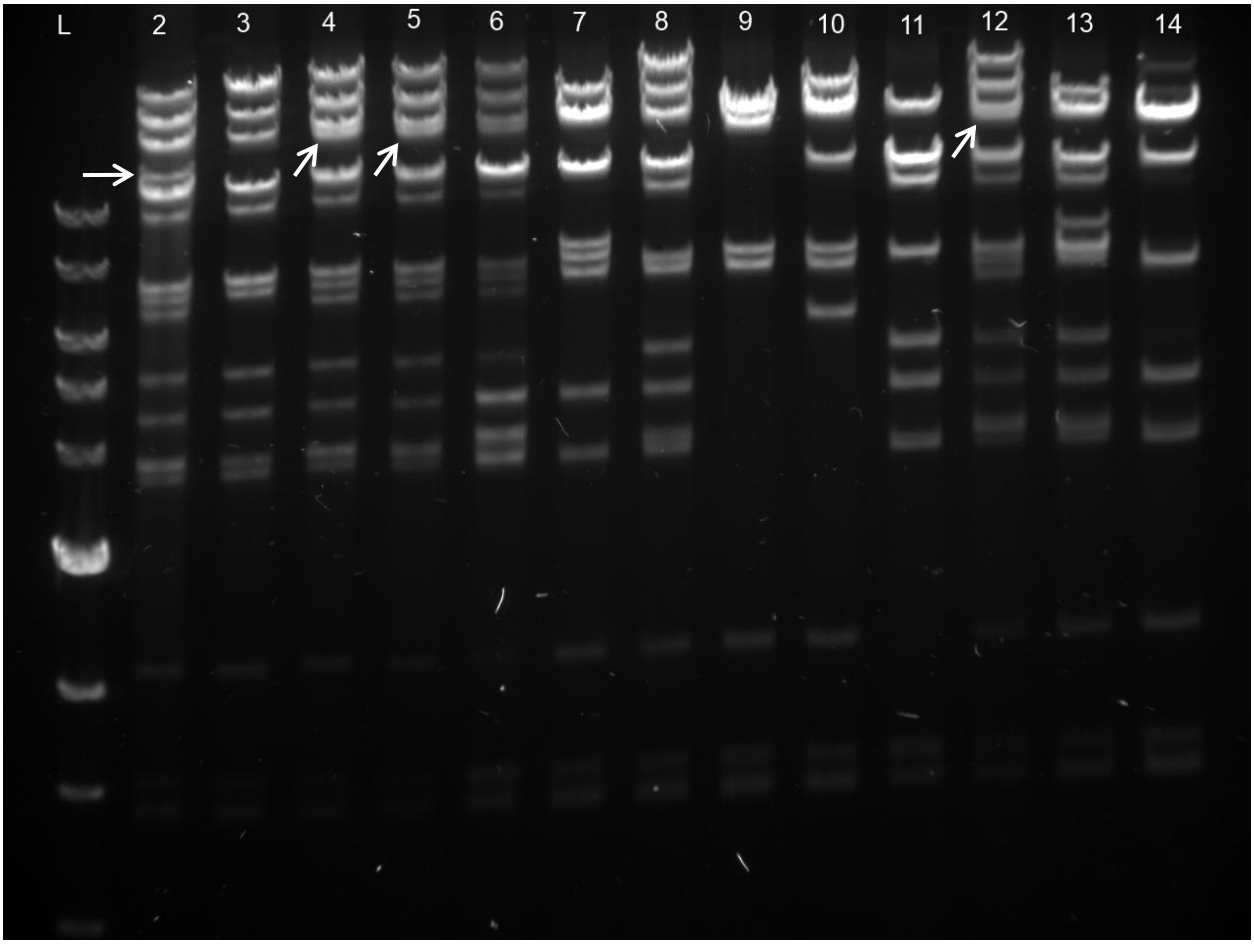

Figure 2.5: Fingerprinting analysis of Amigo2-Cre BAC DNA. A 1 kb ladder (L) was loaded in the first lane. Lane 2 was loaded with a SpeI digest of the unmodified *Amigo2* BAC. Lanes 3-14 are SpeI digests of BAC DNA obtained from individual Amigo2-Cre BAC recombinants. The recombinants shown in lanes 4, 5, and 12 matched the digest pattern of the unmodified BAC shown in lane 2, except for the band marked with the arrow. This part of the BAC contained the recombination site, and thus the band appeared higher on the gel for the recombinants (marked with arrows) due to the addition of the Cre-HSV-polyA cassette.

2.4 CA2-specificity of the transgenic lines

6 Amigo2-Cre founders and 5 Cacng5-Cre founders were generated as determined by PCR amplification of Cre from DNA obtained from tail biopsy of the offspring produced by the females implanted with the BAC-injected embryos.

To test the Cre expression patterns of the founders, the various Cre lines were crossed to the Ai14 reporter line generated by the Allen Institute (Madisen et al., 2010). This line contains, in the Rosa26 locus, a floxed stop cassette upstream of the fluorescent reporter protein tdTomato. This fluorescent protein will only be expressed in Cre-positive cells. Expression of tdTomato in the adult brain, however, does not necessarily reflect the Cre expression pattern in the adult. If Cre is transiently expressed during development, the stop cassette will be excised and tdTomato will be expressed for the lifetime of that cell. To get a readout of adult Cre expression, I injected a Cre-dependent AAV reporter virus (CAG-FLEx-eGFP-WPRE-bGH polyA or EF1α-FLEx-eYFP-WPRE-hGH polyA) generated by the UPenn or UNC vector cores into the dorsal hippocampus of mice from a cross between a founder line and the Ai14 tdTomato reporter line (Figures 2.6, 2.7). A summary of the findings is shown in Table 2.1.

The Amigo2-Cre-1 line demonstrated tdTomato expression in CA1, CA2, and DG, however injection of a Cre-dependent fluorescent reporter AAV revealed CA2-specific expression (Figure 2.6a). The Amigo2-Cre-2 line displayed sparse tdTomato expression scattered throughout the hippocampus including in CA1, CA2, CA3, DG, and interneurons situated in slm. Injection of a Cre-dependent fluorescent reporter AAV revealed similarly scattered expression (Figure 2.6b). The third and sixth Amigo2-Cre founder lines did not produce any Cre-positive offspring. The Amigo2-Cre-4 founder line exhibited tdTomato expression in CA1, CA2 and DG

(Figure 2.6c). While strong CA2 labeling was observed in this line following injection of a Cre-dependent fluorescent reporter AAV, expression in CA1 was also observed (Figure 2.6c). Finally, no tdTomato expression was observed in the Amigo2-Cre-6 founder line suggesting that the Cre protein was not expressed in this line.

Of the 5 Cacng5-Cre founders generated, none produced CA2-specific expression of Cre. Injection of a Cre-dependent fluorescent reporter AAV revealed Cre expression in EC, CA2, CA3, and interneurons scattered throughout the hippocampus. The Cacng5-Cre-2 founder line demonstrated weak CA1, CA2, and DG expression. The Cacng5-Cre-3 founder line did not demonstrate any expression of the fluorescent reporter suggesting that the Cre protein was not expressed in this line. The Cacng5-Cre-4 founder line demonstrated robust CA2 expression, but also weak expression in interneurons scattered throughout the hippocampus (Figure 2.8b). Finally, the Cacng5-Cre-5 founder line did not show hippocampal Cre expression. Instead, expression was observed in layers 2 and 3 of EC (Figure 2.9).

Founder Line	Expression Pattern
Amigo2-Cre-1	Restricted CA2 expression in the adult brain (Figure 2.6a)
Amigo2-Cre-2	Aberrant Cre expression (Figure 2.6b)
Amigo2-Cre-3	No germline transmission of Cre
Amigo2-Cre-4	Aberrant Cre expression (Figure 2.6c)
Amigo2-Cre-5	No Cre activity (no tdTomato expression)
Amigo2-Cre-6	No germline transmission of Cre
Cacng5-Cre-1	Aberrant Cre expression (Figure 2.7)
Cacng5-Cre-2	Aberrant Cre expression (Figure 2.8a)
Cacng5-Cre-3	No Cre expression
Cacng5-Cre-4	Expression in CA2 + some interneurons (Figure 2.8b)
Cacng5-Cre-5	Expression in layers 2 and 3 of EC (Figure 2.9)

Table 2.1: Cre expression patterns in the Amigo2-Cre and Cacng5-Cre founder lines. Summary of the findings obtained from crossing the Cre founders to the Ai14 Cre-reporter line and hippocampal injection of Cre-dependent reporter AAVs.

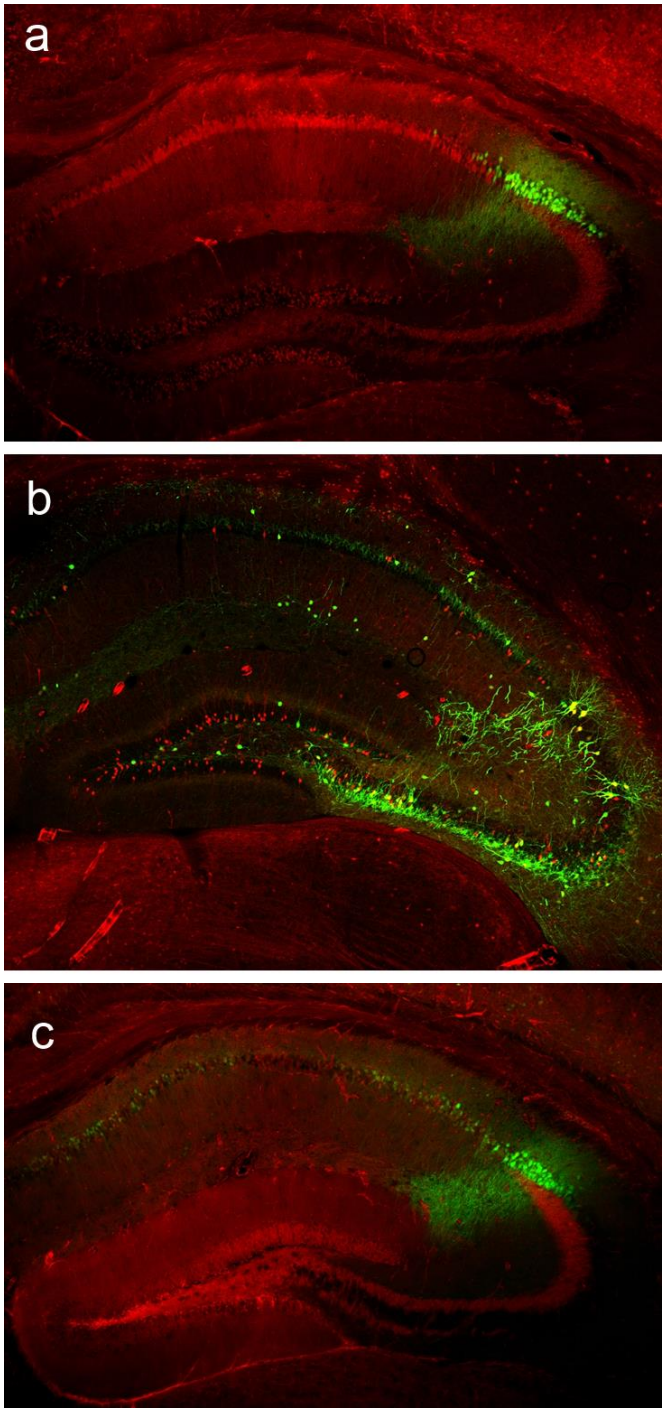

Figure 2.6: Cre expression in the Amigo2-Cre founder lines. The Amigo2-Cre founder lines were crossed with the Ai14 tdTomato reporter line and stereotactically injected with a Cre-dependent eGFP reporter AAV to reveal Cre expression. tdTomato expression is shown in red, and eGFP expression is shown in green. **a,** While the Amigo2-Cre-1 founder line showed relatively unrestricted tdTomato expression, CA2-specific Cre expression was seen in the adult brain with injection of a Cre-dependent AAV carrying the eGFP gene. **b, c,** The Amigo2-Cre-2 **(b)** and Amigo2-Cre-4 **(c)** lines did not demonstrate CA2-specific expression.

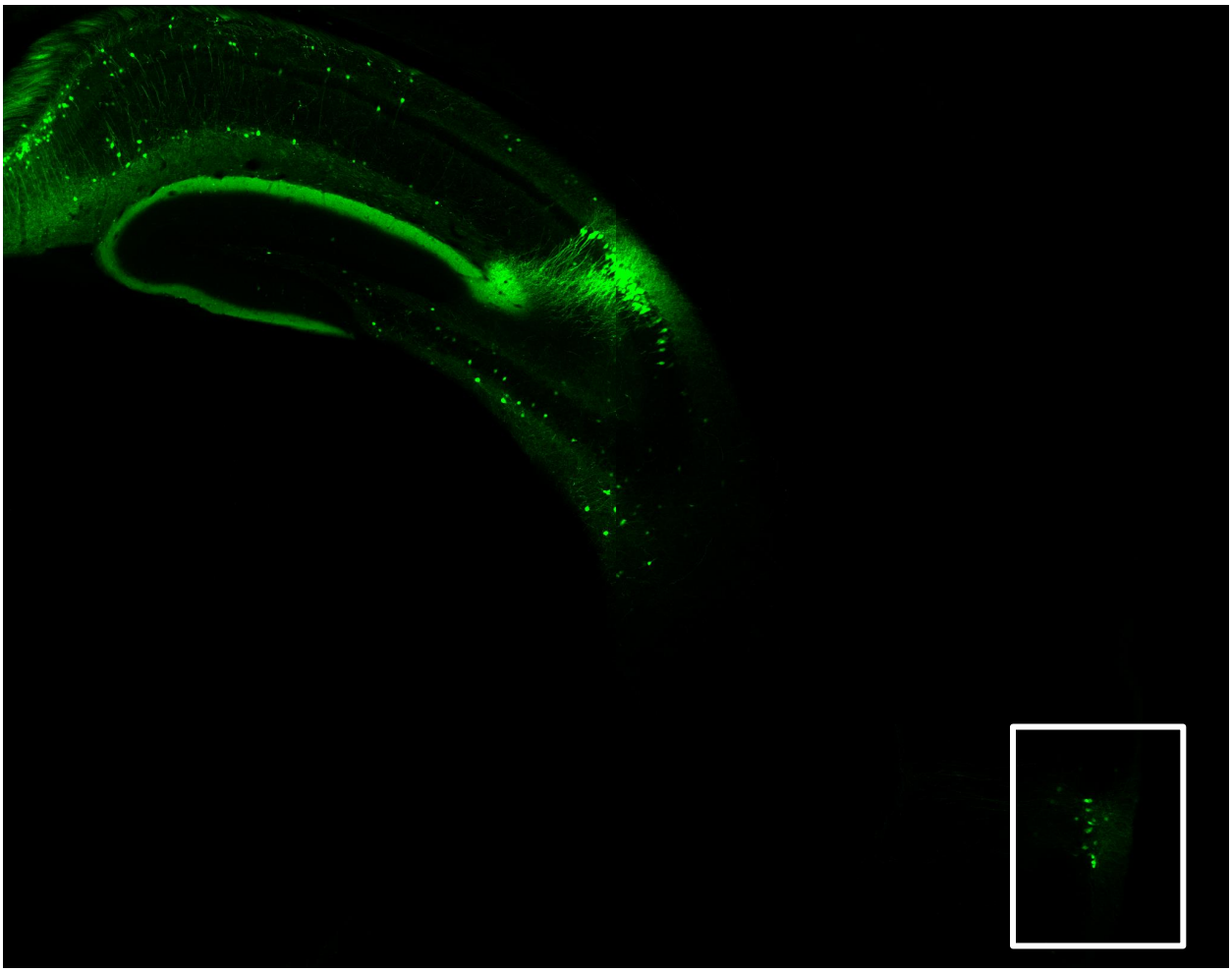

Figure 2.7: Cre expression in the Cacng5-Cre-1 line. A Cre-dependent reporter virus was injected into the dorsal hippocampus to express eYFP in Cre^{+} neurons. eYFP (shown in green) was found in CA2, a variety of interneurons, and the EC (boxed area). EC labeling was presumably the result of retrograde AAV transduction.

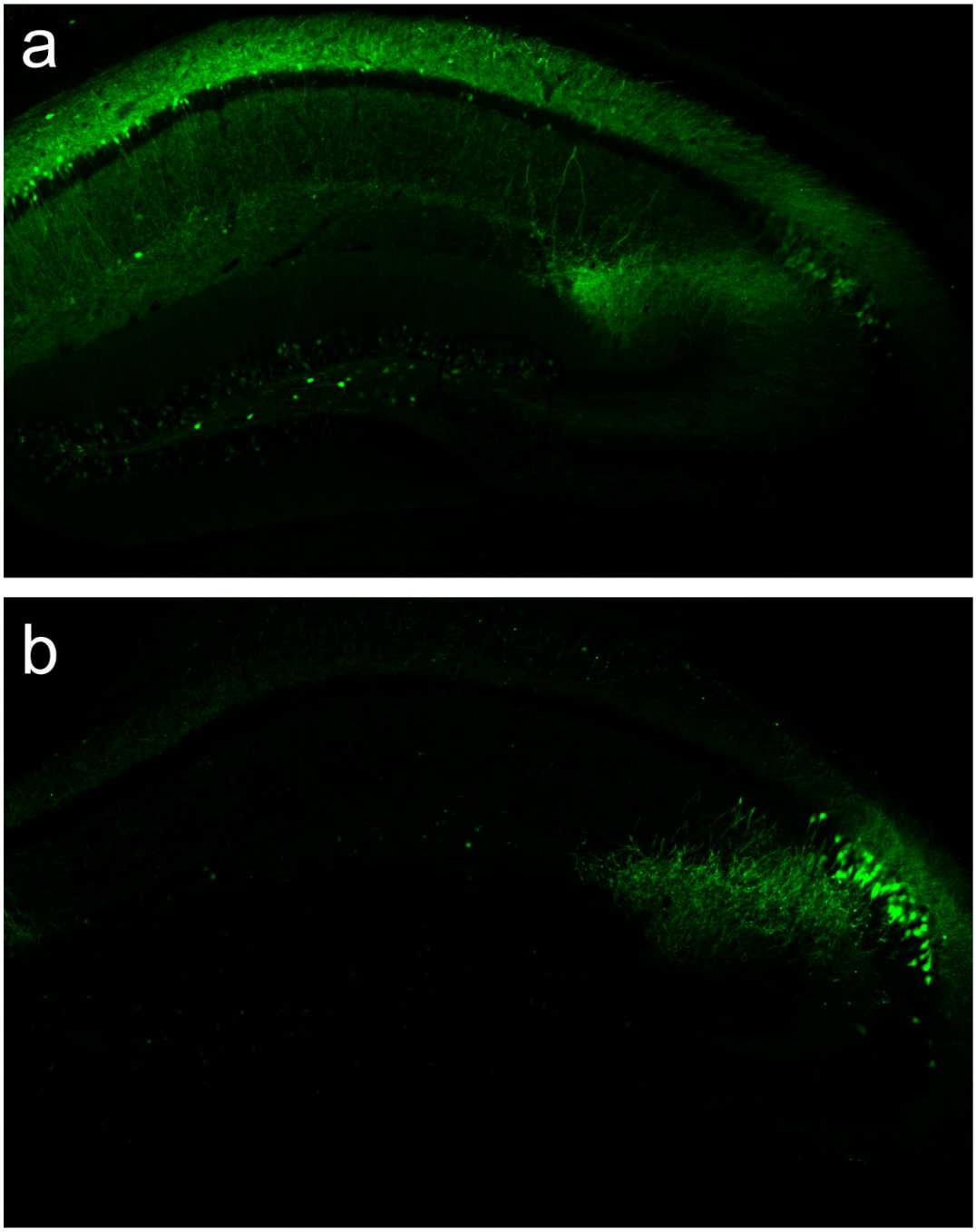

Figure 2.8: Cre expression in the Cacng5-Cre-2 and Cacng5-Cre-4 lines. A Cre-dependent reporter virus was injected into the dorsal hippocampus to express eYFP (shown in green) in Cre^{+} neurons. **a,** The Cacng5-Cre-2 line demonstrated weak Cre expression in CA2, CA1, and DG. **b,** The Cacng5-Cre-4 line demonstrated strong CA2 expression, but also some weak interneuron expression.

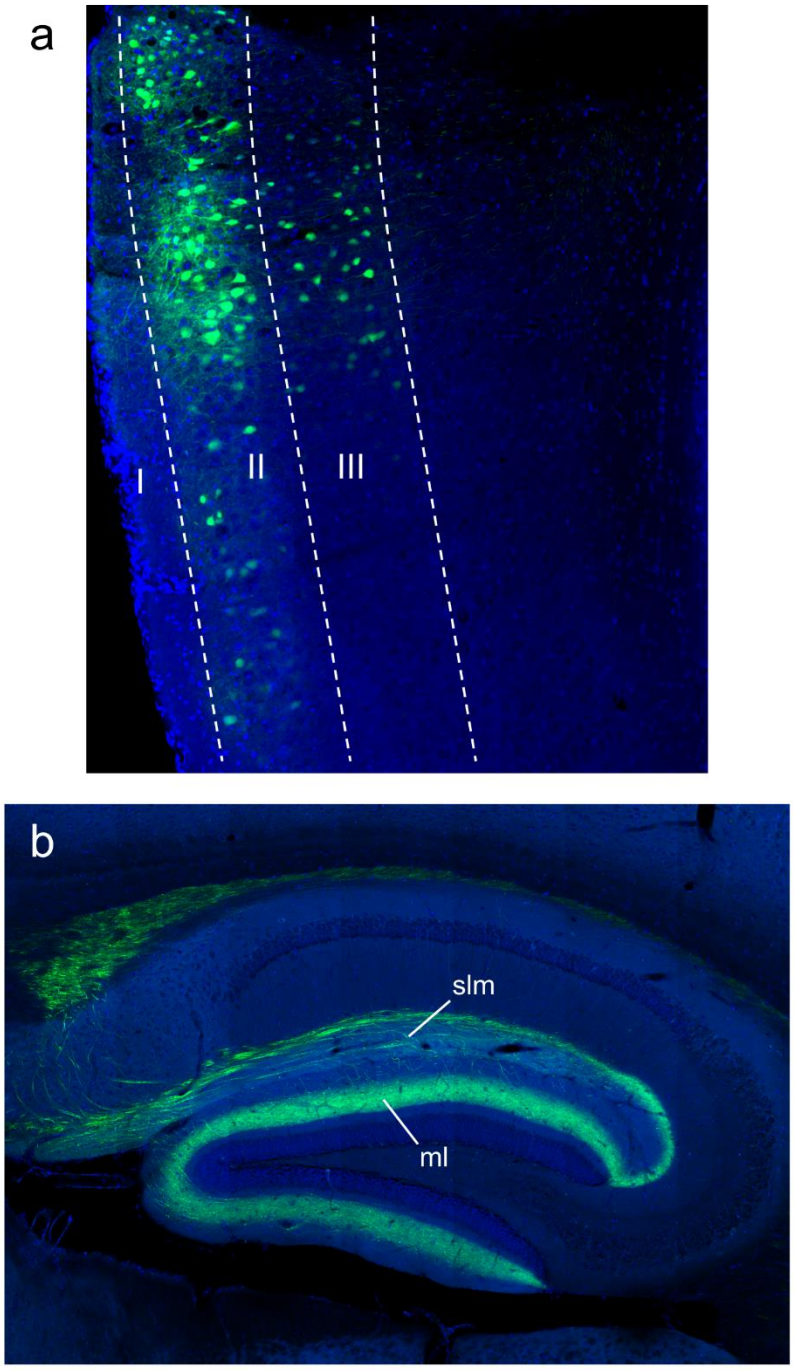

Figure 2.9: Cre expression in the Cacng5-Cre-5 line. A Cre-dependent reporter virus was injected into the EC to express eYFP (shown in green) in Cre^{+} neurons. **a,** Sagittal section of medial EC showing eYFP expression in layers II and III. **b,** Sagittal section of dorsal hippocampus showing eYFP expression of EC LIII axons in stratum lacunosum moleculare (slm) and EC LII axons in the molecular layer (ml) of the DG. DAPI staining shown in blue.

To further investigate the CA2-specificity of the Amigo2-Cre-1 line (Figure 2.6a), I bilaterally injected a Cre-dependent AAV to express yellow fluorescent protein (YFP) in Cre^+ cells (Figure 2.10). I observed selective and robust YFP expression throughout dorsal CA2 (Figure 2.11, Franklin and Paxinos, 2007; Lein et al., 2005). To confirm that these cells were indeed CA2 pyramidal neurons, I stained for RGS14, a marker of CA2 (Figures 2.12 and 2.13; Lee et al., 2010).

Nearly every YFP^+ neuron was also $RGS14^+$ (97.38 ± 0.31%; n = 4 mice, 2546 cells), demonstrating the proper targeting of CA2. Only a minute fraction of YFP^+ neurons were also $GABA^+$ (0.16 ± 0.16%; n = 3 mice, 1539 cells), demonstrating the specific targeting of CA2 excitatory pyramidal neurons (Figures 2.12 and 2.13). Finally, my AAV injection protocol resulted in the targeting of the vast majority of dorsal CA2, measured by the percentage of $RGS14^+$ cells that were also YFP^+ (82.33 ± 2.37%, n = 4 mice, 2992 cells).

To determine if the electrophysiological properties of the Cre^+ neurons matched those previously reported (Chevaleyre and Siegelbaum, 2010) for CA2 neurons, I stereotactically injected a Cre-dependent channelrhodopsin-2 (ChR2) AAV vector into the hippocampi of Amigo2-Cre-1 mice. ChR2 is a light-activated cation channel that allows for activation of transduced neurons with pulses of blue light (Boyden et al., 2005; Sohal et al., 2009). Hence, Cre^+ neurons could be identified as those that responded to pulses of blue light. The electrophysiological properties of the Cre^+ neurons largely matched those previously reported for CA2 neurons (Table 2.2). One electrophysiological property, voltage sag due to hyperpolarization-activated cation current (I_h), was found to be lower than the previously recorded value (1.917 ± 0.503, current study; 4.1 ± 0.2, previous study). This is likely due to the slight differences used in obtaining these values. I recorded the voltage sag following a

hyperpolarizing pulse from -70 mV to -100 mV as in the previous study. However, I recorded these values in whole-cell configuration within a few minutes following break-in. The previously reported value was obtained approximately 10 minutes after break-in, following dialysis of the cell with the internal patch pipette solution. It is important to note that the value found for the Cre^{+} neurons differed from the value previously reported for CA1 neurons. This is significant because a decreased amount of sag is likely due to the decreased expression of hyperpolarization-activated cyclic nucleotide-regulated (HCN) channels in CA2. Furthermore, all of the other electrophysiological properties matched those previously reported for CA2 and differed from the values reported for CA1 (Table 2.2) thus confirming the specific targeting of CA2 pyramidal neurons in the Amigo2-Cre-1 mouse line. This mouse line will henceforth be referred to as CA2-Cre.

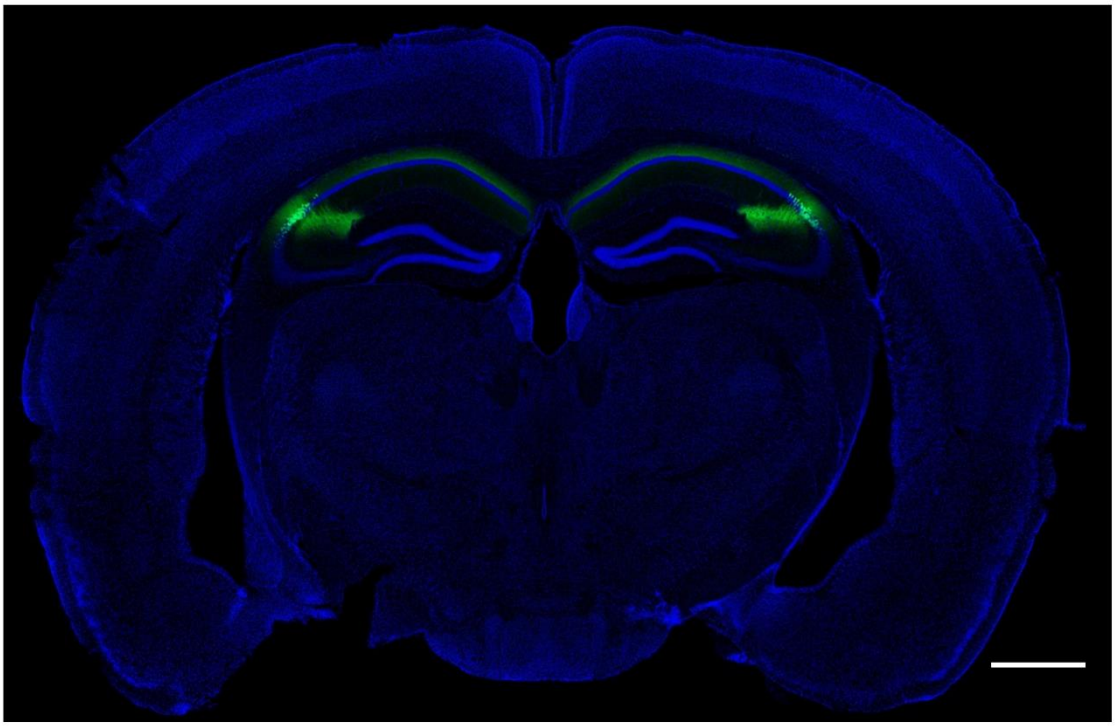

Figure 2.10: Cre expression in the Amigo2-Cre-1 line. A Cre-dependent reporter virus was injected bilaterally into the dorsal hippocampus to express eYFP (shown in green) in Cre^{+} neurons. Coronal section showing robust and selective expression of YFP in CA2. Nissl counterstain shown in blue. Scale bar represents 1 mm.

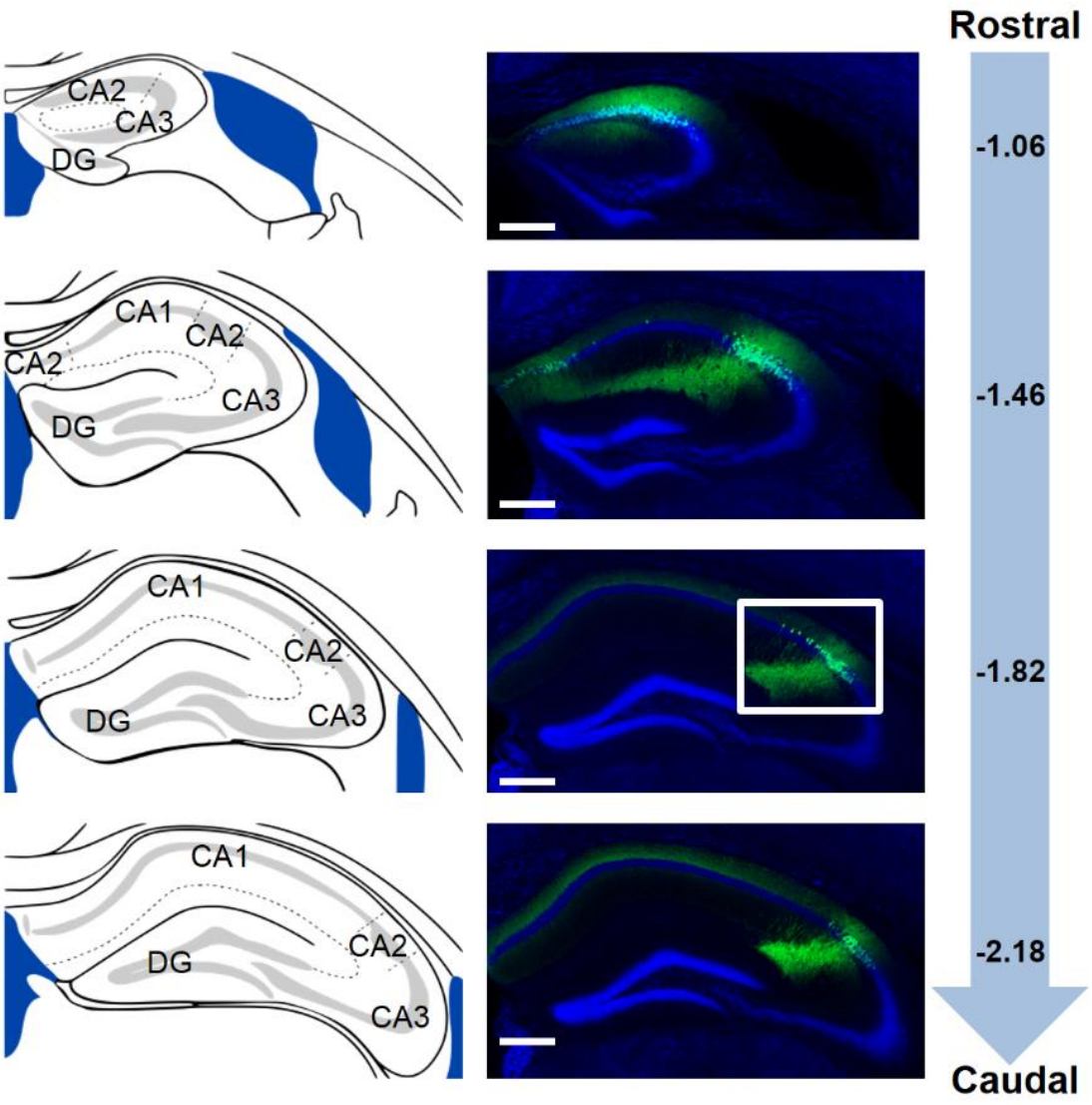

Figure 2.11: Rostrocaudal spread of the AAV transduction. Left, reference atlas images adapted from Franklin and Paxinos, 2007. Center, YFP expression shown in green. Robust and selective expression in CA2 was observed. The boxed area is magnified in Figure 2.12. Right, mm from bregma along rostrocaudal axis. All panels show coronal sections with Nissl counterstain (colored in blue). Scale bars represent 400 μm.

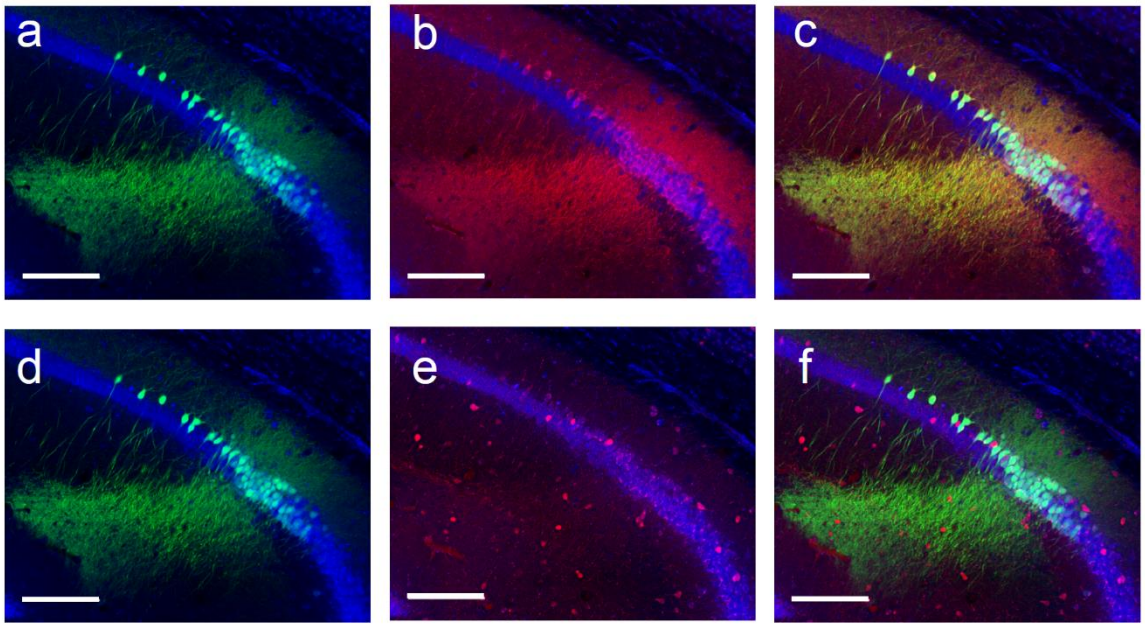

Figure 2.12: YFP$^+$ neurons are positive for RGS14 and negative for GABA. a, d Magnification of area demarcated with a white box in Figure 2.11. YFP expression resulting from transduction of CA2 neurons with the Cre-dependent YFP reporter virus is shown in green. **b,** RGS14 staining shown in red. **c,** Merge of **(a)** and **(b)** illustrating overlap between RGS14 and YFP. **e,** GABA staining shown in red. **f,** Merge of **(d)** and **(e)** demonstrating that YFP$^+$ neurons are not GABAergic. Scale bars represent 200 μm.

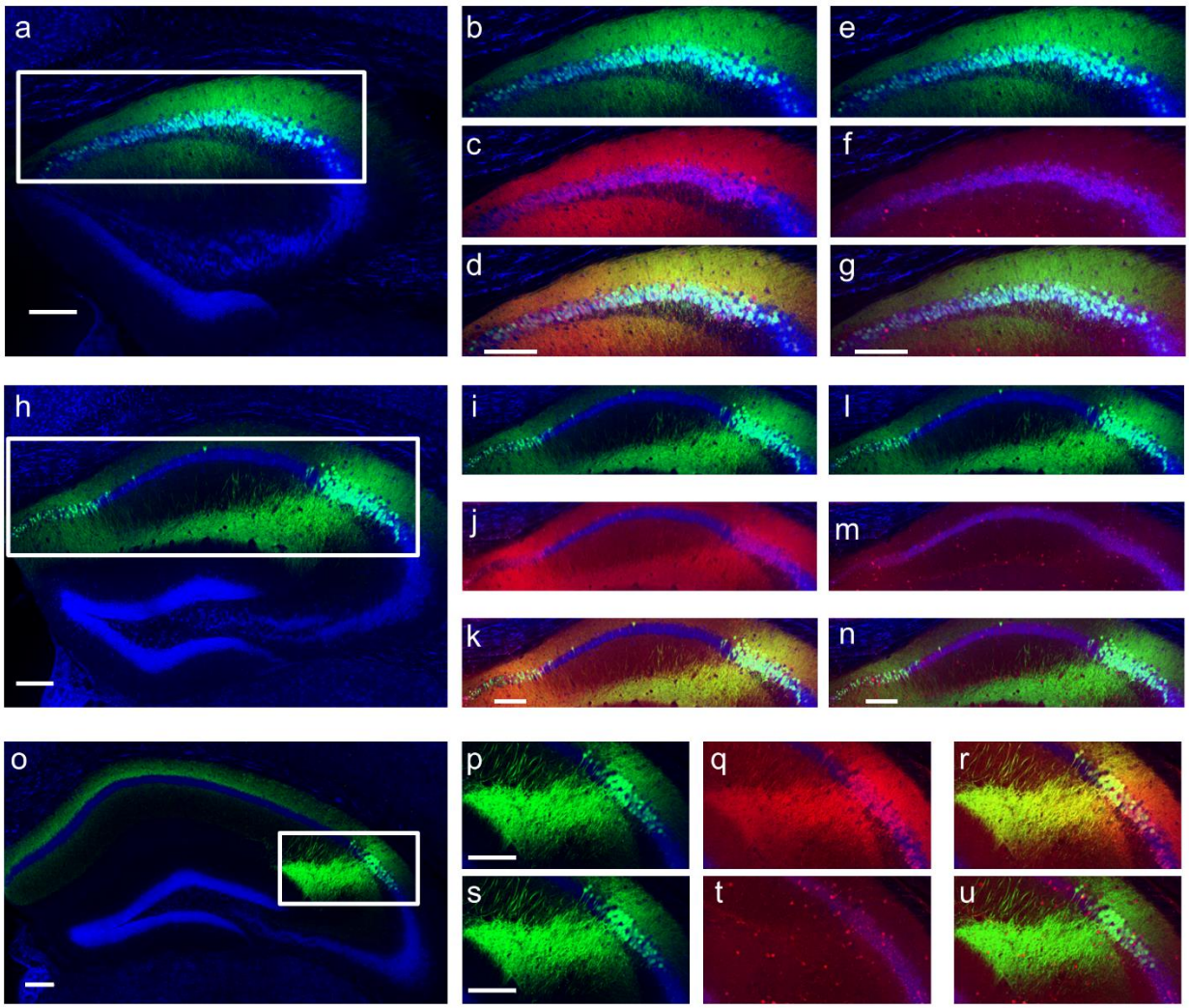

Figure 2.13: YFP$^+$ neurons are excitatory CA2 pyramidal neurons. Cre$^+$ neurons expressing YFP (shown in green) co-label with RGS14 staining (shown in red), but do not co-label with GABA staining (shown in red in separate images). **a,** Reproduction of section -1.06mm shown in Figure 2.11. **b,e** Magnification of area boxed in (**a**). **c,** RGS14 staining of section shown in (**b**). **d,** Merge of (**b,c**) demonstrating YFP and RGS14 co-labeling. **f,** GABA staining of section shown in (**e**). **g,** Merge of (**e,f**) showing no overlap of GABA and YFP. **h,** Reproduction of section -1.46mm shown in Figure 2.11. **i,l** Magnification of area boxed in (**h**). **j,** RGS14 staining of section shown in (i). **k,** Merge of (**i,j**) demonstrating YFP and RGS14 co-labeling. **m,** GABA staining of section shown in (**l**). **n,** Merge of (**l,m**) showing no overlap of GABA and YFP. **o,** Reproduction of section -2.18mm shown in Figure 2.11. **p,s** Magnification of area boxed in (**o**). **q,** RGS14 staining of section shown in (**p**). **r,** Merge of (**p,q**) demonstrating YFP and RGS14 co-labeling. **t,** GABA staining of section shown in (**s**). **u,** Merge of (**s,t**) showing no overlap of GABA and YFP. Scale bars, 200 μm.

	Cre^+ neurons	CA1	CA2	CA3
Input Resistance (MΩ)	68.3 ± 3.032	107 ± 10.7	76.2 ± 11.1	107.5 ± 28.1
Capacitance (pF)	296.0 ± 18.68	170.1 ± 11.4	305.3 ± 20.8	150.1 ± 26.1
Resting Potential (mV)	-76.3 ± 0.63	-71.9 ± 1.2	-75.3 ± 1.0	-74.4 ± 0.8
AP Amplitude (mV)	90.81 ± 2.17	95.3 ± 1.8	84.8 ± 1.6	84.4 ± 4.4
AP Duration (ms)	0.8253 ± 0.02	0.99 ± 0.03	0.78 ± 0.02	0.95 ± 0.03
Sag (mV)	1.917 ± 0.503	8.4 ± 0.3	4.1 ± 0.2	4.3 ± 0.4

Table 2.2: The electrophysiological properties of Cre^+ neurons. Electrophysiological properties of Cre^+ neurons (Column 1) largely matched the properties previously reported (Chevaleyre and Siegelbaum, 2010) for CA2 neurons (Column 3). Whole-cell recordings (n = 5) were conducted to measure input resistance, capacitance, resting potential, action potential (AP) amplitude, AP duration, and sag. Input resistance and capacitance were measured with a -5 mV pulse. The AP amplitude and duration were measured during a 10ms depolarizing pulse and the sag resulting from activation of I_h was measured during a 500ms hyper-polarization from -70 to -100mV. Values previously reported (Chevaleyre and Siegelbaum, 2010) for CA1 and CA3 cells are shown for reference.

2.5 Discussion

In this chapter, I have detailed the generation of a Cre mouse line that enables genetic targeting of the CA2 subfield of the hippocampus. I chose to generate a BAC transgenic, and I introduced the rationale for choosing this method in section 2.3. This method was chosen as a compromise between fidelity of expression and cost, in terms of both time and money. However, this method did not prove as fruitful as anticipated. Following BAC DNA injection of ~360 embryos and screening of 54 potential founders, only 11 Cre^{+} founders were generated. These numbers reflect the inefficiency of BAC transgenesis. This inefficiency is not surprising due to the fact that this technique relies on random DNA integration that is not selected for. Furthermore, as detailed previously in section 2.4, this process only yielded 1 useful transgenic line after the 11 founders were screened for proper expression of Cre that would recapitulate the endogenous expression pattern of the gene used to target CA2. This low success rate was a bit more surprising. The members of the GENSAT (Gene Expression Nervous System Atlas) project previously reported that only three or four founder lines would need to be screened to find a line that would express Cre faithfully (Gong et al., 2007). With this expectation, it was shocking to find such a low success rate for the current project detailed in this thesis. The discrepancy in rate of successful transgenesis may be due to differences in the techniques used by the GENSAT and Columbia transgenic facilities.

Due to my experiences with the inefficiency of BAC transgenesis, in the future I would choose to generate mouse lines with targeted mutations (knock-in lines). These lines take longer to generate because they require DNA recombination in embryonic stem (ES) cells and injection of the ES cells into blastocysts to produce chimeric mice, which must then be bred to produce the transgenic founders. While the generation of the knock-in founders does indeed take more time

than the generation of the BAC transgenic founders, very few founders are required to obtain successful recapitulation of endogenous gene expression patterns. This is a result of the targeted insertion of the transgene in the proper locus. Hence, positional effects due to random DNA insertion associated with the BAC transgenic technique are eliminated with generation of a knock-in transgenic.

Even in the one mouse line that exhibited expression of Cre restricted to CA2, expression was not limited to CA2 throughout development (Figure 2.6a). Therefore, conditional mouse lines cannot be crossed with the CA2-Cre mouse line generated in this study because the conditional allele would be expressed in many regions other than CA2, as evidenced by the neurons expressing tdTomato in Figure 2.6a. This limitation, of course, decreases the usefulness of this line.

The mouse line that yielded CA2-restricted expression (Amigo2-Cre-1) was based on the BAC containing the *Amigo2* gene. As seen in the GENSAT and Allen brain atlases (Figure 2.2), expression of *Amgio2* is also observed in the mossy cells of the dentate gyrus. Expression of Cre in the mossy cells of the DG is observed in the Amigo2-Cre-1 mouse line. Nevertheless, stereotaxic injection of Cre-dependent viruses into the hippocampus proper is sufficient to avoid mossy cell expression (Figures 2.10, 2.11). Additionally, injection of these vectors in adult animals can be used to avoid the undesirable non-specific expression seen during development. This technique is very versatile, because many transgenes may be carried by Cre-dependent viruses. Nearly the only limitation of this technique is the carrying capacity of the viruses used, which is admittedly low for AAV (~5 kb). However, larger DNA viruses such viruses in the herpes virus family can carry ~150 kb of DNA (Luo et al., 2008).

I have demonstrated in this chapter that CA2 can be effectively and specifically targeted genetically using a combination of the CA2-Cre mouse line and stereotaxic injection of Cre-dependent viral vectors. There is a wealth of Cre-dependent tools available to manipulate and observe the activity and connections of specific populations of neurons that are genetically defined by their expression of Cre recombinase. Included in this set of tools are Cre-dependent vectors that can be used to express the TVA receptor and rabies G protein selectively in Cre^+ neurons. Specific expression of these proteins allows for monosynaptic retrograde tracing of inputs to a specific cell population. This technique will be used to explore the connectivity of CA2 in the following chapter. Furthermore, Cre-dependent viral vectors can be used to transduce a neural population with a protein such as tetanus neurotoxin (TeNT) to allow for inactivation of that region. The behavioral result following inactivation of the region can then be assessed. This technique is utilized to explore the behavioral relevance of CA2 in Chapter 4.

Chapter 3

Mapping the inputs and outputs of CA2

3.1 Inputs to CA2

Although aspects of CA2 connectivity have been examined (Cui et al., 2013; Haglund et al., 1984; Kiss et al., 2000; Magloczky et al., 1994; Vertes 1992; Vertes et al., 1999), as discussed in the Introduction to this thesis, these previous studies used non-genetic tracing methods that did not distinguish among the mixture of neuronal subtypes located in the CA2 region or whether an axonal projection formed actual synapses onto CA2 targets. To circumvent these problems, I utilized the CA2-specific Cre mouse line that I generated to map CA2 connectivity using viral tracing strategies that take advantage of the targeting of a genetically defined population of CA2 pyramidal neurons. I labeled monosynaptic inputs to CA2 pyramidal neurons using an EnvA pseudotyped ΔG rabies virus (Figure 3.1; Wall et al., 2013; Wall et al., 2010; Wickersham et al., 2010). EnvA pseudotyped viruses can only infect neurons expressing the avian TVA receptor. Since this receptor is not normally expressed in the mouse brain, expression of the receptor in a specific population of neurons renders only those neurons susceptible to EnvA pseudotyped rabies infection. Hence to target CA2 specifically, a Cre-dependent AAV carrying the TVA gene (AAV5- EF1α-FLEx-TVA-mCherry-WPRE-hGH; Watabe-Uchida et al., 2012) was injected into the hippocampus of the CA2-Cre mice two weeks prior to injection of the EnvA rabies virus.

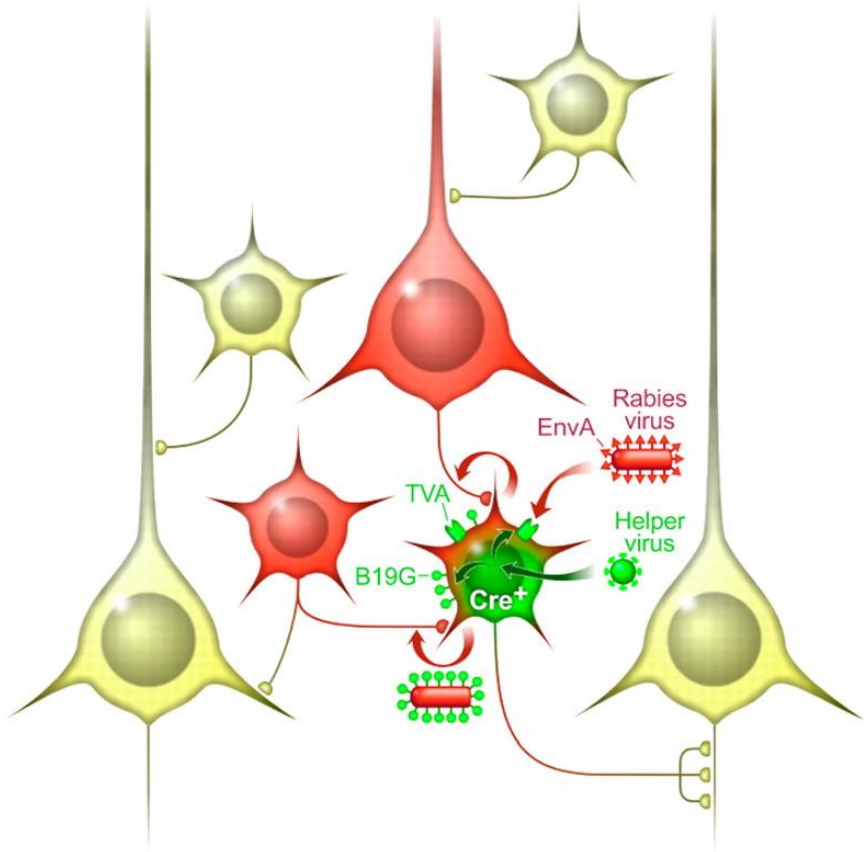

Figure 3.1: EnvA pseudotyped rabies virus tracing. Monosynaptic retrograde tracing with the pseudotyped rabies virus approach is illustrated above. A Cre^+ neuron is transduced with Cre-dependent helper viruses (depicted green) to express the TVA receptor and the B19G glycoprotein only in Cre^+ cells. Then the EnvA pseudotyped rabies virus, which is only capable of infecting neurons that express TVA, is injected. With this strategy, only Cre^+ neurons are initially infected with the rabies virus. The rabies virus encodes mCherry, thus turning the cell red. Because the B19G glycoprotein is expressed in the Cre^+ cell, functional rabies virus particles with the ability to travel transsynaptically in the retrograde direction are made in the Cre^+ neuron. Following transsynaptic spread, monosynaptic inputs are labeled (depicted as red) with the fluorophore encoded for by the rabies virus. These cells do not express G, and hence their inputs (yellow cells) will not be labeled. Furthermore, because rabies travels only in the retrograde direction, targets of Cre^+ cells will not be labeled (cells also depicted in yellow). (Adapted from Wall et al., 2010).

Additionally, since the rabies virus is a ΔG virus (the glycoprotein coat gene has been removed), the rabies virus is not capable of synthesizing new infectious particles without transcomplementation of the glycoprotein G. Therefore, I expressed G specifically in CA2 by injecting a Cre-dependent AAV that carried the G gene (AAV5- CAG-FLEx-rabiesG-WPRE-hGH; Watabe-Uchida et al., 2012) at the same time that I injected the Cre-dependent TVA AAV.

This system (Figure 3.1) has several advantages over traditional tracing techniques. First, rabies virus travels transsynaptically in the retrograde direction. Other retrograde tracers, such as wheat germ agglutinin (WGA), travel transneuronally. Thus, rabies virus tracing will only label functionally connected inputs. Second, the ΔG virus used with this method cannot spread beyond one synapse. Hence, this technique will label only monosynaptic connections. This eliminates the ambiguity of polysynaptic spread associated with other tracing techniques. Finally, the rabies virus is replication competent, thus permitting amplification of the fluorescent reporter. Consequently, weak inputs will be robustly visualized.

To utilize this tracing technique, I unilaterally co-injected two Cre-dependent AAVs to express TVA and G in CA2. Two weeks after injection, I injected EnvA pseudotyped mCherry rabies virus into the dorsal hippocampus (n = 8). One week after the rabies virus injection, I perfused the mice, sliced the brains, and looked for mCherry labeled cells. Unilateral injections revealed bilateral inputs to CA2 from CA3 and CA2 (Figure 3.2).

Strong unilateral input from both lateral and medial EC layer 2 neurons was also observed (Figure 3.3). Some fluorescent cells were occasionally observed in layer 3 of EC, however these were likely due to aberrant leaky expression of the tracing system because EC 3 labeling was observed only when cells in CA1 showed rabies infection. While the EC 2 input to CA2 was expected, the lack of EC layer 3 labeling was surprising given that previous reports

have documented a connection between EC3 and CA2 (Chevaleyre and Siegelbaum, 2010). This discrepancy can be explained by the fact that Chevaleyre and Siegelbaum used electrophysiological recordings to observe a connection between EC 3 and CA2. More specifically, an electrode was placed in slm to excite putative EC 3 fibers and post-synaptic responses were observed in CA2. While this is a standard technique and EC 3 axons do course through slm, this data does not exclude the possibility that axons other than those from EC 3 run through and make synapses onto the distal dendrites of CA2 neurons.

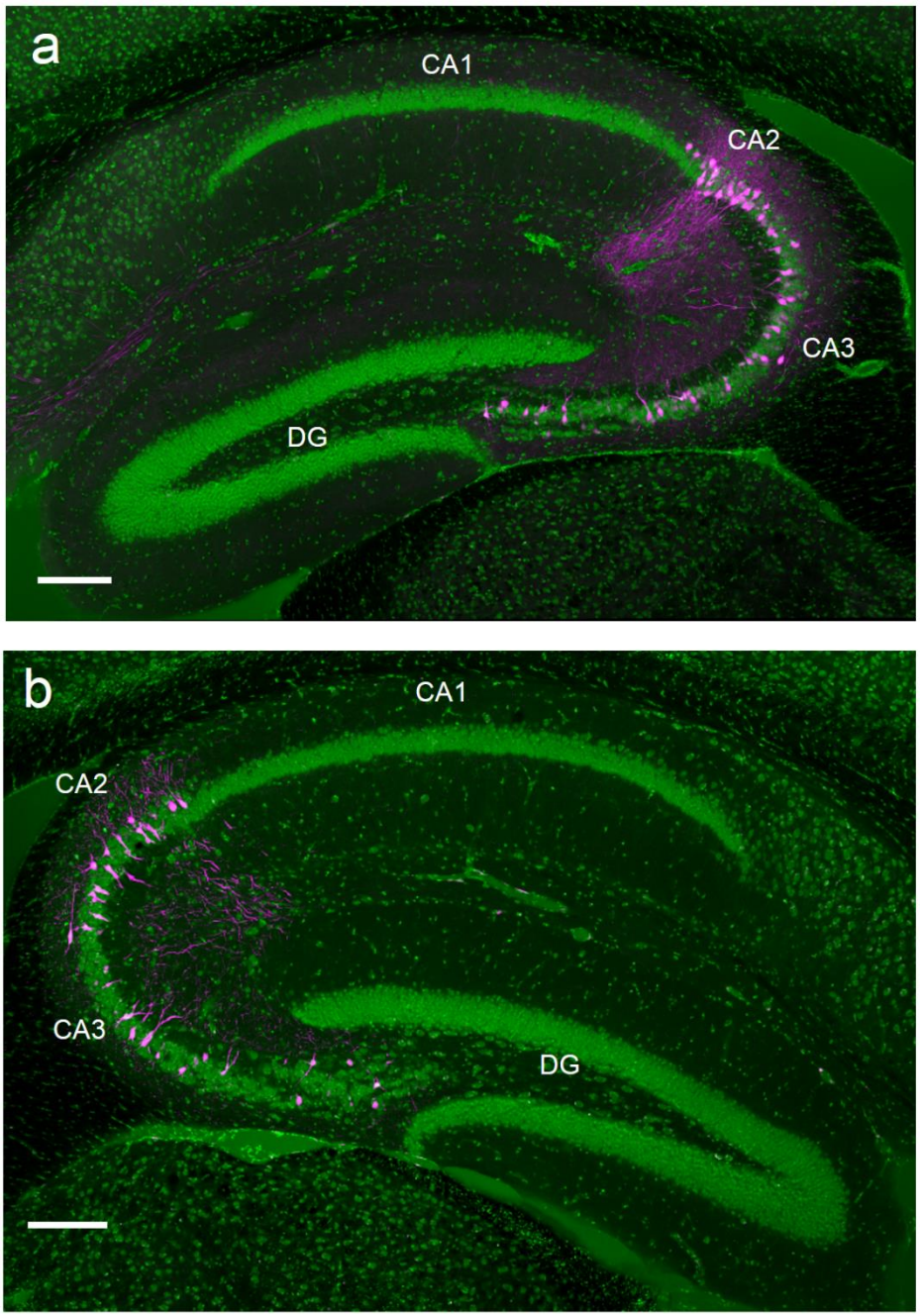

Figure 3.2: CA2 and CA3 project bilaterally to CA2. Rabies virus labeling (mCherry signal) shown in magenta. Nissl stain shown in green. **a,** Hemisphere ipsilateral to the side of virus injection. Robust mCherry signal is seen in CA2 (principally infected cells) and in CA3, which makes monosynaptic connections to CA2. **b,** mCherry was also seen in contralateral CA2 and CA3, indicating that CA2 and CA3 project bilaterally to CA2. All panels show sagittal sections. Scale bars represent 200 μm.

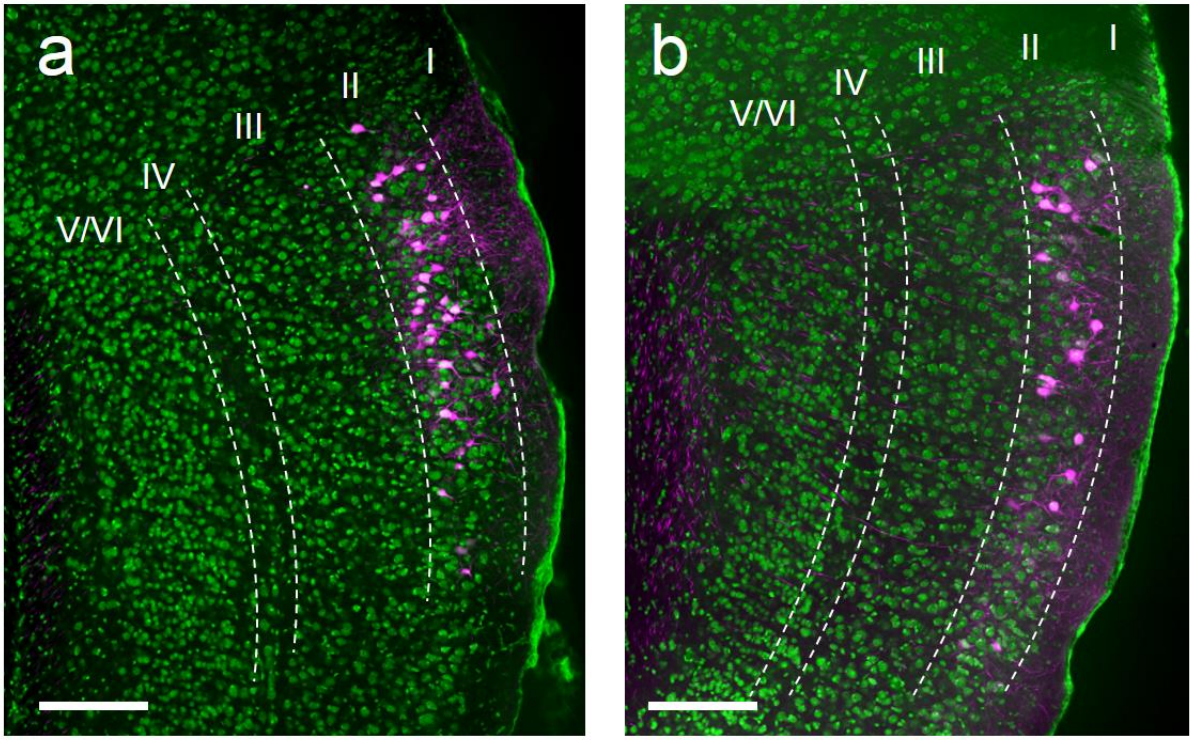

Figure 3.3: Layer 2 of medial and lateral EC project to CA2. Rabies virus labeling (mCherry signal) shown in magenta. Nissl stain shown in green. **a,** Layer 2 of lateral EC monosynaptically projects to CA2. **b,** Layer 2 of medial EC monosynaptically projects to CA2. All panels show sagittal sections. Scale bars represent 200 μm.

In addition, synaptic inputs were detected from other cortical and subcortical nuclei, including medial septum and diagonal band (Figure 3.4a), median raphe nucleus (Figure 3.4b), and the supramammillary nucleus of hypothalamus (Figure 3.4c).

To ensure that the rabies virus was pseudotyped properly with little to no contamination of unpseudotyped virus, the EnvA rabies virus was injected into the dorsal hippocampus of CA2-Cre mice that were not previously injected with the helper TVA and G adeno-associated viruses (n = 3). One week following injection, the mice were perfused and the brains were examined for mCherry expression. If the viral stock were contaminated with unpseudotyped virus, I would have observed mCherry labeling. However, I did not observe any mCherry expression (Figure 3.5) indicating that the EnvA virus was not contaminated with unpseudotyped virus.

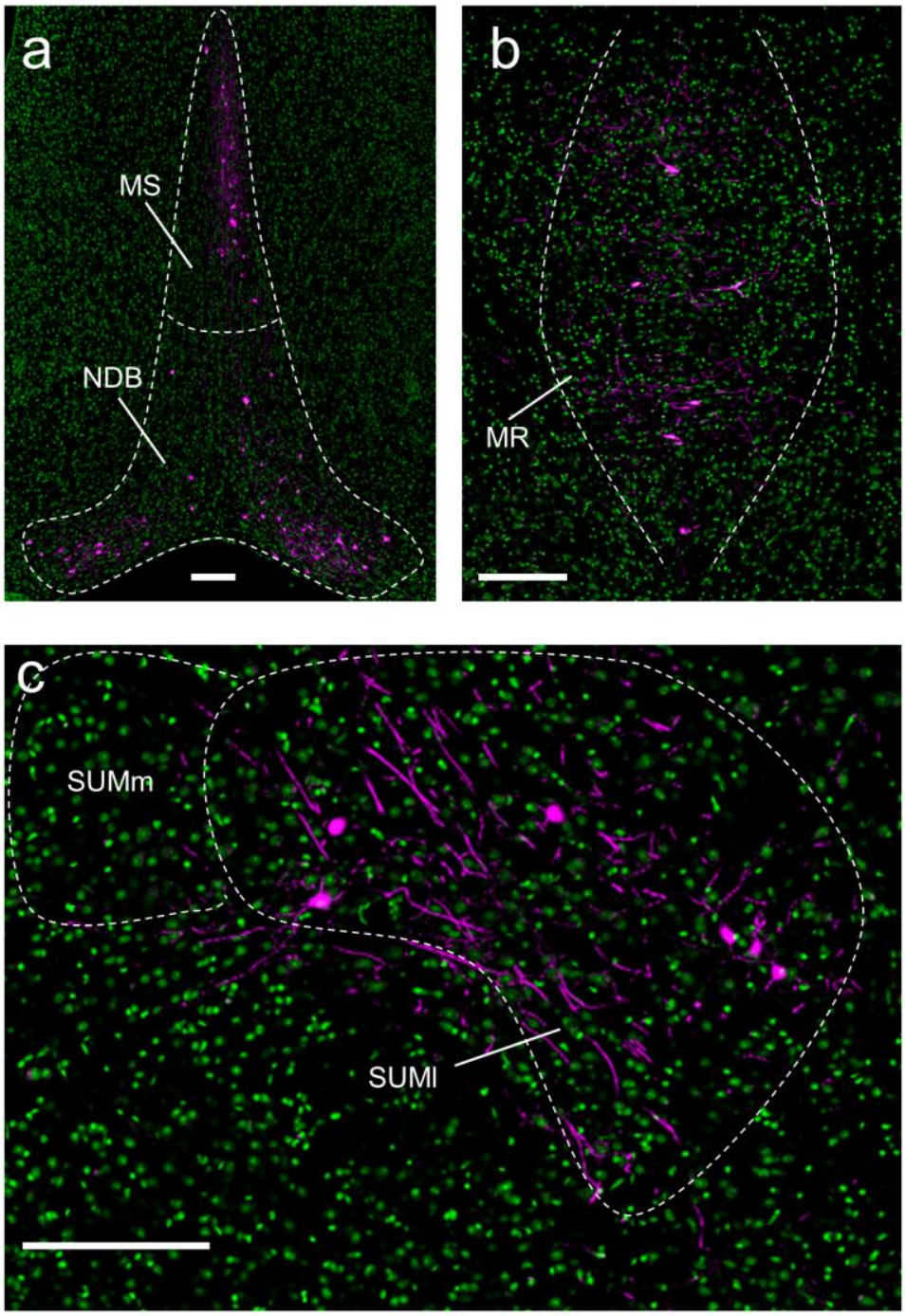

Figure 3.4: Subcortical projections to CA2. Rabies virus labeling (mCherry signal) shown in magenta. Nissl stain shown in green. **a,** The medial septum (MS) and nucleus of the diagonal band (NDB) project to CA2. **b,** The median raphe (MR) projects to CA2. **c,** The lateral supramammillary (SUMl) nucleus projects to CA2. All panels show coronal sections. Scale bars represent 200 μm.

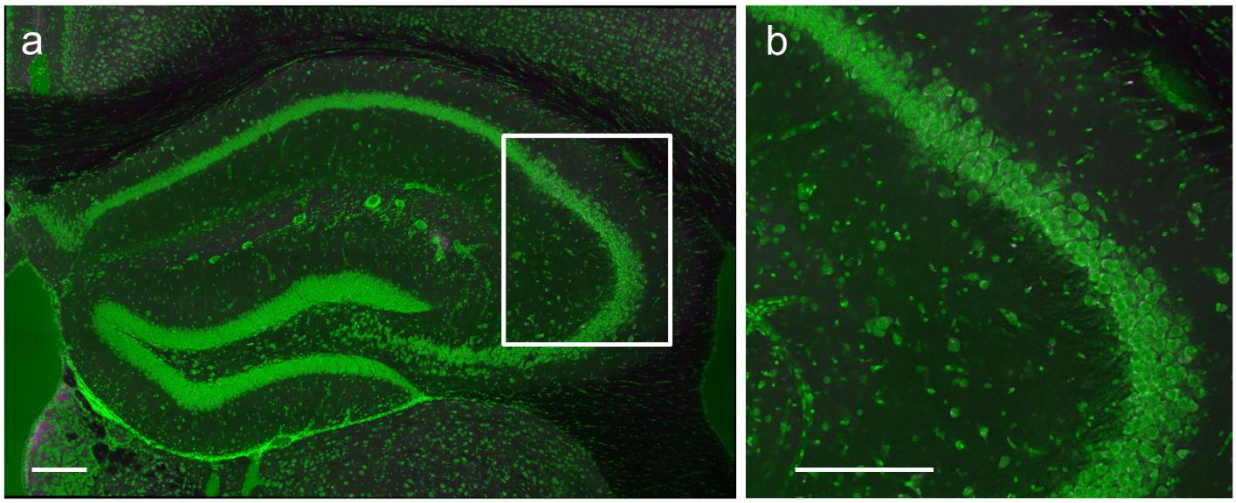

Figure 3.5: Specificity of the pseudotyped rabies virus. a, b, No labeled cells were observed (*n* = 3 mice) following injection of the (EnvA)SAD-ΔG-mCherry virus when TVA was not expressed in CA2. **b,** Magnification of boxed area in (**a**). Rabies labeling would have appeared in magenta; Nissl stain shown in green. Scale bars, 200 μm.

3.2 Outputs from CA2

Projections from CA2 to other brain areas were determined by expressing YFP in CA2 (as in Figure 2.10) and examining brains for YFP fluorescent axons. I unilaterally injected a Cre-dependent AAV (EF1α-FLEx-eYFP-WPRE-hGH polyA) to express YFP in CA2 (n = 6). Two weeks following injection, the mice were perfused, the brains were sliced, and the slices were imaged with confocal microscopy to search for YFP-positive axons. I observed strong bilateral labeling in stratum oriens (SO) and stratum radiatum (SR) of CA1, CA2, and CA3 (Figure 3.6).

I did not observe extra-hippocampal CA2 output. However, previous studies have reported CA2 output to the supramammillary nucleus (Cui et al., 2013) and to layer 2 of the entorhinal cortex (Rowland et al., 2013). Possible explanations for these discrepancies are discussed in the following section.

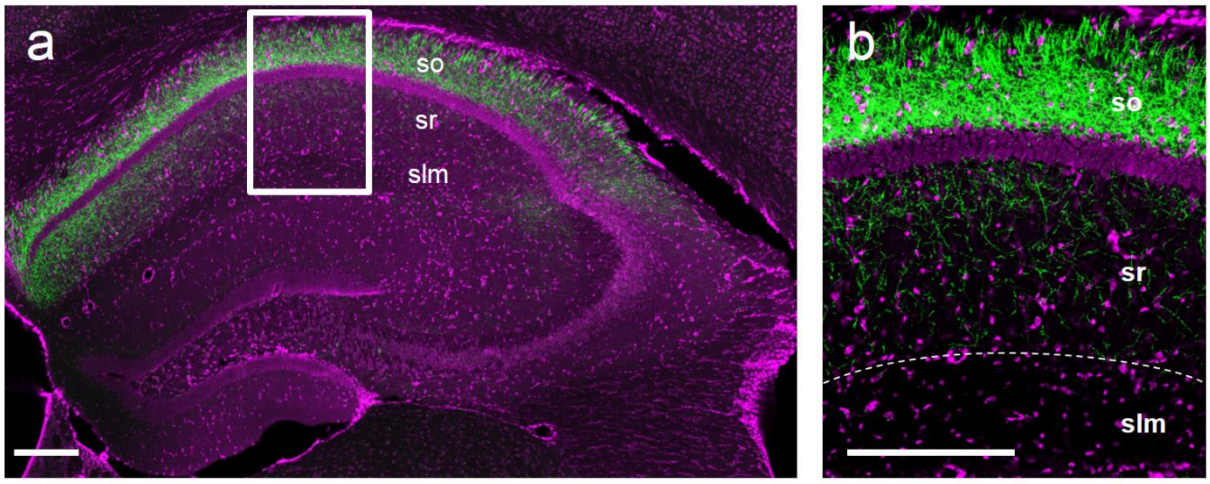

Figure 3.6: CA2 projections. Unilateral injections of Cre-dependent AAV in CA2-Cre mice were done to express YFP (shown in green) selectively in CA2. **a,** Image of the dorsal hippocampus contralateral to the injected hemisphere demonstrating YFP-positive axons in stratum oriens (so) and stratum radiatum (sr). Axons were not seen in stratum lacunosum moleculare (slm). **b,** Magnification of the area boxed in **(a)**. All panels show coronal sections. Nissl stain shown in magenta. Scale bars represent 200 μm.

3.3 Discussion

These anatomical results generally support previous findings from conventional tracing studies (Cui et al., 2013; Haglund et al., 1984; Kiss et al., 2000; Magloczky et al., 1994; Vertes 1992; Vertes et al., 1999). However, I failed to confirm vasopressinergic input to CA2 from the paraventricular nucleus of the hypothalamus (Cui et al., 2013). This is likely due to an inability of the transsynaptic rabies tracing system to label nontraditional synapses (Wall et al., 2013).

While this technique did not reveal any novel inputs to CA2, these results provide a more definitive list of monosynaptic inputs to CA2. Furthermore, the finding that CA2 receives significant input from lateral EC (Figure 3.3a), median raphe (Figure 3.4b), and lateral supramammillary nucleus (Figure 3.4c) suggests that it may be critical for certain forms of non-spatial memory (Hargreaves et al., 2005; Hensler 2006; Pan and McNaughton, 2004).

The subcortical projections to CA2 are of particular interest because these structures are largely responsible for the release of various neuromodulators. The medial septum (MS) and the nucleus of the diagonal band (NDB) release acetylcholine (Griguoli and Cherubini, 2012), which is thought to be important in attention and in pathologic states such as Alzheimer's disease (Zaborszky et al., 1999). The median raphe (MR) is predominately a serotonergic nucleus (Hensler, 2006). Serotonin is thought to signal emotional valence and motivational states and is important in disease processes such as major depression (Hensler, 2006; Meneses and Liy-Salmeron, 2012). Finally, the supramammillary nucleus (SUM) contains a large variety of cell types including dopaminergic, calretinin positive, glutamatergic, substance P positive, CCK positive, and VIP positive neurons (Pan and McNaughton, 2004). Hence, this nucleus is likely to mediate a diverse array of emotional and cognitive behaviors (Pan and McNaughton, 2004).

As indicated in section 3.2, I did not observe extra-hippocampal CA2 output. This is in contrast to previous studies that have reported CA2 output to the supramammillary nucleus (Cui et al., 2013) and to layer 2 of the entorhinal cortex (Rowland et al., 2013).

A possible explanation for my failure to observe SUM output is that Cui and colleagues did not utilize genetically targeted axon tracing (Cui et al., 2013). Hence, they labeled both inhibitory and excitatory CA2 neurons. As my approach labeled only excitatory CA2 neurons, the previously reported CA2 output to the supramammillary nucleus may be a long-range inhibitory projection. Indeed, a previous study has demonstrated projections of non-pyramidal neurons from hippocampus to the supramammillary nucleus (Ino et al., 1988).

Using genetically targeted rabies tracing, Rowland and colleagues have demonstrated output of CA2 to layer 2 of EC (Rowland et al., 2013). Like the output of CA2 to the supramammillary nucleus, the proposed output to EC may also represent a long-range inhibitory projection (Tamamaki and Nojyo, 1995). However, Rowland and colleagues reported that these neurons did not represent an inhibitory neuronal population because they were parvalbumin and GAD67 immunonegative. An alternative explanation is that the axonal YFP signal that I used to look for CA2 outputs did not reach EC. This is an unlikely explanation because the axonal YFP signal was visualized in the contralateral hippocampus following unilateral AAV injections (Figure 3.6). Alternatively, this discrepancy may be due to the ability of the rabies virus tracing system to label weak inputs to a particular brain region. Finally, this result may represent non-specific expression of the TVA receptor and/or the rabies glycoprotein in the mouse line that Rowland and colleagues used to specifically target layer 2 of EC, thus allowing for inappropriate labeling of CA2.

Chapter 4

The *in vivo* function of CA2 in learning and memory

4.1 Genetic inactivation of CA2

To study the *in vivo* relevance of CA2, I genetically inactivated this hippocampal subfield with the CA2-Cre line detailed in Chapter 1. A variety of tools have been developed to silence genetically targeted neurons. These methods include the MISTs, allatostatin receptor, halorhodopsin, tetanus neurotoxin (TeNT), and the DREADDs (Luo et al., 2008; Ferguson et al., 2011). Halorhodopsin is ideal for tight temporal control, because it is a light activated Cl^- pump that can be rapidly turned on and off. This technique, however, requires additional equipment and high expression of the pump. Furthermore, the volume of tissue silenced is limited by the spread of the light. This method would not be ideal for the current study because even though CA2 is a small region in the medial-lateral axis, it spans a great distance in the rostral-caudal direction. The light spread would not cover all of CA2, and a potential phenotype could possibly go undetected. The MISTs, allatostatin receptor system, and the DREADDs provide a means of silencing neurons via injection of a drug/ligand. Thus, all of these systems provide for inducible silencing of neurons on a timescale slower than that of halorhodopsin, but without the equipment setup complications. The allatostatin receptor and the DREADDs do not mediate silencing directly; they do so by activating GIRK channels. Unfortunately, this makes the silencing dependent on GIRK channel expression. Additionally, allatostatin and the MIST "dimerizers" must be administered intracranially (Karpova et al., 2005; Luo et al., 2008).

I chose to silence CA2 neurons using a Cre-dependent AAV viral vector that I have synthesized that expresses TeNT (Ef1α-FLEx-eGFP-TeNT-WPRE-hGH polyA). To avoid

developmental effects of CA2 silencing, the vector was injected intracranially in adult mice. TeNT is a metalloprotease that cleaves vesicle-associated membrane protein 2 (VAMP2), a critical component of the exocytotic machinery (Tonello et al., 1999; Yamamoto et al., 2003). Hence, injection of this virus into the hippocampus of CA2-Cre mice would result in abolition of CA2 output.

To confirm that injection of this virus into the hippocampi of CA2-Cre mice would result in inactivation of CA2 output, I co-expressed the light-activated cation channel channelrhodopsin-2 (ChR2) (Boyden et al., 2005; Sohal et al., 2009) with either TeNT or YFP by injection of two independent AAVs and recorded electrophysiological activity of CA1 and CA2 neurons in response to light stimulation of CA2 in acute hippocampal brain slices. Low intensity illumination (using 2-ms pulses of 470 nm light at 3 $mW \cdot mm^{-2}$) focused on CA2 in hippocampal slices expressing ChR2 reliably triggered action potentials in CA2 PNs, as seen by the presence of large action currents in cell-attached patch recordings (Figure 4.1). Spiking was similarly elicited in neurons that co-expressed either YFP (Figure 4.1b, $n = 6$) or TeNT (Figure 4.1c, $n = 4$) with ChR2, indicating that the TeNT did not inhibit the excitability of CA2 neurons.

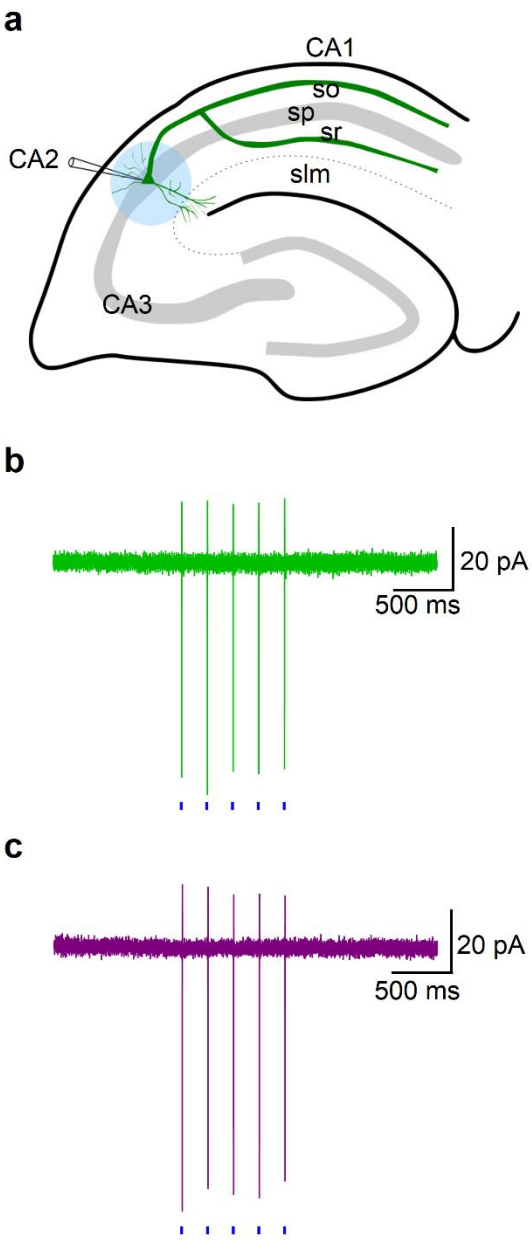

Figure 4.1: Optogenetic stimulation of CA2. a, Experimental setup. Cell-attached voltage clamp recordings were made from CA2 neurons that expressed ChR2 with either YFP or TeNT. The CA2 neuron and its axons coursing through stratum oriens (so) and stratum radiatum (sr) is depicted in green. **b,** Cell-attached recording of CA2 neuron expressing ChR2 and YFP demonstrating action currents in response to 2 ms blue light (470 nm) stimulation (blue bars underneath trace). **c,** Light-induced action currents were also observed in CA2 neurons expressing ChR2 and TeNT.

Next, I examined the strength of synaptic transmission from CA2 to CA1 pyramidal neurons and the efficacy of TeNT silencing. Whole-cell current-clamp recordings were used to measure light-evoked postsynaptic potentials (PSPs) in CA1 pyramidal neurons in hippocampal slices in which CA2 neurons co-expressed ChR2 with either YFP or TeNT (Figure 4.2). In agreement with our anatomical mapping (Chapter 3) and previous paired recordings (Chevaleyre and Siegelbaum, 2010) focal photostimulation delivered to the SO and SR regions of CA1 in slices expressing ChR2 and YFP (n = 14) evoked robust EPSPs in nearby CA1 PNs (Figure 4.2b). Increasing the light power recruited progressively larger PSPs, presumably due to an increase in the number of optically activated CA2 axons (Figure 4.2b, c). In stark contrast, in slices in which TeNT was co-expressed with ChR2 in CA2 (n = 14), illumination over a wide range of intensities produced little or no synaptic response in CA1 neurons (Figure 4.2b, c), demonstrating the efficacy of the genetic lesion.

The aforementioned experiments were performed without the addition of any pharmacological agents in the either the patch pipette or the bath of the slice. Hence, the recorded PSPs represent the sum of excitation from CA2 to CA1 and feed-forward inhibition of CA1 recruited by CA2. To assess the strength of the inhibition recruited by CA2, this experiment could be repeated with the $GABA_A$ and $GABA_B$ antagonists picrotoxin and CGP 55845A. With inhibitory transmission blocked, pulses of blue light would result in excitatory PSPs (EPSPs) in CA1. With the EPSPs isolated, the inhibitory PSPs (IPSPs) could be inferred by subtracting the net PSP (e.g. Figure 4.2b) from the isolated EPSP.

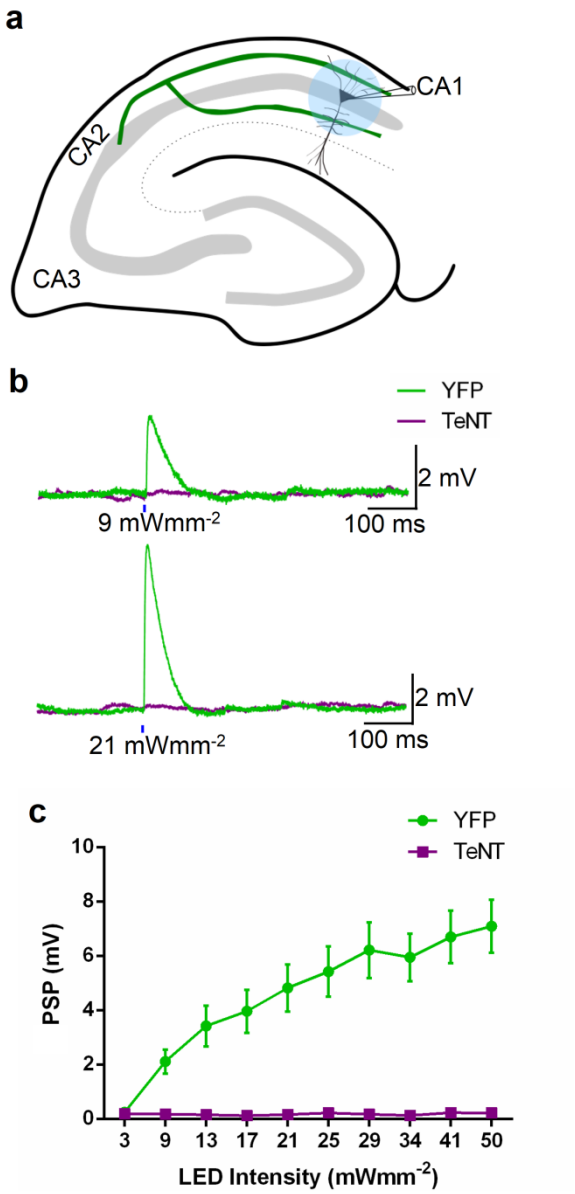

Figure 4.2: Electrophysiological confirmation of genetic CA2-inactivation. a, Experimental setup. Whole-cell current-clamp recordings were made in CA1 neurons (shown in black). CA2 axons that expressed ChR2 are shown in green. **b,** Light evoked (blue bars underneath traces) PSPs were observed in CA1 neurons when ChR2 was co-expressed with YFP (green traces). PSPs were not seen in CA1 when ChR2 was co-expressed with TeNT in CA2 (magenta traces). **c,** Larger PSPs were measured in CA1 with increasing light intensities when ChR2 was expressed with YFP in CA2. When TeNT was co-expressed with ChR2 in CA2, increasing the light intensity did not uncover PSPs in CA1, indicating the efficacy of the TeNT-based inactivation of CA2. Data are presented as mean ± s.e.m.

4.2 A number of behaviors are unaltered by CA2-inactivation

What are the behavioral consequences of inactivation of CA2? To address this question, I examined the behavior of control (YFP expressed in CA2, CA2-YFP) and CA2-inactivated (TeNT expressed in CA2, CA2-TeNT) CA2-Cre littermate mice in a number of tasks.

a. Locomotor activity and anxiety-like behavior. Functional inactivation of dorsal CA2 did not alter locomotor activity as assayed by the open field test (Figure 4.3). Furthermore, inactivation of CA2 did not alter anxiety-like behavior as assayed by the elevated plus maze test (Figure 4.4).

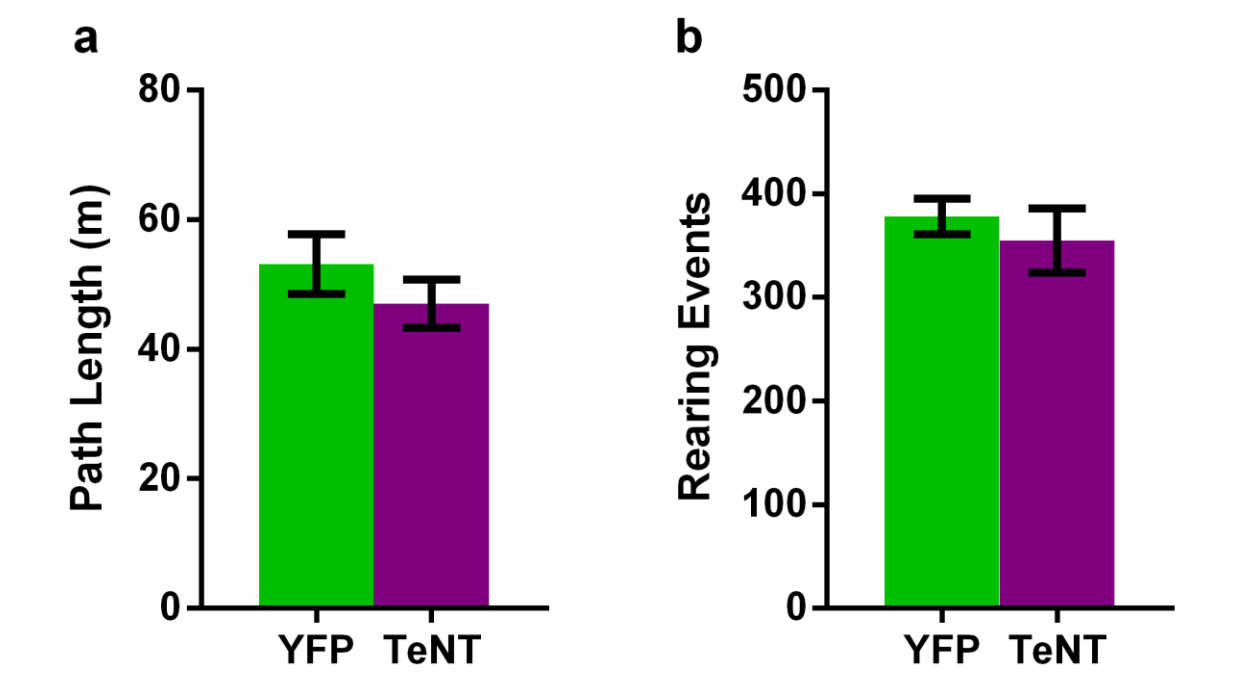

Figure 4.3: CA2-inactivation does not alter locomotor activity. Locomotor activity was assayed by the open field test. Briefly, mice were placed in an open plastic arena and distance traveled (path length) and rearing events (number of times a mouse stood upright on its hind paws) were measured. **a,** Path length (YFP, 53.14 ± 4.62m, *n* = 8; TeNT, 47.04 ± 3.70m, *n* = 10) was no different in CA2-inactivated mice compared to control mice (P = 0.31, two-tailed unpaired t-test). **b,** Number of rearing events (YFP, 378.0 ± 17.36, *n* = 8; TeNT, 354.7 ± 30.99, *n* = 10) was no different in CA2-inactivated mice compared to control mice (P = 0.55, two-tailed unpaired t-test). Results are presented as mean ± s.e.m.

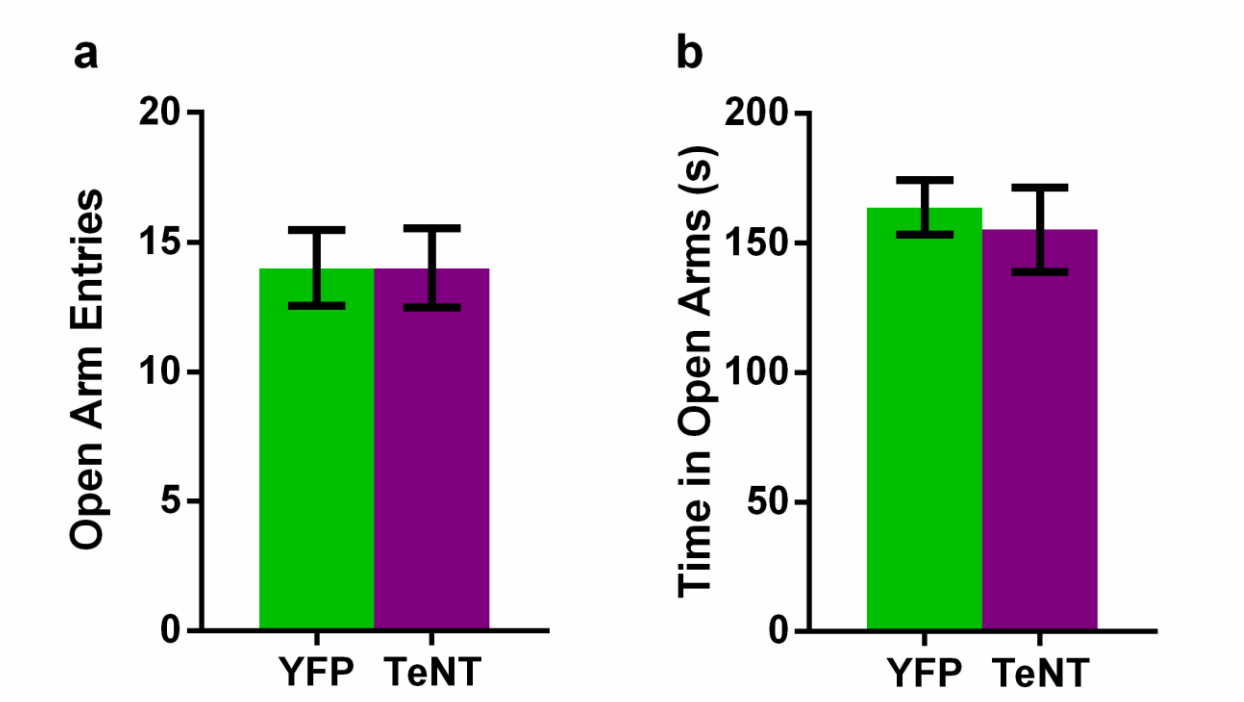

Figure 4.4: CA2-inactivation does not alter anxiety-like behavior. Anxiety-like activity was assayed by the elevated plus maze test. Briefly, mice were placed in the center of an elevated maze built in a plus shape with 4 arms. Two arms were closed (high walls) and two arms were open (no walls). **a,** The number of open arm entries was not significantly different ($P > 0.99$, two-tailed unpaired t-test) between the groups (YFP, 14.00 ± 1.46, $n = 8$; TeNT, 14.00 ± 1.54, $n = 10$). **b,** The time spent in the open arms (YFP, 163.7 ± 10.43s, $n = 8$; TeNT, 155.1 ± 16.38s, $n = 10$) did not differ significantly ($P = 0.68$, two-tailed unpaired t-test) between the groups. Results are presented as mean ± s.e.m.

b. Spatial memory. The above results showing that loss of CA2 does alter performance in the open field or elevated plus maze are not surprising because previous studies have demonstrated that lesions of the entire dorsal hippocampus do not result in alterations in locomotor activity as assayed by the open field test (Markowska and Lukaszewska, 1981) or anxiety-like behavior as assayed by the elevated plus maze test (McHugh et al., 2004). In contrast, the dorsal hippocampus has been shown to be essential for spatial memory as assayed by the Morris water maze task (Morris et al., 1982; Squire 1992). Hence, I next assessed the performance of CA2-inactivated mice in the Morris water maze task.

The experimental protocol I used is outlined in Figure 4.5a. Water is innately aversive to mice; hence when placed in a water tank (maze), mice will attempt to find an escape from the tank. First, I trained the mice to find a platform that was marked with a flag to render it visible (Days 1-2). This phase of the task does not require the hippocampus and was done to ensure that no deficits in swim speed or vision were present in the CA2-inactivated group. Then, the flag was removed to hide the platform, which was located 1 cm below the surface of water opacified with white paint. The mice were then trained to find this platform over the course of 5 days (days 3-7). On day 8, the platform was removed to conduct a probe trial to assay spatial memory. An increase in the amount of time spent in the target quadrant (where the platform was previously located) indicated intact spatial memory. Then, the platform was moved to the opposite quadrant for reversal training, a test of cognitive flexibility. Learning during training was assayed by measuring the distance the mouse traveled before reaching the platform (path length, Figure 4.5b) and latency to find the platform (Figure 4.5c). Spatial memory assayed during the probe trials was assessed as percent time spent in each quadrant of the water maze (Figure 4.6).

As the mice learned the task, both path length to the platform and latency to find the platform decreased (Figure 4.5b, c). Both groups learned the task as evidenced by the decrement in these measurements during the cued learning (days 1-2) and hidden platform learning (days 3-7 and days 9-13) periods. While not significant, there was a slight trend for slower learning in the CA2-inactivated group (on day 4), which was more pronounced during reversal training (day 10). This may indicate a slight deficit in cognitive flexibility in the CA2-TeNT group. However, the two groups performed similarly in the probe trials on days 8 and 14 (Figure 4.6). Both groups showed a preference for the quadrant in which the platform was located in during training. These probe trial results indicate that spatial memory was intact in the CA2- inactivated group.

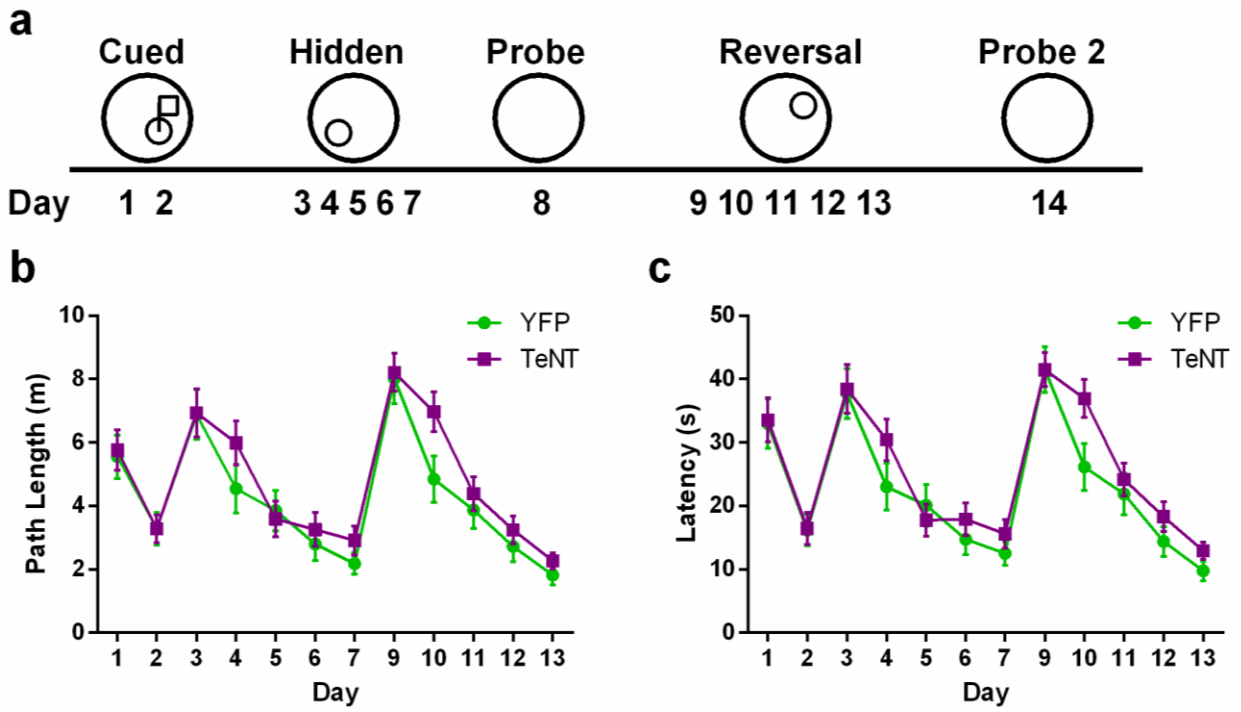

Figure 4.5: CA2-inactivation does not alter Morris water maze performance. a, Schema of the experimental design. On days 1 and 2, mice were trained to find a platform with a visible flag. On days 3-7, mice were trained to find a hidden platform located in the SW quadrant of the water maze. Spatial memory was assayed on day 8 with the platform removed. Reversal training was conducted on days 9-13 with the platform now hidden in the NW quadrant. Spatial memory of the novel location was tested on day 14. **b,** Path length to the platform was not altered by CA2-inactivation (two-way repeated measures ANOVA: Treatment x Time $F(11,770) = 0.67$, $P = 0.77$; Time $F(11,770) = 21.87$, $P < 0.0001$; Treatment $F(1,70) = 2.85$, $P = 0.10$). **c,** Latency to find the platform did not differ between the two groups (two-way repeated measures ANOVA: Treatment x Time $F(11,770) = 0.78$, $P = 0.66$; Time $F(11,770) = 25.23$, $P < 0.0001$; Treatment $F(1,70) = 2.84$, $P = 0.10$). YFP, $n = 8$; TeNT, $n = 10$. Results are presented as mean ± s.e.m.

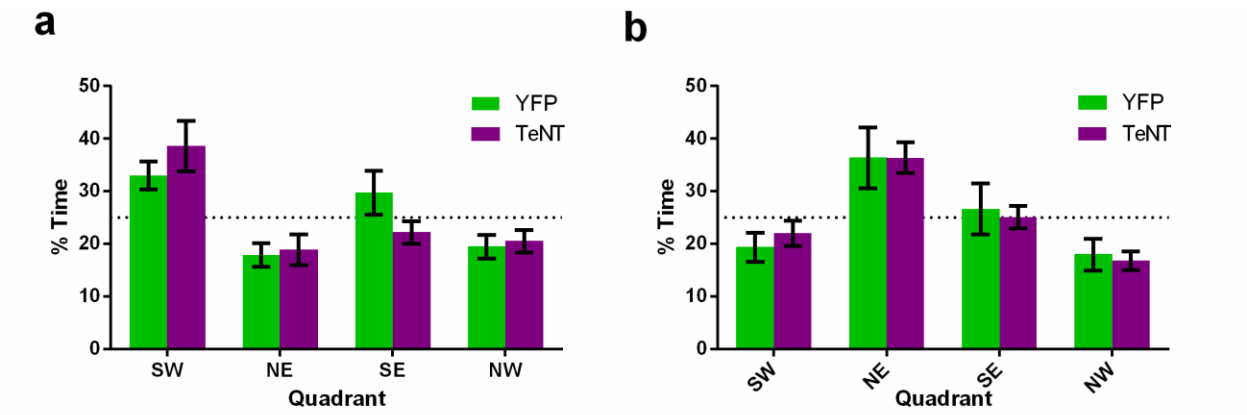

Figure 4.6: CA2-inactivation does not impair spatial memory. a, Spatial memory during the probe trial was unaffected by CA2-inactivation. The percent of time spent in the target quadrant (YFP, 33.00 ± 2.66%; TeNT, 38.6 ± 4.79%) was not significantly different between the two groups (P = 0.36, two-tailed unpaired t-test). **b,** Spatial memory following reversal training was unaffected by CA2-inactivation. There was no significant difference between the groups in percent time spent in the target quadrant during the probe trial following reversal training (YFP, 36.38 ± 5.75%; TeNT, 36.40 ± 2.92%; P > 0.99, two-tailed unpaired t-test). YFP, *n* = 8; TeNT, *n* = 10. Results are presented as mean ± s.e.m.

c. Contextual memory. In addition to spatial memory, the hippocampus has also been shown to be critically involved in contextual memory, most commonly assayed by the contextual fearing conditioning paradigm (Gewirtz et al., 2000; Squire 1992). I used a delay fear conditioning protocol to assay both hippocampal-dependent contextual fear memory and amygdala-dependent auditory fear memory in CA2-inactivated (CA2-TeNT) and control (CA2-YFP) mice. The experimental design of this 3-day test is outlined in Figure 4.7a. On day 1, mice were placed in context A, which consisted of 3 plexiglass walls, 1 opaque wall with black and white stripes, and a steel grid floor. 1% acetic acid was placed as the dominant odor, and the house fan was turned on. After 150s in the chamber, a tone (30s, 2.8 kHz, 85 dB) was played and co-terminated with a shock (2s, 0.7 mA). Mice were removed from the chamber 30s after the shock. Hence, on day 1 mice were trained to associate both context A (conditioned stimulus, CS) and the tone (CS) with the aversive unconditioned stimulus (US), the shock. On day 2, contextual fear memory was assayed by placing the mice back in context A for 300s. On day 3, the mice were brought to the testing room that was now dimly illuminated with red light. The mice were placed in context B, which was outfitted very differently from context A. Context B consisted of an enclosure with 3 solid gray colored walls, 1 plexiglass wall with a circular door, and a red, flat plastic roof. The floor of the enclosure was a white piece of plastic, 0.25% benzaldehyde was the dominant odor. After 180s in context B, the tone from day 1 was sounded for 60s. Percent time spent freezing (defined as the absence of all movement except for respiration) was measured throughout these experiments and served as an index of fear memory. Mice exhibiting fear memory will demonstrate an increase in freezing after training on day 1. Both groups exhibited low levels of freezing on day 1, indicating that the mice were not inappropriately fearful of the context before training (Figure 4.7b, c). On day 2 both the CA2-

inactivated and control groups exhibited a similar level of increased freezing in response to context A after training, with no statistically significant difference (see Fig 4.7). On day 3, both groups demonstrated similarly low levels of freezing to context B, indicating that the fear memory was not inappropriately generalized. In contrast, similar levels of robust freezing were observed in both groups during the presentation of the tone on day 3 indicating intact auditory fear memory (Figure 4.7b, c).

These results indicate that CA2 is not essential for the expression of hippocampal-dependent contextual fear memory. In contrast, a robust deficit in contextual fear memory was observed when CA3-inactivated mice were tested using the same delay conditioning protocol I employed (Nakashiba et al., 2008). Together, these results support the hypothesis that the parallel tri-synaptic and di-synaptic pathways mediate and support different forms of learning and memory. It is important to note that CA2 may be partly involved in contextual fear memory or spatial memory as tested by the MWM, and that the functional CA3 region in these mice fully compensated for the loss of CA2 activity.

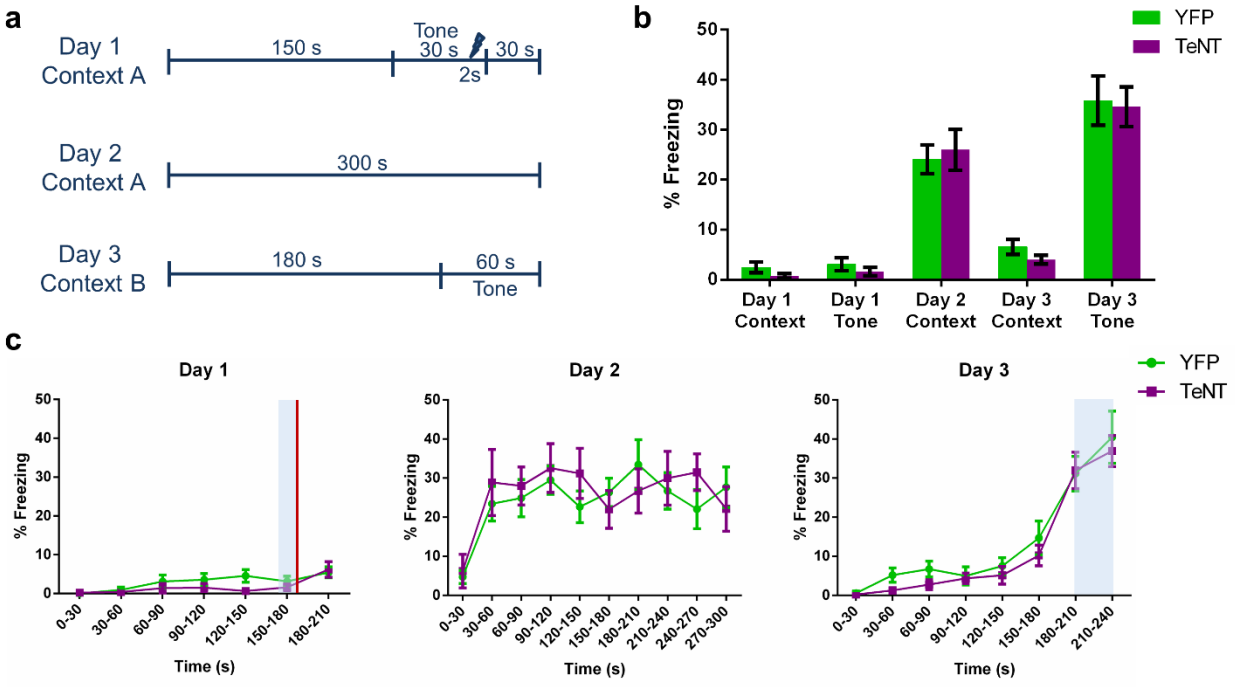

Figure 4.7: CA2-inactivation does not impair contextual or auditory fear memory. a, Schema of the experimental design. Delay fear conditioning was employed to test hippocampal-dependent contextual fear memory and amygdala-dependent auditory fear memory. **b,** There was no significant difference in percent freezing between the groups (two-way repeated measures ANOVA: Treatment x Day $F(4,68) = 0.31$, $P = 0.87$; Treatment $F(1,17) = 0.13$, $P = 0.73$; Day $F(4,68) = 100.8$, $P < 0.0001$; YFP, $n = 11$; TeNT, $n = 8$). Prior to training on day 1, neither group exhibited a fear response to context A (YFP, 2.45 ± 1.06%; TeNT, 0.75 ± 0.49%) or to the tone (YFP, 3.09 ± 1.31%; TeNT, 1.63 ± 0.84%). On day 2 after training, robust fear responses to context A were measured in both groups (YFP, 24.09 ± 2.88%; TeNT, 26.00 ± 4.10%). Both groups exhibited low levels of freezing on day 3 in novel context B (YFP, 6.55 ± 1.52%; TeNT, 4.00 ± 0.87%) demonstrating context specificity of the fear memory and a lack of fear generalization. Both groups exhibited robust freezing to the tone on day 3 (YFP, 35.82 ± 4.93%; TeNT, 34.63 ± 3.96%), demonstrating intact auditory fear memory. **c,** Freezing data plotted in 30s bins. Shaded areas represent tone presentation. Red line represents shock delivery. Left, two-way repeated measures ANOVA revealed no significant difference between groups in freezing on day 1 (Treatment x Time $F(6,102) = 1.135$, $P = 0.3474$; Treatment $F(1,17) = 1.116$, $P = 0.3056$; Time $F(6,102) = 6.348$, $P < 0.0001$). Middle, two-way repeated measures ANOVA

revealed no significant difference between groups in freezing on day 2 (Treatment x Time $F(9,153) = 0.9741$, $P = 0.4637$; Treatment $F(1,17) = 0.1326$, $P = 0.7203$; Time $F(9,153) = 6.335$, $P < 0.0001$). Right, two-way repeated measures ANOVA revealed no significant difference between groups in freezing on day 3 (Treatment x Time $F(7,119) = 0.2490$, $P = 0.9716$; Treatment $F(1,17) = 0.6517$, $P = 0.4307$; Time $F(7,119) = 50.87$, $P < 0.0001$). Results are presented as mean ± s.e.m.

d. Novel object recognition. Mice possess innate curiosity and when presented with two objects, one that they've previously encountered and a novel object, they will spend more time interacting with and exploring the novel object (Bevins and Besheer 2006). This behavior requires innate preference for novelty and intact object recognition memory. The hippocampal-dependence of object recognition memory is controversial with studies both supporting (Cohen et al., 2013) and refuting (Winters et al., 2004) its importance. To assess whether or not CA2 was necessary for object recognition memory, I subjected CA2-TeNT and CA2-YFP mice to two novel object tasks (Figures 4.8, 4.9). The protocol employed for the first test is outlined in Figure 4.8a. Briefly, mice were placed into an arena with 2 different objects and were habituated to the objects and the arena over the course of four 5-minute trials. After a 1 hour inter-trial interval (ITI), the mice were presented with a novel object and one of the previously encountered objects. Time spent investigating the object (snout within 2 cm of the object) was measured throughout all trials by an overhead camera and tracking software. The second variation of the novel object task is outlined in Figure 4.9a. In this version, the mice were habituated to the empty arena for 3 days. On the fourth day, the mice were presented with two identical objects. After one hour, the old object and a novel object were presented together. The CA2-inactivated and control mice exhibited a similar extent of preference for the novel object (Figures 4.8 and 4.9). This indicates that CA2-inactivation does not impair object recognition memory, nor does it abolish preference for novelty.

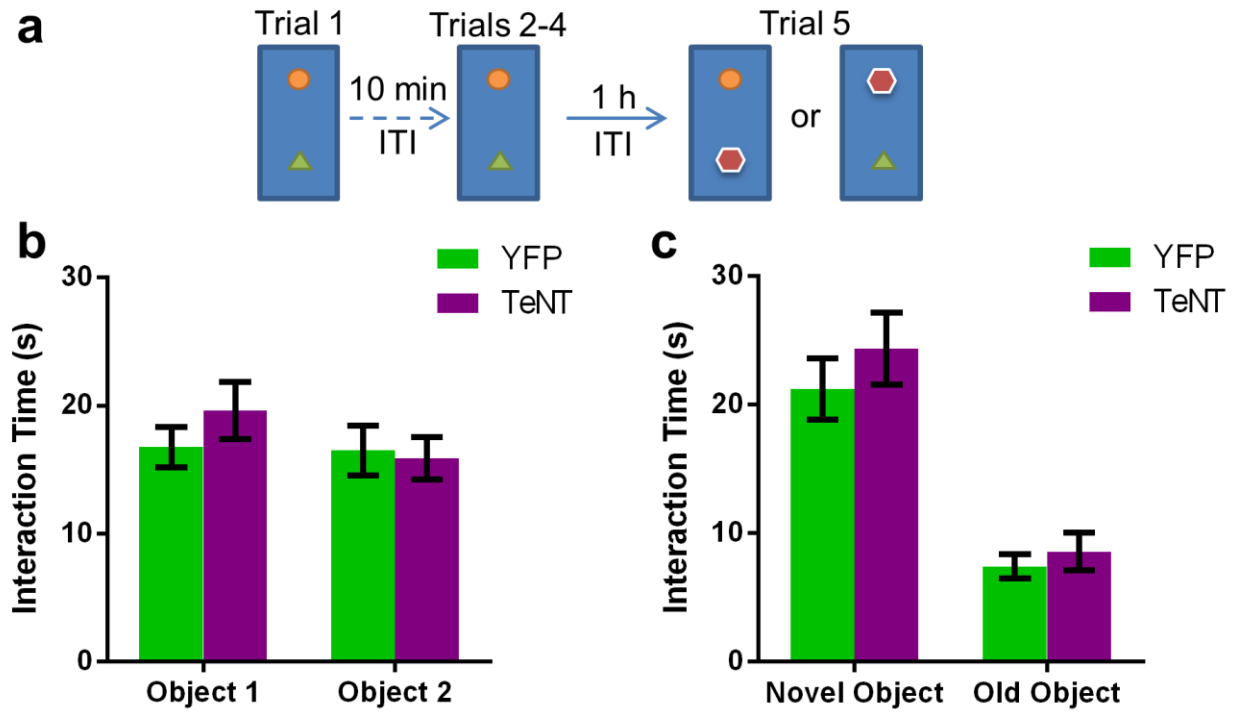

Figure 4.8: CA2-inactivation does not impair object recognition memory. a, Schema of the experimental design for the novel object recognition task. **b,** The groups did not differ significantly in exploration of object 1 (YFP, 16.75 ± 1.57s; TeNT, 19.60 ± 2.24s) or object 2 (YFP, 16.50 ± 1.97s; TeNT, 15.90 ± 1.66s) averaged over the course of the first 4 trials (two-way ANOVA: Treatment x Object $F(1,32) = 0.80$, $P = 0.38$; Object $F(1,32) = 1.05$, $P = 0.31$; Treatment $F(1,32) = 0.34$, $P = 0.56$; YFP, $n = 8$; TeNT, $n = 10$). **c,** Both groups explored the novel object (YFP, 21.23 ± 2.37s; TeNT, 24.37 ± 2.81s) more than the familiar object (YFP, 7.41 ± 0.92s; TeNT, 8.57 ± 1.48s). Statistical analysis revealed a significant effect of object, but not CA2 inactivation or interaction of the two (two-way ANOVA: Treatment x Object $F(1,28) = 0.22$, $P = 0.64$; Object $F(1,28) = 48.46$, $P < 0.0001$; Treatment $F(1,28) = 1.02$, $P = 0.32$). Multiple comparison testing revealed a significant difference between exploration of the novel object compared to exploration of the old object for both the YFP group ($P = 0.0002$) and the TeNT group ($P < 0.0001$). Results are presented as mean ± s.e.m.

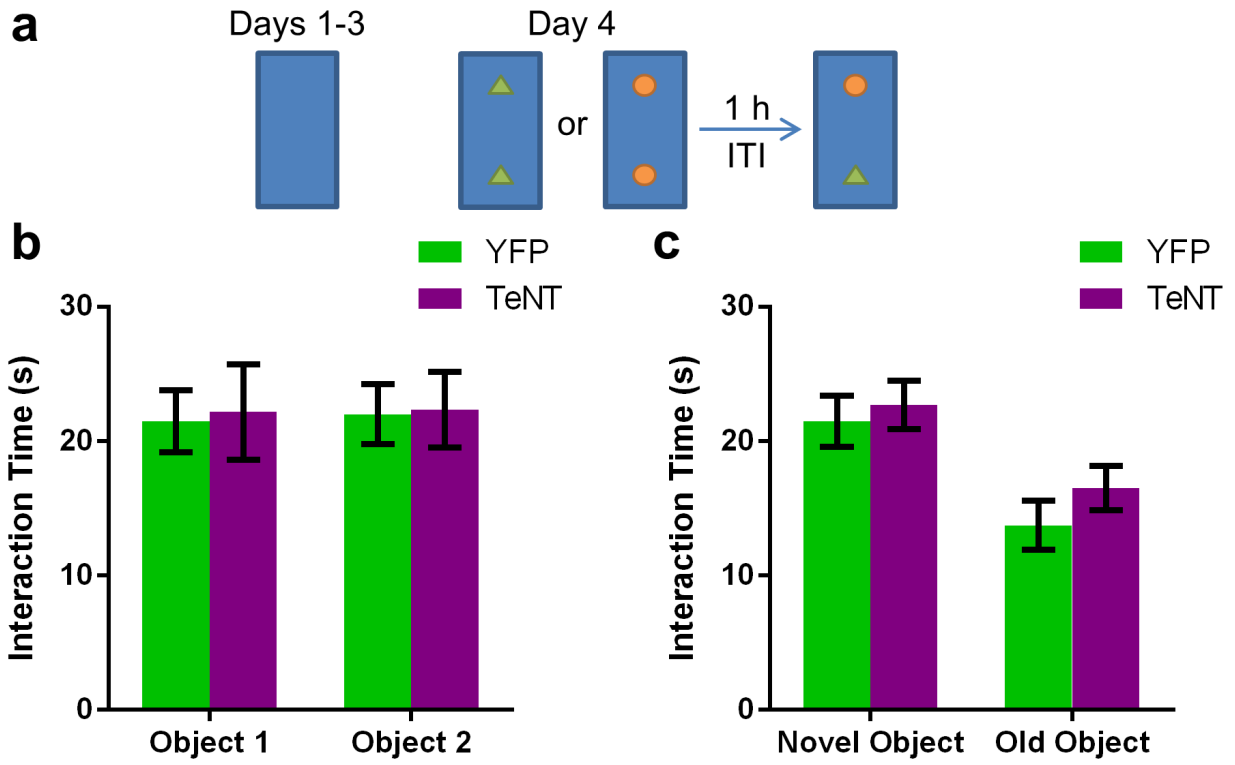

Figure 4.9: Confirmation that CA2-inactivation does not impair object recognition memory. a, Schema of the experimental design for another variation of the novel object recognition task. **b,** The groups did not differ significantly in time spent exploring object 1 (YFP, 21.50 ± 2.31s; TeNT, 22.18 ± 3.57s) or object 2 (YFP, 22.02 ± 2.23s; TeNT, 22.36 ± 2.81s) during trial 1 of day 4 (two-way ANOVA: Treatment x Object $F(1,44) = 0.004$, $P = 0.95$; Object $F(1,44) = 0.02$, $P = 0.90$; Treatment $F(1,44) = 0.03$, $P = 0.85$; YFP, $n = 12$; TeNT, $n = 12$). **c,** Both groups explored the novel object (YFP, 21.49 ± 1.91s; TeNT, 22.73 ± 1.82s) more than the familiar object (YFP, 13.74 ± 1.83s; TeNT, 16.53 ± 1.64s). Statistical analysis revealed a significant effect of object, but not CA2 inactivation or interaction of the two (two-way ANOVA: Treatment x Object $F(1,44) = 0.18$, $P = 0.67$; Object $F(1,44) = 15.02$, $P = 0.0004$; Treatment $F(1,44) = 1.25$, $P = 0.27$). Multiple comparison testing revealed a significant difference between exploration of the novel object compared to exploration of the old object for both the YFP group ($P = 0.008$) and the TeNT group ($P = 0.02$). Results are presented as mean ± s.e.m.

e. Olfaction. Mice rely on their incredible sense of smell for many behaviors, including normal social interaction (Brennan and Zufall, 2006). Most previous studies suggest that the hippocampus is not necessary for recognition or discrimination of odors (Dudchenko et al., 2000; DeVito and Eichenbaum, 2011). Because my experiments involved selective manipulation of a subregion of the hippocampus, I did not expect the mice to exhibit any deficits in odor detection. However, to ensure that any deficits observed in CA2-inactivated mice were not caused by olfactory impairment, I first conducted a test in which mice had to detect the presence of food buried under a deep layer of cage bedding by its odor alone. The CA2-TeNT mice performed the task as well as CA2-YFP mice (Figure 4.10a), indicating intact olfaction. To further probe the effects of CA2-inactivation on olfactory discrimination, including discrimination between social odors, I ran the olfactory habituation/dishabituation test (Figure 4.10b). In this test both non-social (almond and banana) and social odors are presented for three successive trials. Habituation is defined as the decrease in olfactory investigation upon repeated presentation of an odor, and dishabituation is defined as increased olfactory investigation upon presentation of a novel odor. Both the CA2-YFP and CA2-TeNT groups demonstrated normal habituation and dishabituation to both the non-social and social odors presented (Figure 4.10b). Hence, CA2-inactivation did not impair olfactory discrimination of non-social or social odors.

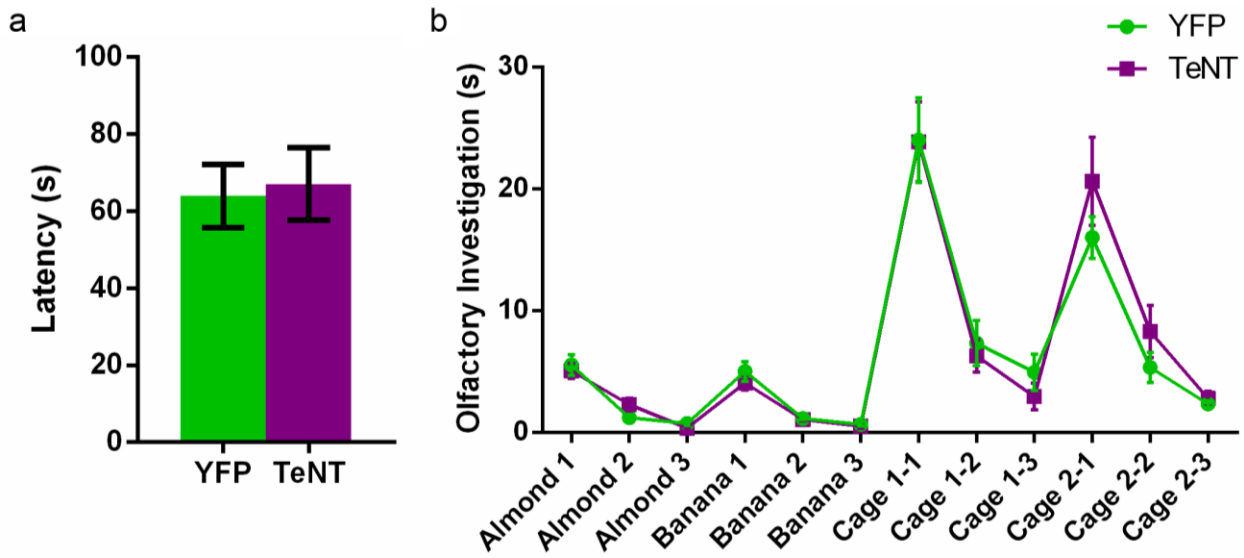

Figure 4.10: CA2-inactivation does not impair olfaction. a, There was no significant difference between the groups in latency to find a buried food pellet (YFP, 63.93 ± 8.22s, *n* = 15; TeNT, 67.06 ± 9.42s *n* = 16; P = 0.81, two-tailed unpaired t-test). Results are presented as mean ± s.e.m. **b,** Both groups (YFP, *n* = 15; TeNT, *n* = 14) demonstrated habituation (decreased olfactory investigation) to the repeated presentation of both non-social (almond and banana) and social odors. Additionally, both control and CA2-inactivated groups demonstrated dishabituation (increased olfactory investigation) upon the presentation of a novel non-social or social odor.

4.3 CA2-inactivation abolishes social memory

In the previous section, I detailed the many behaviors unaltered by CA2-inactivation. The anatomical findings presented in Chapter 3 suggested that CA2 may be involved in other non-spatial hippocampal processes. Namely, the finding that CA2 pyramidal neurons integrate synaptic input from lateral EC, which conveys non-spatial information (Hargreaves et al., 2005), with subcortical input from both the hypothalamic supramammillary nucleus (Pan and McNaughton, 2004) and the serotonergic median raphe nucleus (Hensler, 2006) suggested a role for this region in non-spatial hippocampal tasks that involve emotional components.

Furthermore, previous studies have shown that the vasopressin 1b receptor (AVPR1b) mRNA is strongly expressed in CA2 (Young et al., 2006) and that unconditional deletion of this gene results in a deficit in social recognition memory (Wersinger et al., 2002; DeVito et al., 2009). This has led to the suggestion that CA2 is important for social recognition and social memory (Young et al., 2006). However, AVPR1b mRNA is expressed in many areas of the brain outside the hippocampus (Young et al., 2006) and its deletion results in changes in a number of non-hippocampal dependent behaviors, including reduced aggression and decreased sociability (Wersinger et al., 2002; DeVito et al., 2009). Such findings raise questions as to the selective role of CA2 in the behavioral changes seen in the AVPR1b knockout mice (Stevenson and Caldwell, 2012).

To assess directly the role of CA2 in social behavior, I first compared the performance of CA2-YFP versus CA2-TeNT mice in a three-chamber test of sociability (DeVito et al., 2009), which assesses the normal preference of a subject mouse for a chamber containing a littermate versus an empty chamber (Figure 4.11a). CA2-TeNT mice did not significantly differ from CA2-YFP mice in this sociability test (two-way ANOVA: Treatment x Chamber $F(1,44) = 0.013$, $P =$

0.91; Treatment $F(1,44) = 1.566$, $P = 0.22$; Chamber $F(1,44) = 17.49$, $P = 0.0001$). Multiple comparison testing revealed that both groups displayed a significant preference for the compartment containing the littermate, signifying normal sociability (Figure 4.11a). Additionally, the difference scores (time spent exploring the chamber containing the mouse minus time spent exploring the empty chamber) of the two groups were similar (Figure 4.11). These results suggest that altered sociability seen in the AVPR1b knockout mice involves a brain region distinct from CA2.

In contrast to their normal sociability, CA2-TeNT mice displayed a profound deficit in social memory as determined by the social novelty test (Figure 4.11b). In this three-chamber test (DeVito et al., 2009), social memory is assessed by the increased time a subject mouse spends interacting with a novel unrelated mouse present in one chamber compared to the time it spends interacting with a familiar co-housed littermate present in another chamber. CA2-TeNT mice displayed a significant deficit in performance on this test compared to CA2-YFP mice (two-way ANOVA: Treatment x Chamber $F(1,44) = 11.25$, $P = 0.0016$). Multiple comparison testing revealed that the CA2-YFP group demonstrated a significant preference for the compartment containing the novel animal whereas the CA2-TeNT group did not (Figure 4.11b). Moreover, the difference score (time spent exploring the novel mouse minus time spent exploring the familiar mouse) of the CA2-TeNT group was significantly less than the difference score of the CA2-YFP group (Figure 4.11b). Hence, the CA2-TeNT mice displayed a profound deficit in social recognition. Furthermore, this deficit was not due to a lack of interest in novelty, *per se*, as the CA2-TeNT mice demonstrated normal preference for a novel object as assayed by two different novel object recognition protocols (Figures 4.8 and 4.9).

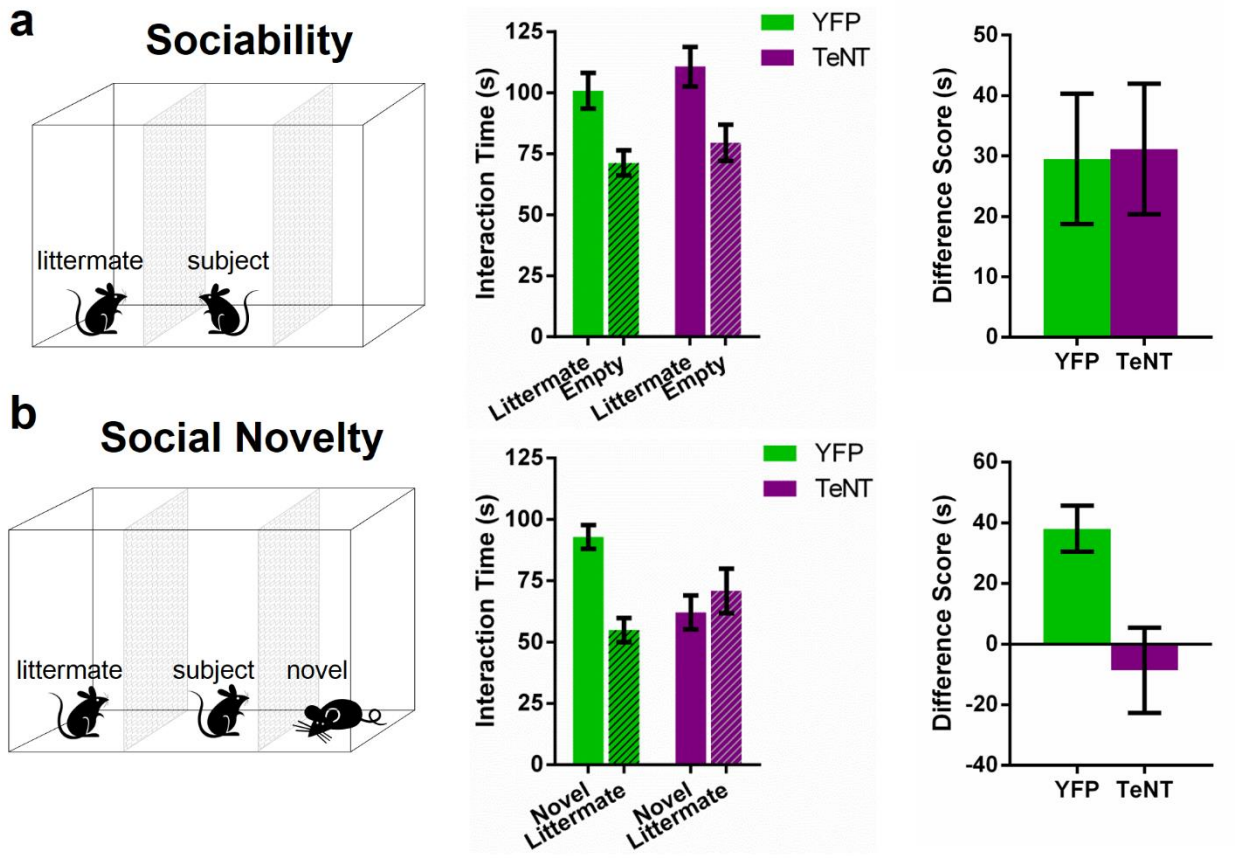

Figure 4.11: CA2-inactivation impairs social memory but not sociability. a, Left, experimental setup for the sociability test. A subject mouse in the middle chamber can interact with a littermate in one adjacent chamber or with an empty chamber. Middle, the YFP (n = 11) and TeNT (n = 13) groups both preferred the chamber with a littermate (YFP, P = 0.0083; TeNT, P = 0.0055; multiplicity adjusted P values). Right, the difference scores of the groups were similar (P = 0.9154, two-tailed t-test). **b,** Left, experimental setup for the social novelty test. The subject was allowed to interact with a littermate in one chamber or a novel, unfamiliar mouse in another chamber. Middle, only the YFP group showed a preference for the novel animal (YFP, P = 0.0012; TeNT, P = 0.3593; multiplicity adjusted P values). Right, the difference score of the CA2-TeNT group was less than that of the CA2-YFP group (P = 0.0109, two-tailed t-test). Data are presented as mean ± s.e.m.

To further explore these findings, I conducted a second test of social memory, the direct interaction test (Kogan et al., 2000). In this test, a subject mouse was first exposed to an unfamiliar mouse in trial 1 placed together with the subject mouse in the same cage. After a 1h inter-trial interval (ITI), the subject mouse was exposed either to a second unfamiliar mouse (Figure 4.12a) or re-exposed to the same mouse encountered in trial 1 (Figure 4.12b). When a novel mouse was introduced in trial 2, both groups exhibited similar social interaction times for the two trials, with comparable difference scores (Figure 4.12a). In contrast, I observed a significant difference in interaction times between the groups in trial 2 when the subjects were re-exposed to the mouse initially encountered during trial 1 (Figure 4.12b; two-way repeated measures ANOVA: Treatment x Trial $F(1,29) = 24.23$, $P < 0.0001$). Whereas the CA2-YFP group spent significantly less time exploring the same mouse in trial 2 compared to trial 1, demonstrating the presence of social memory, the CA2-TeNT group spent a similar amount of time exploring the mouse in both trials (Figure 4.12b), indicating a loss of social memory. Moreover, the difference score (time spent exploring the mouse on trial 1 minus time spent exploring the mouse on trial 2) of the CA2-TeNT group was significantly less than that of the CA2-YFP group (Figure 4.12b).

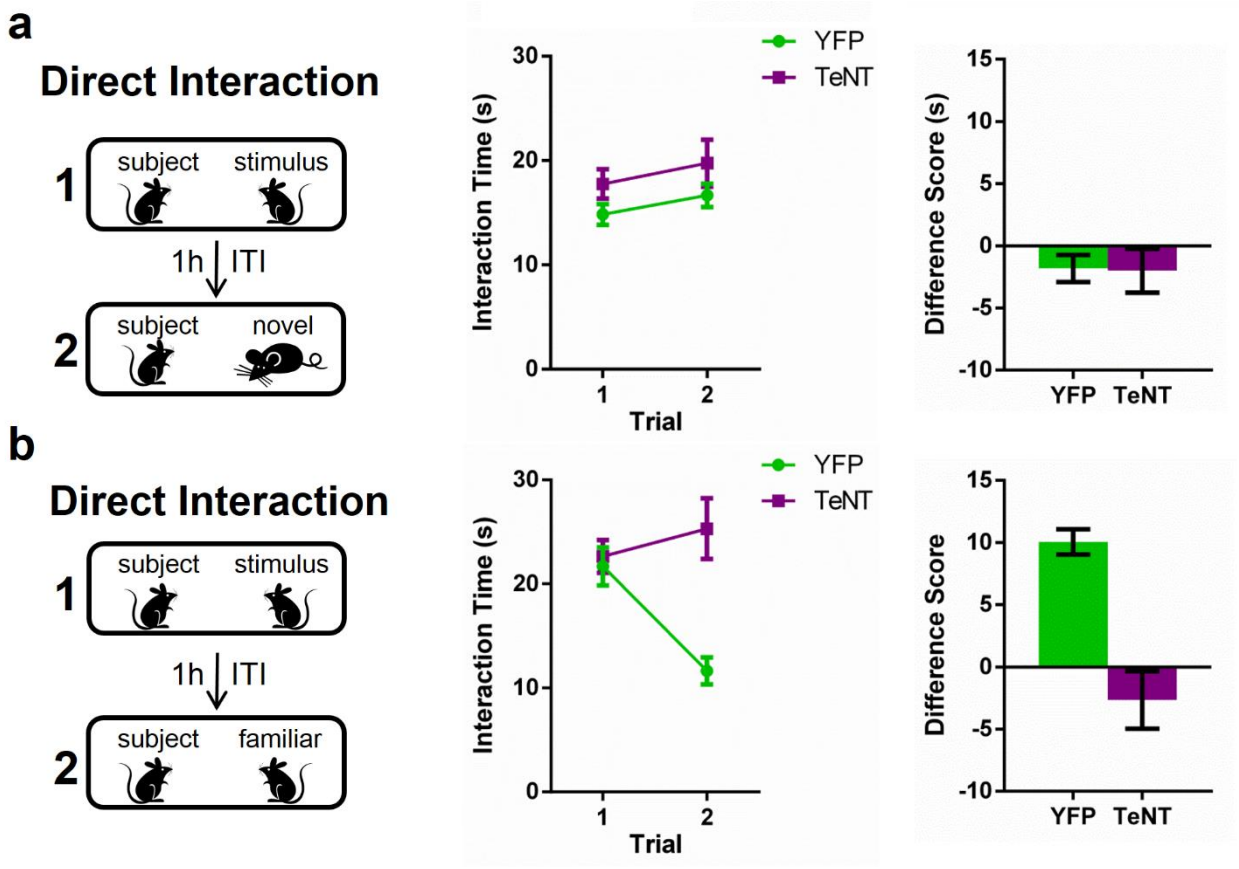

Figure 4.12: Direct interaction assay confirms social memory deficit in CA2-inactivated mice. a, Left, experimental setup for the direct interaction test in which a different stimulus animal was presented in each trial. Middle, the two groups (YFP, *n* = 15; TeNT, *n* = 16) explored the two stimulus animals for a similar amount of time (two-way repeated measures ANOVA: Treatment x Trial $F(1,29) = 0.0068$, $P = 0.93$; Treatment $F(1,29) = 2.405$, $P = 0.13$; Trial $F(1,29) = 3.278$, $P = 0.0806$). Right, the difference scores of the groups were similar ($P = 0.93$, two-tailed t-test). b**,** Left, experimental setup for the direct interaction test in which the same stimulus animal was presented for both trials. Middle, only the YFP group displayed recognition of the familiar animal, evidenced by the decrement in social investigation on trial 2 (YFP, $P < 0.0001$; TeNT, $P = 0.1499$; multiplicity adjusted P values). Right, the difference score of the CA2-TeNT group was less than that of the CA2-YFP group ($P < 0.0001$; two-tailed t-test). Data are presented as mean ± s.e.m.

To further investigate the social memory deficit following CA2-inactivation, I next ran a 5-trial social memory assay (Figure 4.13a). This test was run as previously described (Ferguson et al., 2000; Bielsky et al., 2004). Briefly, subject mice were individually housed for 7 days prior to testing. On the day of testing, the subject mice were presented with an adult ovariectomized female stimulus mouse for 4 successive 1 minute trials separated by a 10 minute ITI. On the fifth trial, a novel stimulus animal was presented. Mice with intact social memory will habituate to the presentation of the stimulus mouse over the course of the first 4 trials and dishabituate when a novel stimulus animal is presented on the fifth trial. The control CA2-YFP group displayed this behavior and thus intact social memory (Figure 4.13b). Conversely, the CA2-TeNT group did not demonstrate habituation to the repeated presentation of the stimulus mouse during the first four trials thus reaffirming the social memory deficit seen in the CA2-inactivated group (Figure 4.13b). Furthermore, statistical analysis confirmed a significant difference between the control and CA2-inactivated groups (two-way repeated measures ANOVA: Treatment x Trial $F(4,108) = 7.26$, $P < 0.0001$; Treatment $F(1,27) = 7.862$, $P = 0.0092$; Trial $F(4,108) = 15.41$, $P < 0.0001$).

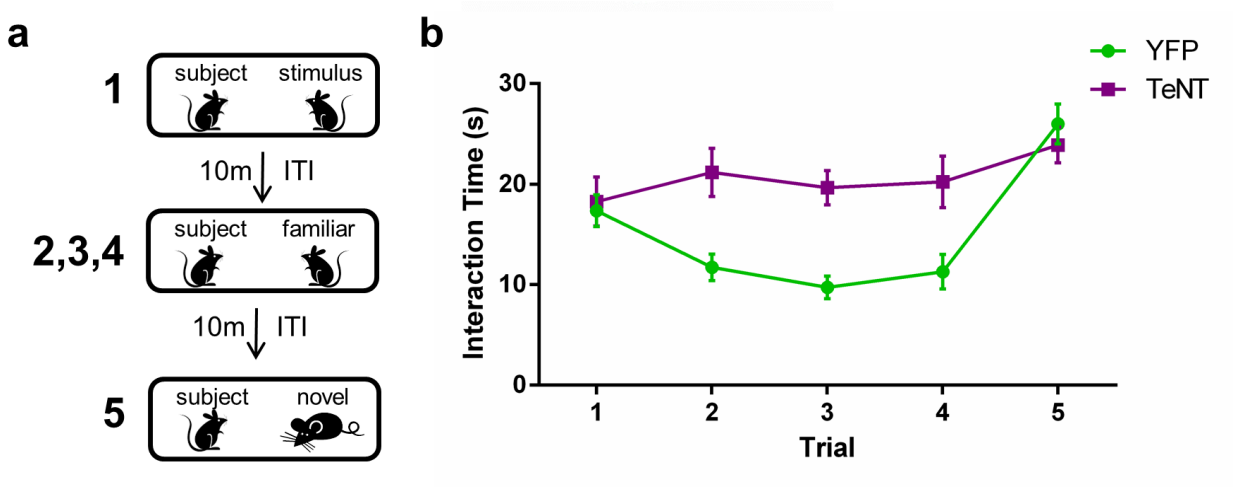

Figure 4.13: 5-trial social memory assay confirms social memory deficit in CA2-inactivated mice. a, Experimental paradigm. A stimulus animal was presented to the subject mouse for 4 successive trials separated by a 10 minute ITI. On the fifth trial, a novel mouse was introduced. **b,** The CA2-YFP control group (n = 15) displayed habituation to repeated presentation of the stimulus animal and dishabituation when a novel stimulus animal was introduced on the fifth trial. Conversely, the CA2-TeNT group (n = 14) did not display either habituation or dishabituation during the 5 trials indicating a severe deficit in social memory. Two-way repeated measures ANOVA revealed a significant interaction between treatment and trial (Treatment x Trial $F(4,108) = 7.26$, $P < 0.0001$; Treatment $F(1,27) = 7.862$, $P = 0.0092$; Trial $F(4,108) = 15.41$, $P < 0.0001$).

Olfaction is crucial for normal social interaction (Brennan and Zufall, 2006). Hence, a deficit in olfaction could result in an apparent social memory impairment. In the previous section however, I demonstrated intact olfaction in the CA2-inactivated mice based on the buried food and olfactory habituation/dishabituation tests (Figure 4.10). With the ability to detect and discriminate between both non-social and social odors, it is highly unlikely that the social memory deficit observed in the CA2-TeNT mice was due to olfactory impairment.

Chapter 5

Conclusions

5.1 CA2 joins the hippocampal circuit

In this thesis, I have detailed the development and validation of a CA2-Cre mouse line that enables precise genetic targeting of excitatory CA2 pyramidal neurons. This mouse line has enabled selective mapping of the inputs and outputs of this largely unexplored region (Chapter 3). Furthermore, I have demonstrated that the CA2 subfield is essential for social memory (Chapter 4.3). The importance of human hippocampus for social memory is famously illustrated by the case of Henry Molaison (patient H.M.) who, following bilateral medial temporal lobe ablation, could not remember people who had worked with him for years, indicating a profound deficit in social memory (Corkin, 2002). Patients with lesions limited to the hippocampus demonstrate similar dysfunction (Rempel-Clower et al., 1996). Furthermore, previous studies have demonstrated hippocampal dependence of social memory in rodents (Kogan et al., 2000). The data presented in this thesis argue for a central role of CA2 in mediating these mnemonic processes.

Although the cognitive deficits of psychiatric disorders have been the subject of much investigation, little is known about the underlying physiology of the social deficits in such diseases. My finding of a central role of CA2 in sociocognitive processing suggests that alterations in information processing in this subregion may contribute to the social endophenotypes of disorders such as schizophrenia and autism. This possibility is further suggested by the finding that individuals with schizophrenia and bipolar disorder have a reduced

number of inhibitory neurons in CA2 (Benes et al., 1998), and findings that suggest a link between autism and vasopressin (Meyer-Lindenberg et al., 2011), whose 1b receptors are strongly concentrated in CA2 (Caruana et al., 2012; Young et al., 2006).

It is important to note that although I observed a specific deficit in social memory, CA2 likely participates in other hippocampal-dependent tasks. The lack of an effect of CA2-inactivation on performance of classical hippocampal-dependent tasks, such as contextual fear conditioning and the Morris water maze, may result from the ability of non-CA2-dependent hippocampal circuits, such as the trisynaptic pathway, to carry out these tasks. In this context, it is of interest that a genetic lesion of CA3 also fails to impair memory in the Morris water maze, although contextual fear conditioning memory is abolished (Nakashiba et al., 2008). Such results indicate that distinct hippocampal circuits, such as the disynaptic CA2-dependent and trisynaptic CA3-dependent paths, may mediate both common and unique functions in hippocampal memory storage (Figure 5.1). Future combined lesion studies or *in vivo* physiology could help to disentangle these complexities.

Similarly, my finding that CA2 is essential for social memory does not rule out the participation of upstream regions of the hippocampal circuit, including DG and CA3, in social memory. Future investigation of social memory in DG-inactivated or CA3-inactivated mice will be required to establish whether or not these subregions also participate in social memory processing.

Inactivation of individual subregions of the entorhinal-hippocampal circuit often produces subtle deficits in learning and memory, presumably due to compensation from the other intact and functional subregions (the present work; Nakashiba et al., 2008; Nakashiba et al.,

2012; Suh et al., 2011). Due to the robustness of this circuit, mnemonic functions that can be ascribed to particular subregions are likely a result of properties unique to that subregion. In this regard, several properties unique to CA2 support its essential role in mnemonic processing of social information. The specific expression of the vasopressin 1b receptor in CA2 (in comparison to other areas of the hippocampal circuit) likely enables signaling of social valence. Sensory information from the environment is abundant; much is filtered and not stored in memory. Hence, valence signals are required to designate which information should be remembered and which information should be forgotten. Because of vasopressin's important role as a social hormone, it is a likely candidate for this function. Furthermore, the input that CA2 receives from the supramammillary nucleus may also be important in signaling valence as this region has been shown to include a wide variety of cell types, many of which secrete various neuropeptides (Pan and McNaughton, 2004). Finally, layer 2 of the lateral entorhinal cortex likely provides the sensory information to CA2 necessary to encode social memory as this region of the entorhinal cortex has been shown to be involved in non-spatial memory (Hargreaves et al., 2005).

The work presented in this thesis is likely to spur a greater interest in the CA2 subfield of the hippocampus. Most notably, I have demonstrated a specific behavioral function of this hippocampal area. With an *in vivo* function of CA2 established, motivation for further exploration of this area's circuitry, physiology, and pathophysiology is certain to ensue.

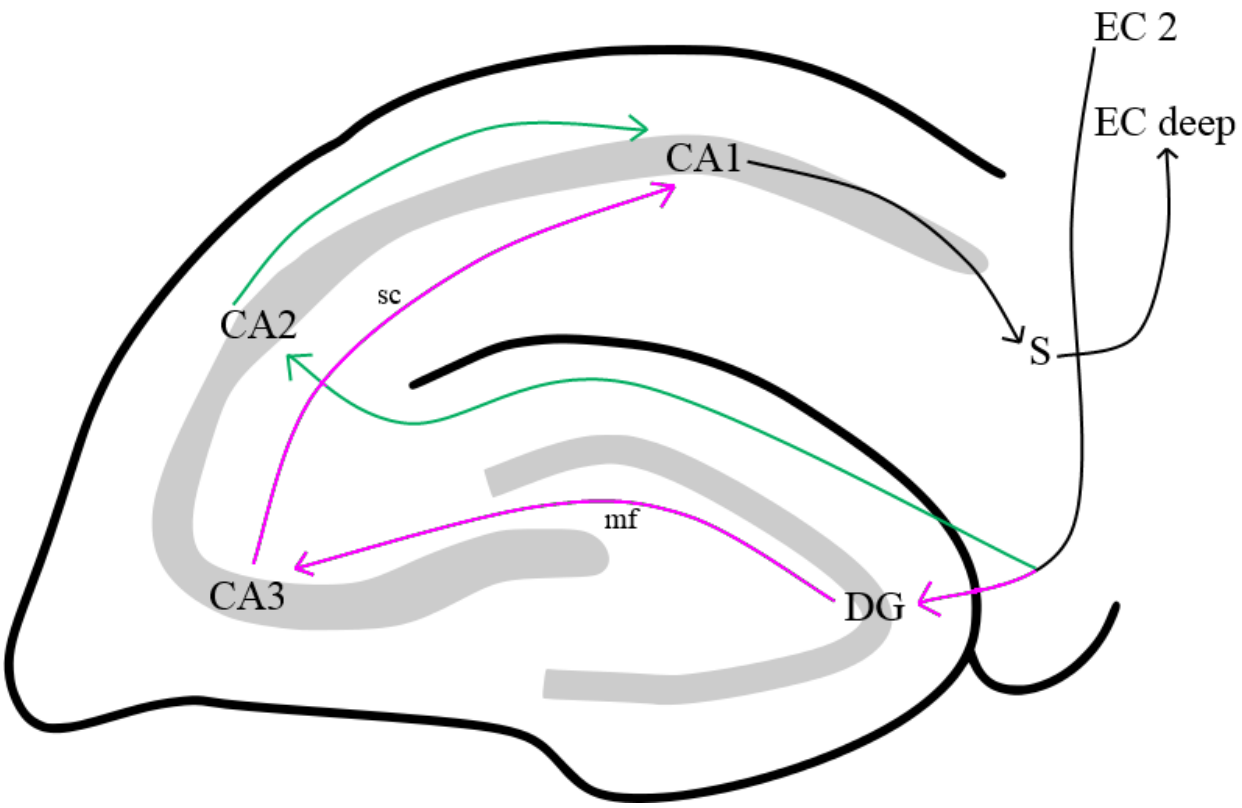

Figure 5.1: The trisynaptic and disynaptic circuits. The trisynaptic circuit is illustrated in magenta and the disynaptic circuit is illustrated in green. The trisynaptic circuit connects layer 2 of entorhinal cortex (EC 2) to CA1 via dentate gyrus (DG) and CA3. In this circuit, EC 2 projects to DG via the perforant path. The DG sends its output to CA3 via the mossy fibers (mf), and CA3 synapses on CA1 neurons via the Schaffer collaterals (sc). The disynaptic pathway connects EC 2 to CA1 via CA2. EC 2 neurons make direct connections with CA2 (see Chapter 3.1), and CA2 sends its output to CA1 (see Chapters 3.2 and 4.2).

5.2 Future directions

The generation of a CA2-Cre line will provide a valuable tool for genetic targeting of this subfield for future studies. This mouse line may be used to drive expression of nearly any gene selectively to CA2. For example, a Cre-dependent channelrhodopsin-2 (ChR2) virus (Boyden et al., 2005; Sohal et al., 2009) may be used to selectively express this light-activated cation channel in CA2 (see Chapter 4.2). In this thesis, ChR2 expression in CA2 was used to assay the efficacy of the TeNT silencing strategy employed to elucidate the behavioral role of CA2. However, this tool may also be used to more carefully explore the circuitry of CA2. As inhibitory postsynaptic potentials (IPSPs) were observed in CA1 following the light stimulation induced EPSPs, it is likely that CA2 recruits large feed-forward inhibition. With ChR2 expressed in CA2, postsynaptic responses in CA1 can be measured both in the presence and absence of GABA blockers. In this way, a pure excitatory component of the CA1 EPSP (GABA blockers present) can be obtained. The combined EPSP (no blockers present) can be subtracted from the pure excitatory EPSP to obtain an estimation of the feed forward IPSP. Furthermore, light-induced excitatory postsynaptic currents (EPSCs) and inhibitory postsynaptic currents (IPSCs) can be directly measured from CA1 when the cell is voltage clamped. By voltage clamping the neuron at -70 mV (the reversal potential for Cl^-), the EPSC can be isolated, and by voltage clamping the cell at +10 mV, the IPSC can be isolated. Determination of the balance of excitation and inhibition is critical for the understanding of normal circuit function.

As outlined in Chapter 1.1, CA2 has been implicated in diseases such as epilepsy and schizophrenia. This mouse line may aid in the study of CA2's involvement in these pathological processes as well. For example, ablating CA2 in a model of temporal lobe epilepsy might demonstrate CA2's epileptogenic role *in vivo*. This may be done by expressing the

pharmacologically selective actuator module (PSAM) in CA2 by injection of a Cre-dependent PSAM vector in the CA2-Cre line (Magnus et al., 2011). PSAM is a genetically engineered ligand-binding ion channel. Upon administration of the synthetic ligand PSEM, the channel opens and Cl^- passes through the ion pore domain (from the glycine receptor) of the PSAM. Cl^- influx will silence the CA2 neuron. With PSAM expressed in CA2, the PSEM can be administered at any time point to temporarily inactivate CA2. To explore CA2's role in epilepsy, animals that express PSAM in CA2 can be kindled to induce a model of temporal lobe epilepsy. Then, PSEM can be administered at different time points to determine if CA2-inactivation decreases the number of seizure events or if it increases the threshold for generating persistent epileptic activity in these mice. To test CA2's involvement in schizophrenia, the CA2-Cre line can be crossed to a mouse model of schizophrenia, for example the 22q11.2 microdeletion model (Fénelon et al., 2013), and CA2 can be inactivated or activated to explore if CA2 activity alters physiological or behavioral activity in these mice.

Finally, this line can also be used in future studies to delve further into the social memory phenotype of CA2-inactivated mice. CA2-dependece of additional, possibly more ethological behaviors such as the social transmission of food preference test (Wrenn, 2004) may be examined. Furthermore, the work outlined in this thesis employed a TeNT-based inactivation strategy that resulted in chronic ablation of CA2 activity. This prevented me from testing whether CA2 is necessary for encoding, consolidation, and/or retrieval of social memory. To differentiate between these possibilities acute inactivation of CA2 is required. As described above, tools like the PSAM/PSEM system are currently available to enable temporally specific inactivation of CA2. Hence, with genetically targeted expression of PSAM in CA2, PSEM injections can be used to acutely inactivate CA2. PSEM ligand may be infused at various time

points to assess the role of CA2 in social memory encoding and retrieval. The direct interaction test can be run with the PSAM/PSEM approach to address this question. These experiments would entail PSAM expression in CA2 and PSEM injection before the first trial to test the necessity of CA2 for encoding social memories. PSEM injection after the first trial, but before the second retrieval trial would be done to assess the role of CA2 in social memory retrieval.

As indicated earlier, the present work does not exclude a role of other hippocampal regions including the DG and CA3 in the encoding or retrieval of social memory. To formally test the hypothesis that CA2 is uniquely essential for social memory, the social memory tasks outlined in Chapter 4.3 would need to be repeated in DG-inactivated and CA3-inactivated mice. This could be achieved using the same strategy detailed in this thesis (Chapter 4.1). Namely, the Cre-dependent TeNT virus that I have prepared could be utilized in conjunction with the CA3-Cre (Nakashiba et al., 2008) and DG-Cre (Nakashiba et al., 2012) mouse lines to genetically inactivate these subregions. Additionally, the PSAM/PSEM system described above could also be employed to achieve acute inactivation of these hippocampal subfields.

CA2 inactivation (present work) and CA3 inactivation (Nakashiba et al., 2008) produced surprisingly little deficit in spatial learning and memory, which has been shown to be hippocampal-dependent. A possible explanation for this is that CA3 compensates for the lack of CA2 activity when CA2 is inactivated, and CA2 compensates for the lack CA3 activity when CA3 is inactivated. An alternate explanation for these findings is that the direct EC projections to CA1 are capable of supporting spatial memory as assayed by the Morris water maze task. To differentiate between these possibilities, the CA3-Cre mouse line (Nakashiba et al., 2008) can be crossed to the CA2-Cre mouse line to generate a mouse that expresses Cre in CA2 and CA3. Then, the TeNT-based inactivation approach outlined in Chapter 4 could be used to inactivate

both of these subfields simultaneously. This would isolate CA1 from its disynaptic and trisynaptic pathway inputs. Hence, the capability of the perforant path EC input to CA1 to support spatial memory could be assessed.

The experiments described above are only a small sampling of possible future directions for this work. Because CA2 has been largely ignored in the past, the realm of potential prospective work is vast.

Chapter 6

Methods

Generation of CA2-Cre mouse line

Atlases of gene expression in the mouse brain (Heintz, 2003; Lein, 2007) were consulted to ascertain which genes are expressed exclusively, with respect to the hippocampus, in CA2. Both the GENSAT and Allen Brain Atlas indicated the CA2-specificity of Amigo2 expression. The RP23-288P18 bacterial artificial chromosome (BAC) that contained the Amigo2 gene and its surrounding regulatory elements was obtained from the BACPAC Resource Center (de Jong, 2000). Recombineering with galK selection and the SW102 bacterial strain (Warming et al., 2005) was employed to seamlessly modify RP23-288P18 so that a Cre-HSV-polyA cassette was inserted at the translation start site of the Amigo2 gene. Specifically, the Cre expression cassette was PCR amplified from pLD53.SC-Cre (Gong et al., 2007) The homology arms used for the recombineering were 5' arm: 5’ ATTGGTGGGAGACTGAGCTGATGAGAAGCGACTGGCAAGAGACTCAGAGGCGACCATA-3’ and 3’ arm: 5’ ATGTCGTTAAGGTTCCACACACTGCCCACCCTGCCTAGAGCTGTCAAACCGGGTTGCAGAGA-3’. This modified BAC was injected into B6CBA/F2 pronuclei and embryos were implanted into pseudopregnant females. PCR was used to identify the offspring that were Cre-positive. These founders were crossed to the Ai14 Cre-reporter line (Madisen et al., 2010) to examine the specificity of Cre expression. At 12 weeks of age, the Cre^{+} offspring were transcardially perfused with 4% paraformaldehyde (PFA) in phosphate buffered saline (PBS) and

expression of tdTomato was examined in 50 μm coronal slices. CA2-specific expression of tdTomato was not observed in any of the founder lines. However, injection of the EF1α-FLEx-eYFP-WPRE-hGH Cre-reporter adeno-associated virus (AAV) into the hippocampus of adult mice (> 8 weeks old) revealed CA2-specific expression in 1 of the 6 founder lines. This line was used for all of the studies presented here. The line was backcrossed to C57BL/6J a minimum of 6 times before any behavioral or physiological experiments were performed.

Subjects

The Amigo2-Cre line was maintained as a hemizygous line on the C57BL/6J background by breeding Cre+ males to C57BL/6J females. Only Cre+ males were used for these experiments. Mice > 8 weeks old were injected with virus under stereotactic control into the hippocampus. All anatomical, behavioral, and physiological experiments were conducted 2-4 weeks following injection. All procedures were approved by the Institutional Animal Care and Use Committee at Columbia University and the New York State Psychiatric Institute.

Virus constructs

AAV5- EF1α-FLEx-eYFP-WPRE-hGH (4×10^{12} virus molecules ml^{-1}) was injected to label CA2 pyramidal neurons and trace their axons. (EnvA)SAD-ΔG-mCherry (1×10^{8} infectious particles ml^{-1}) pseudotyped rabies virus was produced as previously described (Wickersham et al., 2010) and used to label monosynaptic inputs to CA2. This virus can only infect cells expressing the TVA receptor (Wickersham et al., 2010; Watabe-Uchida et al., 2012). Before rabies virus injection, AAV5- EF1α-FLEx-TVA-mCherry-WPRE-hGH (Watabe-Uchida et al., 2012) (3×10^{12} virus molecules ml^{-1}) was injected to express TVA in CA2. To permit

retrograde synaptic transport of the ΔG virus, AAV5- CAG-FLEx-rabiesG-WPRE-hGH (Watabe-Uchida et al., 2012) (2×10^{12} virus molecules ml^{-1}) was co-injected with the TVA virus to express G in CA2. The aforementioned AAVs were obtained from the University of North Carolina vector core. To specifically excite CA2 pyramidal neurons, AAV5- EF1α-FLEx-hChR2(H134R)-EYFP-WPRE-hGH (2×10^{12} genome copies ml^{-1}) was injected to express ChR2 in the CA2 neurons. This vector was obtained from the University of Pennsylvania (UPenn) vector core. To ablate CA2 pyramidal cell output, tetanus neurotoxin light chain (TeNT) was expressed selectively in these cells. A Cre-dependent AAV vector carrying eGFP-TeNT was created by PCR amplifying eGFP-TeNT from pTRE2-eGFP-TeNT-PEST19 and subcloning it into pAAV- EF1α-DIO-hChR2-mCherry-WPRE (Addgene plasmid 20297) between the NheI and AscI sites in the inverse orientation. The resulting vector, pAAV- EF1α-FLEx-eGFP-TeNT-WPRE-hGH was sent to the UPenn vector core for custom production of AAV5- EF1α-FLEx-eGFP-TeNT-WPRE-hGH (1×10^{13} genome copies ml^{-1}).

Stereotaxic injection

Mice were anesthetized with isoflurane (2-5%) and placed in a stereotaxic apparatus (Digital Just for Mice Stereotaxic Instrument, Stoelting). The head was fixed, and the skull was exposed. Burr holes were made and a glass micropipette (Drummond Scientific) was slowly lowered into the hippocampus at -1.6 mm anteroposterior, ±1.6 mm mediolateral, and -1.7 mm dorsoventral relative to bregma. The pipettes were formed with 20 μm diameter tips using a P-2000 laser puller (Sutter Instrument). For the mouse line validation, anterograde tracing, and behavioral experiments, 180 nl of virus was pressure injected into each hemisphere. For the retrograde tracing experiments, 180 nl of a 1:5 mix of AAV expressing TVA and AAV

expressing rabies G was injected unilaterally. For the electrophysiological experiments, 360 nl of a 1:1 mix of ChR2 AAV and either YFP or TeNT AAV was injected. After injection, the pipette remained in place for 5 minutes and then was slowly retracted. The mice were placed on a heating pad (TR-200, Fine Science Tools) throughout the duration of the surgery. Following injection, the scalp was sutured, saline was administered subcutaneously, and buprenorphine (0.05-0.1 mg/kg) was administered intraperitoneally for analgesia. The mice were placed under heating lamps during recovery from anesthesia. For the retrograde tracing experiments, these procedures were repeated two weeks after the initial AAV injection to inject 360 nl of (EnvA)SAD-ΔG-mCherry rabies virus. To test the specificity of the rabies virus, a subset of animals was injected with 360 nl of the (EnvA)SAD-ΔG-mCherry rabies virus without prior injection of AAVs expressing TVA and G. All injections were verified histologically. No injections were mistargeted, hence no subjects were excluded from analysis due to injection failure.

Immunohistochemistry and confocal microscopy

Mice were administered ketamine/xylazine (150 mg/kg, 10 mg/kg) and transcardially perfused with ice-cold PBS followed by ice-cold 4% PFA in PBS. Brains were postfixed overnight in 4% PFA in PBS and 50μm slices were prepared (Vibratome 3000 Plus, The Vibratome Company). Antigen retrieval (Jiao et al., 1999) was performed for RGS14 staining. Briefly, free-floating sections were incubated at 80°C for 30min in 50mM sodium citrate (pH = 8.5). Slices were permeabilized with 0.2% Triton X-100 in PBS and blocked with 10% goat serum in PBS. The sections were incubated at 4°C overnight in primary antibody (1:50 dilution, 73-170, NeuroMab). For GABA staining, sections were permeabilized and blocked as above and then incubated in primary antibody (1:500 dilution, A2052, Sigma-Aldrich) at 4°C overnight.

Sections were washed the following day and incubated for 2h with Alexa 555 or 647 secondary antibody (1:500 dilution, A21422, A21428, or A21245, Invitrogen) and NeuroTrace (1:500 dilution, N21479 or N21483, Invitrogen). Slices were then mounted with either Prolong Gold (P36930, Invitrogen) or VECTASHIELD (H-1000, Vector Laboratories) and imaged. An inverted laser scanning confocal microscope (LSM 700, Zeiss) was used for fluorescence imaging followed by analysis in ImageJ (Rasband, 1997). For cell counting experiments, every sixth slice throughout the extent of the dorsal hippocampus was examined.

Electrophysiology

2-3 weeks following AAV injection, mice were anesthetized with isoflurane (5%) and transcardially perfused with an ice-cold dissection solution that contained (in mM): 10 NaCl, 195 sucrose, 2.5 KCl, 10 glucose, 25 NaHCO3, 1.25 NaH2PO4, 2 Na Pyruvate, 0.5 CaCl2 and 7 MgCl2. The hippocampi were dissected out and 400 μm slices were cut (VT1200S, Leica) perpendicular to the longitudinal axis of the hippocampus. The slices were then transferred to a chamber containing a 1:1 mixture of dissection solution and artificial cerebrospinal fluid (aCSF). The aCSF contained (in mM): 125 NaCl, 2.5 KCl, 22.5 glucose, 25 $NaHCO_3$, 1.25 NaH_2PO_4, 3 Na Pyruvate, 1 Ascorbic Acid, 2 $CaCl_2$ and 1 $MgCl_2$. Slices were incubated at 30 °C for 30 minutes and then at room temperature for at least 1.5 hours before recording. Slices were transferred to a recording chamber (Warner Instruments), perfused with aCSF, and maintained at 33 °C. All solutions were saturated with carbogen (95% O_2 and 5% CO_2). Whole-cell recordings were obtained from pyramidal neurons with a patch pipette (3–5 MΩ) containing (in mM): 135 $KMeSO_4$, 5 KCl, 0.1 EGTA-Na, 10 HEPES, 2 NaCl, 5 ATP, 0.4 GTP, 10 phosphocreatine at pH 7.2 and osmolarity of 280–290 mOsm. Series resistance, which was always less than 30 MΩ, was monitored and compensated throughout the experiment. Cells with a 15% or greater change

in series resistance were excluded from analysis. To activate ChR2, 2 ms pulses of blue (470 nm) light (M470L2-C1, Thor Labs) were delivered through a 20X objective. Light power from the objective was measured with a power meter (PM100D, Thor Labs). The objective was centered on the neuron that was being recorded during the experiment. For the CA2 cell-attached recordings, a gigaohm seal was made and action currents were measured in voltage-clamp mode (cell clamped at -70 mV) while 5 pulses of blue light were delivered. For the input-output curves, whole-cell recordings were made from CA1 cells in current-clamp mode and the objective was centered on the patched CA1 neuron. This provided illumination over stratum oriens (SO), stratum pyramidale (SP), and stratum radiatum (SR) thus activating the CA2 projections to CA1 that course through SO and SR.

Behavioral tests

Mice were housed 2-5 per cage and were given ad lib access to food and water. They were kept on a 12h (6 a.m. to 6 p.m.) light–dark cycle in a room maintained at 21 °C. All tests were conducted during the light cycle. Mice were habituated to handling and transport from the colony room to the behavioral room for 3 days before behavioral tests were begun. Mice were given 1 hour to habituate after transport to the behavioral room before any tests were conducted. The experimenter was blind to the treatment groups. The control group (CA2-YFP) was injected with AAV5- EF1α-FLEx-eYFP-WPRE-hGH while the CA2-inactivated group (CA2-TeNT) was injected with AAV5- EF1α-FLEx-eGFP-TeNT-WPRE-hGH. To blind the experimenter, virus aliquots were stored as pairs of coded cryotubes. Half of the mice in each home cage were injected with the YFP virus, while the other half were injected with the TeNT virus. The identity of the groups was revealed only after testing was completed. For the elevated plus maze, novel

object, Morris water maze, and 3-chamber tests, mice were tracked with an overhead FireWire camera (DMK 31AF03-Z2, The Imaging Source) and ANY-maze (Stoelting). Freezing during fear conditioning was tracked with a Fire-i (unibrain) camera and analyzed with ANY-maze (Stoelting). All apparatuses and testing chambers were cleaned with 70% isopropanol wipes (VWR) between animals unless otherwise indicated below.

Open field

Mice were placed in an open field (ENV-510S, Med Associates, Inc.) for 30 minutes and locomotor and rearing activity was monitored via IR beam breaks and recorded by the Activity Monitor (Med Associates, Inc.) software. The entire apparatus was enclosed in a sound attenuating cubicle.

Elevated plus maze

Mice were placed in the center of a maze (Stoelting) constructed in the shape of a plus with two enclosed arms (15 cm high walls) and two open arms. The maze was elevated 40 cm from the ground. Mice were allowed to explore the maze for 8 minutes. Entry into an arm was scored only after 85% of the animal's tracked body area was in the arm.

Novel object

Two variations of the novel object task were run. Both were conducted in a 50 cm long x 25 cm wide x 30.5 cm high arena. For both tests, the snouts of the mice were tracked and object interaction was measured as time spent with snout within 2 cm of the object. The objects (a glass chess piece, a small metal lock, and a small plastic box) were secured to the arena with neodymium magnets to render them immovable. In the first variation, mice were habituated to

the arena and objects 1 and 2 over the course of four 5 minute trials separated by an intertrial interval (ITI) of 10 minutes. Mice were then tested for object recognition memory 1 hour after the fourth trial during the 5-minute-long fifth trial. Either object 1 or object 2 (counterbalanced) was swapped for object 3 during the fifth trial. In the second variation of this test, the mice were habituated to the empty arena for 10 minutes each day for 3 consecutive days. On day 4, the mice were exposed to a pair of either object 1 or object 2 for 5 minutes. Object recognition memory was tested 1 hour after this trial by exposure to objects 1 and 2 for 5 minutes. In both protocols, object recognition memory was measured as the increased time spent investigating the novel object.

Morris water maze

The Morris water maze task was run over the course of 14 days in a 120 cm diameter pool filled with water that was opacified with non-toxic white paint (Prang tempera paint, VWR). The water was maintained at 19-20 °C. Four 1 minute trials were administered per day, and mice were run in groups of 8. On days 1-2, cued learning was conducted. During this procedure, mice were trained to find a circular platform (10 cm in diameter) submerged 1 cm below the surface of the water and marked with a flag. Distal cues in the room were obscured by a black curtain that encircled the tank. The mouse was removed from the tank and returned to its home cage 15 s after locating the platform. If a mouse failed to locate the platform during the minute-long trial, it was gently guided towards the platform. The mice were released from different start points at the beginning of each trial, and the platform location also varied between trials. On days 3-7, the flag was removed from the platform, rendering it hidden, and the curtains were removed, which allowed the mice to now use distal cues to locate the hidden platform. The platform was kept in the middle of the SW quadrant of the maze during days 3-7. On day 8,

spatial memory was assayed with a 1min probe trial in which the platform was removed. Reversal training was conducted on days 9-13 with the platform now hidden in the NW quadrant. Spatial memory of the novel location was tested with a 1min probe trial on day 14. Release and platform locations were adapted from previous studies (Vorhees et al., 2006).

Fear conditioning

A 3-day delay fear conditioning protocol was employed to test hippocampal-dependent contextual fear memory and amygdala-dependent auditory fear memory. On day 1, the mice were placed in an enclosure (17 cm x 17 cm x 25 cm) with a steel grid floor. This enclosure was located in a sound-attenuating chamber that contained a FireWire camera, light, and speaker. On day 1, the enclosure was outfitted as context A which consisted of 3 plexiglass walls and 1 opaque wall with black and white stripes. 1% acetic acid was placed as the dominant odor, and the house fan was turned on. The enclosure was cleaned with 70% isopropanol between animals. Mice were moved from their home cage to a transfer cage with no bedding and after 15-20s were placed in the fear conditioning chamber. After 150s, a tone (30s, 2.8 kHz, 85 dB) was played and co-terminated with a shock (2s, 0.7 mA). Mice were removed from the chamber 30s after the shock. On day 2, contextual fear memory was assayed by placing the mice back in context A for 300s. On day 3, the mice were brought to the testing room that was now dimly illuminated with red light. The mice were placed in context B, which consisted of an enclosure with 3 solid gray colored walls, 1 plexiglass wall with a circular door, and a red, flat plastic roof. The floor of the enclosure was a white piece of plastic, 0.25% benzaldehyde was the dominant odor, and the enclosure was cleaned between animals with Vimoba. Mice were first moved from their home cage to a circular bucket and then to the testing chamber. After 180s, the tone from day 1 was

sounded for 60s. Percent time spent freezing (defined as the absence of all movement except for respiration) was measured throughout these experiments and served as an index of fear memory.

Buried food test

To ensure palatability of the food, mice were given 1g reward treats (F05472-1, Bio-Serv) in their home cages one day before testing. All pellets were consumed. The mice were then food deprived for 18 hours before the test to improve sensitivity (Yang and Crawley, 2009). A treat was hidden under 1.5cm of standard cage bedding, a mouse was placed in the cage, and the latency to consumption of the treat was recorded.

Olfactory habituation/dishabituation test

This test was run as previously described (Yang and Crawley, 2009) with the exclusion of the first 3 trials in which a water-soaked cotton swab is presented. A trained observer measured and recorded olfactory investigation of the odorant-soaked cotton swab.

Sociability and social novelty

This test was performed as previously described (DeVito, et al. 2009). Briefly, mice were placed in an arena divided into 3 equal-sized compartments by plastic mesh. On day 1, a 5 minute sociability trial was conducted. A littermate was placed in the left or right compartment (systematically alternated) and the test subject was placed into the center compartment. The time the test subject spent investigating each compartment (snout within 2cm of the mesh barrier) was measured and a difference score was computed. On day 2, a 5 minute social novelty test was conducted in which a littermate was placed in either the left or right compartment, and a novel animal (C57BL/6J, 3-month-old, male) was placed in the other compartment. The test subject

was placed in the center compartment, investigation time was measured, and a difference score, determined by subtracting the time spent investigating the two compartments, was computed.

Direct interaction

This test was adapted from Kogan et al., 2000. Under low light (12 lux), mice were placed in a standard clean cage and a novel mouse (C57BL/6J, 4-5-week-old, male) was introduced. Activity was monitored for 5 minutes and scored online for social behavior (anogenital and nose-to-nose sniffing, following, and allogrooming) initiated by the test subject. After an ITI of 1 hour, the test was run again with either the previously encountered mouse or a novel mouse. The time spent in social interaction during trial 1 was subtracted from the social interaction time during trial 2 to obtain the difference score.

5-trial social memory assay

This test was run as previously described (Ferguson et al., 2000; Bielsky et al., 2004). Briefly, subject mice were individually housed for 7 days prior to testing. On the day of testing, the subjects were presented with a 10 week old CD-1 ovariectomized female mouse for 4 successive 1 minute trials. On the fifth trial, a novel stimulus animal was presented.

Statistical Analysis

Prism 6 (GraphPad) was used for statistical analysis and to graph data. Statistical significance was assessed by two-tailed unpaired Student's t-tests, 2-way ANOVA, or 2-way repeated measures ANOVA where appropriate. Significant main effects or interactions were followed up with multiple comparison testing using Holm-Sidak's correction. Results were considered significant when $P < 0.05$. α was set equal to 0.05 for multiple comparison tests.

References

Altman, J. and Das, G.D. (1965). Autoradiographic and histological evidence of postnatal hippocampal neurogenesis in rats. Journal of Comparative Neurology 124, 319–335.

Amaral, D.G., and Witter, M.P. (1989). The three-dimensional organization of the hippocampal formation: a review of anatomical data. Neuroscience 31, 571-591.

Andrioli, A., Alonso-Nanclares, L., Arellano, J.I., and DeFelipe, J. (2007). Quantitative analysis of parvalbumin-immunoreactive cells in the human epileptic hippocampus. Neuroscience 149, 131-143.

Bartesaghi, R. and Gessi, T. (2004). Parallel activation of field CA2 and dentate gyrus by synaptically elicited perforant path volleys. Hippocampus 14, 948–963.

Bartesaghi, R., Migliore, M., and Gessi, T. (2006). Input-output relations in the entorhinal cortex-dentate-hippocampal system: evidence for a non-linear transfer of signals. Neuroscience 142, 247–265.

Benes, F.M., Kwok, E.W., Vincent, S.L., and Todtenkopf, M.S. (1998). A reduction of nonpyramidal cells in sector CA2 of schizophrenics and manic depressives. Biological Psychiatry 44, 88–97.

Benes, F.M. and Todtenkopf, M.S. (1999). Effect of age and neuroleptics on tyrosine hydroxylase-IR in sector CA2 of schizophrenic brain. NeuroReport 10, 3527–3530.

Bevins, R.A. and Besheer, J. (2006). Object recognition in rats and mice: a one-trial non-matching-to-sample learning task to study 'recognition memory'. Nature Protocols 1, 1306-11.

Bielsky, I.F., Hu, S., Szegda, K.L., Westphal, H., and Young, L.J. (2004). Profound Impairment in Social Recognition and Reduction in Anxiety-Like Behavior in Vasopressin V1a Receptor Knockout Mice. Neuropsychopharmacology 29, 483–493.

Bird, C.M. and Burgess, N. (2008). The hippocampus and memory: insights from spatial processing Nature Reviews Neuroscience 9, 182-194.

Bolshakov, V.Y. and Siegelbaum, S.A. (1995). Regulation of hippocampal transmitter release during development and long-term potentiation. Science 269, 1730-4.

Boulanger, L.M., Lombroso, P.J., Raghunathan, A., During, M.J., Wahle, P., and Naegele, J.R. (1995). Cellular and molecular characterization of a brain-enriched protein tyrosine phosphatase. The Journal of Neuroscience 15, 1532-1544.

Boyden, E. S., Zhang F., Bamberg, E., Nagel, G., and Deisseroth K. (2005). Millisecond-timescale, genetically targeted optical control of neural activity. Nature Neuroscience 8, 1263-8.

Brennan, P. A. and Zufall, F. (2006). Pheromonal communication in vertebrates. Nature 444, 308-315.

Brun, V.H., Otnass, M.K., Molden, S., Steffenach, H.A., Witter, M.P., Moser, M.B., and Moser, E.I. (2002). Place cells and place recognition maintained by direct entorhinal-hippocampal circuitry. Science 296, 2243-2246.

Caruana, D. A., Alexander, G. M., and Dudek, S. M. (2012). New insights into the regulation of synaptic plasticity from an unexpected place: hippocampal area CA2. Learning and Memory 19, 391-400.

Chevaleyre, V., and Siegelbaum, S.A. (2010). Strong CA2 pyramidal neuron synapses define a powerful disynaptic cortico-hippocampal loop. Neuron 66, 560-572.

Chun, M.M. and Phelps, E.A. (1999). Memory deficits for implicit contextual information in amnesic subjects with hippocampal damage. Nature Neuroscience 2, 844–847.

Cohen, S.J., Munchow, A.H., Rios, L.M., Zhang, G., Asgeirsdóttir, H.N., Stackman, R.W. Jr. (2013). The rodent hippocampus is essential for nonspatial object memory. Current Biology 23, 1685-90.

Corkin, S. (2002). What's new with the amnesic patient H.M.? Nature Reviews Neuroscience 2, 153-60.

Cui, Z., Gerfen, C. R., and Young, W. S. 3rd. (2013). Hypothalamic and other connections with dorsal CA2 area of the mouse hippocampus. Journal of comparative neurology 521, 1844-66.

de Jong P. J. BAC Clones Distribution Center – BACPAC Resources Center. https://bacpac.chori.org/ (2000).

DeVito, L.M. and Eichenbaum, H. (2011). Memory for the order of events in specific sequences: contributions of the hippocampus and medial prefrontal cortex. Journal of Neuroscience 31, 3169-75.

DeVito, L.M., Konigsberg, R., Lykken, C., Sauvage, M., Young, W.S. 3rd, and Eichenbaum, H. (2009). Vasopressin 1b receptor knock-out impairs memory for temporal order. Journal of Neuroscience 29, 2676-83.

Dudchenko, P.A., Wood, E.R., and Eichenbaum, H. (2000). Neurotoxic hippocampal lesions have no effect on odor span and little effect on odor recognition but produce significant impairments on spatial span, recognition, and alternation. Journal of Neuroscience 20, 2964-77.

Eriksson, P.S., Perfilieva, E., Björk-Eriksson, T., Alborn, A.M., Nordborg, C., Peterson, D.A., and Gage, F.H. (1998). Neurogenesis in the adult human hippocampus. Nature Medicine 4, 1313–1317.

Fénelon, K., Xu, B., Lai, C.S., Mukai, J., Markx, S., Stark, K.L., Hsu, P.K., Gan, W.B., Fischbach, G.D., Macdermott, A.B., Karayiorgou, M., and Gogos, J.A. (2013). The Pattern of Cortical Dysfunction in a Mouse Model of a Schizophrenia-Related Microdeletion. Journal of Neuroscience 33, 14825-14839.

Ferguson, S.M., Eskenazi, D., Ishikawa, M., Wanat, M.J., Phillips, P.E., Dong, Y., Roth, B.L., and Neumaier, J.F. (2011). Transient neuronal inhibition reveals opposing roles of indirect and direct pathways in sensitization. Nature Neuroscience 14, 22-24.

Ferguson, J.N., Young, L.J., Hearn, E.F., Matzuk, M.M., Insel, T.R., Winslow, J.T. (2000). Social amnesia in mice lacking the oxytocin gene. Nature Genetics 25, 284–288.

Franklin, K. and Paxinos, G. The Mouse Brain in Stereotaxic Coordinates (Academic Press, 2007).

Fukaya, M., Yamazaki, M., Sakimura, K., and Watanabe, M. (2005). Spatial diversity in gene expression for VDCCgamma subunit family in developing and adult mouse brains. Neuroscience Research 53, 376-383.

Gewirtz, J.C., McNish, K.A., and Davis, M. (2000). Is the hippocampus necessary for contextual fear conditioning? Behavioural Brain Research 110, 83-95.

Golding, N.L., Staff, N.P., and Spruston, N. (2002). Dendritic spikes as a mechanism for cooperative long-term potentiation. Nature 418, 326–331.

Gómez-Pinilla, F., Lee, J.W., and Cotman, C.W. (1994). Distribution of basic fibroblast growth factor in the developing rat brain. Neuroscience 61, 911-923.

Gong, S., Doughty, M., Harbaugh, C.R., Cummins, A., Hatten, M.E., Heintz, N., and Gerfen, C.R. (2007). Targeting Cre recombinase to specific neuron populations with bacterial artificial chromosome constructs. Journal of Neuroscience 27, 9817-23.

Gong, S., Zheng, C., Doughty, M.L., Losos, K., Didkovsky, N., Schambra, U.B., Nowak, N.J., Joyner, A., Leblanc, G., Hatten, M.E., and Heintz, N. (2003). A gene expression atlas of the central nervous system based on bacterial artificial chromosomes. Nature 425, 917-925.

Griguoli, M. and Cherubini E. (2012). Regulation of hippocampal inhibitory circuits by nicotinic acetylcholine receptors. Journal of Physiology 590, 655-66.

Haglund, L., Swanson, L.W., and Kohler, C. (1984). The projection of the supramammillary nucleus to the hippocampal formation: an immunohistochemical and anterograde transport study with the lectin PHA-L in the rat. Journal of Comparative Neurology 229, 171–185.

Hargreaves, E. L., Rao, G., Lee, I., and Knierim, J. J. (2005). Major dissociation between medial and lateral entorhinal input to dorsal hippocampus. Science 308, 1792-4.

Heintz, N. GENSAT Brain Atlas of gene expression in EGFP Transgenic Mice. http://www.gensat.org (2003).

Hensler, J. G. Serotonergic modulation of the limbic system. (2006). Neuroscience and Biobehavioral Reviews 30, 203-14.

Ino, T., Itoh, K., Kamiya, H., Shigemoto, R., Akiguchi, I., and Mizuno, N. (1988). Direct projections of non-pyramidal neurons of Ammon's horn to the supramammillary region in the cat. Brain Research 460, 173-7.

Jiao, Y., Sun, Z., Lee, T., Fusco, F.R., Kimble, T.D., Meade, C.A., Cuthbertson, S., and Reiner, A. (1999). A simple and sensitive antigen retrieval method for free-floating and slide-mounted tissue sections. Journal of Neuroscience Methods 93, 149-62.

Karpova, A.Y., Tervo, D.G., Gray, N.W., and Svoboda, K. (2005). Rapid and reversible chemical inactivation of synaptic transmission in genetically targeted neurons. Neuron 48, 727-735.

Kawai, J. et al. (2001). Functional annotation of a full-length mouse cDNA collection. Nature 409, 685-690.

Kiss, J., Csaki, A., Bokor, H., Shanabrough, M., and Leranth, C. (2000). The supramammillohippocampal and supramammilloseptal glutamatergic/aspartatergic projections in the rat: a combined [3H]D-aspartate autoradiographic and immunohistochemical study. Neuroscience 97, 657–669.

Kogan, J. H., Frankland, P. W., and Silva, A.J. (2000). Long-term memory underlying hippocampus-dependent social recognition in mice. Hippocampus 10, 47-56.

Lee, S.E. et al. (2010). RGS14 is a natural suppressor of both synaptic plasticity in CA2 neurons and hippocampal-based learning and memory. Proceedings of the National Academy of Sciences of the USA 107, 16994-16998.

Lein, E. S. ISH Data :: Allen Brain Atlas: Mouse Brain. http://mouse.brain-map.org/ (2007).

Lein, E.S., Callaway, E.M., Albright, T.D., and Gage, F.H. (2005). Redefining the boundaries of the hippocampal CA2 subfield in the mouse using gene expression and 3-dimensional reconstruction. The Journal of Comparative Neurology 485, 1–10.

Lein, E. et al. (2007). Genome-wide atlas of gene expression in the adult mouse brain. Nature 445(7124), 168-176.

Lein, E.S., Zhao, X., and Gage, F.H. (2004). Defining a molecular atlas of the hippocampus using DNA microarrays and high-throughput in situ hybridization. The Journal of Neuroscience 24, 3879-3889.

Leranth, C., and Ribak, C.E. (1991). Calcium-binding proteins are concentrated in the CA2 field of the monkey hippocampus: a possible key to this region's resistance to epileptic damage. Experimental Brain Research 85, 129-136.

Lorente de Nó, R. (1934). Studies on the structure of the cerebral cortex II. Continuation of the study of the ammonic system. Journal für Psychologie und Neurologie 46, 113-175.

Luo, L., Callaway, E.M., and Svoboda, K. (2008). Genetic Dissection of Neural Circuits. Neuron 57, 634-660.

Madisen, L., Zwingman, T.A., Sunkin, S.M., Oh, S.W., Zariwala, H.A., Gu, H., Ng, L.L., Palmiter, R.D., Hawrylycz, M.J., Jones, A.R., Lein, E.S., and Zeng, H. (2010). A robust and high-throughput Cre reporting and characterization system for the whole mouse brain. Nature Neuroscience 13, 133-140.

Magdaleno, S. et al. (2006). BGEM: an in situ hybridization database of gene expression in the embryonic and adult mouse nervous system. PLoS Biology 4, e86.

Magloczky, Z., Acsady, L., and Freund, T.F. (1994). Principal cells are the postsynaptic targets of supramammillary afferents in the hippocampus of the rat. Hippocampus 4, 322–334.

Magnus, C.J., Lee, P.H., Atasoy, D., Su, H.H., Looger, L.L., and Sternson, S.M. (2011). Chemical and genetic engineering of selective ion channel-ligand interactions. Science 333, 1292-6.

Markowska, A. and Lukaszewska, I. (1981). Open-field behavior in rats with frontomedial cortical, neostriatal or hippocampal lesions. Acta Neurobiologiae Experimentalis (Warsaw) 41, 197-210.

McHugh, S.B., Deacon, R.M., Rawlins, J.N., and Bannerman, D.M. (2004). Amygdala and ventral hippocampus contribute differentially to mechanisms of fear and anxiety. Behavioral Neuroscience 118, 63-78.

Meneses, A. and Liy-Salmeron, G. (2012). Serotonin and emotion, learning and memory. Reviews in the Neurosciences 23, 543-53.

Meyer-Lindenberg, A., Domes, G., Kirsch, P., and Heinrichs, M. (2011). Oxytocin and vasopressin in the human brain: social neuropeptides for translational medicine. Nature Reviews Neuroscience 12, 524-38.

Morris, R.G., Garrud, P., Rawlins, J.N., and O'Keefe, J. (1982). Place navigation impaired in rats with hippocampal lesions. Nature 297, 681-683.

Mouse Genome Sequencing Consortium et al. (2002). Initial sequencing and comparative analysis of the mouse genome. Nature 420, 520-562.

Munoz, D.G. (2004). The distribution of chromogranin A-like immunoreactivity in the human hippocampus coincides with the pattern of resistance to epilepsy-induced neuronal damage. Annals of Neurology 27, 266-275.

Nakashiba, T., Cushman, J.D., Pelkey, K.A., Renaudineau, S., Buhl, D.L., McHugh, T.J., Rodriguez Barrera, V., Chittajallu, R., Iwamoto, K.S., McBain, C.J., Fanselow, M.S., Tonegawa S. (2012). Young dentate granule cells mediate pattern separation, whereas old granule cells facilitate pattern completion. Cell 149, 188-201.

Nakashiba, T., Young, J.Z., McHugh, T.J., Buhl, D.L., and Tonegawa, S. (2008). Transgenic inhibition of synaptic transmission reveals role of CA3 output in hippocampal learning. Science 319, 1260-1264.

Ochiishi, T., Saitoh, Y., Yukawa, A., Saji, M., Ren, Y., Shirao, T., Miyamoto, H., Nakata, H., and Sekino, Y. (1999). High level of adenosine A1 receptor-like immunoreactivity in the CA2/CA3a region of the adult rat hippocampus. Neuroscience 93, 955-967.

Osoegawa, K., Tateno, M., Woon, P.Y., Frengen, E., Mammoser, A.G., Catanese, J.J., Hayashizaki, Y., and de Jong, P.J. (2000). Bacterial artificial chromosome libraries for mouse sequencing and functional analysis. Genome Research 10, 116-128.

Pan, W.X. and McNaughton, N. (2004). The supramammillary area: its organization, functions and relationship to the hippocampus. Progress in Neurobiology 74, 127-66.

Piskorowski, R.A. and Chevaleyre V. (2012). Synaptic integration by different dendritic compartments of hippocampal CA1 and CA2 pyramidal neurons. Cellular and Molecular Life Sciences 69, 75-88.

Ramón y Cajal, S. (1893). Estructura del asta de Ammon y fascia dentata. Anales de la Sociedad Española de Historia Natural 22, 53–126.

Rampon, C., Tang, Y., Goodhouse, J., Shimizu, E., Kyin, M., and Tsien, J.Z. (2000). Enrichment induces structural changes and recovery from nonspatial memory deficits in CA1 NMDAR1-knockout mice. Nature Neuroscience 3, 238-244.

Rasband, W. S. Image J. http://imagej.nih.gov/ij/ (1997)

Rempel-Clower, N. L., Zola, S. M., Squire, L. R., and Amaral, D. G. (1996). Three cases of enduring memory impairment after bilateral damage limited to the hippocampal formation. Journal of Neuroscience 16, 5233-55.

Rowland, D.C., Weible, A.P., Wickersham, I.R., Wu, H., Mayford, M., Witter, M.P., and Kentros, C.G. (2013). Transgenically targeted rabies virus demonstrates a major monosynaptic projection from hippocampal area CA2 to medial entorhinal layer II neurons. Journal of Neuroscience 33, 14889-98.

Sadowski, M., Wisniewski, H.M., Jakubowska-Sadowska, K., Tarnawski, M., Laza-rewicz, J.W., and Mossakowski, M.J. (1999). Pattern of neuronal loss in the rat hippocampus following experimental cardiac arrest-induced ischemia. Journal of the Neurological Sciences 168, 13-20.

Schnütgen, F., Doerflinger, N., Calléja, C., Wendling, O., Chambon, P., and Ghyselinck, N.B. (2003). A directional strategy for monitoring Cre-mediated recombination at the cellular level in the mouse. Nature Biotechnology 21, 562-565.

Sekino, Y., Obata, K., Tanifuji, M., Mizuno, M., and Murayama, J. (1997). Delayed signal propagation via CA2 in rat hippocampal slices revealed by optical recording. The Journal of Neurophysiology 78, 1662–1668.

Sohal, V.S., Zhang, F., Yizhar, O., and Deisseroth, K. (2009). Parvalbumin neurons and gamma rhythms enhance cortical circuit performance. Nature 459, 698-702.

Squire, L.R. (1992). Memory and the hippocampus: a synthesis from findings with rats, monkeys, and humans. Psychological Review 99, 195-231.

Stevenson, E.L. and Caldwell, H.K. (2012). The vasopressin 1b receptor and the neural regulation of social behavior. Hormones and Behavior 61, 277-82.

Suh, J., Rivest, A.J., Nakashiba, T., Tominaga, T., and Tonegawa, S. (2011). Entorhinal cortex layer III input to the hippocampus is crucial for temporal association memory. Science 334, 1415-20.

Szymczak, A.L., Workman, C.J., Wang, Y., Vignali, K.M., Dilioglou, S., Vanin, E.F., and Vignali, D.A. (2004). Correction of multi-gene deficiency in vivo using a single 'self-cleaving' 2A peptide-based retroviral vector. Nature Biotechnology 22, 589-594.

Talley, E.M., Solórzano, G., Lei, Q., Kim, D., and Bayliss, D.A. (2001). CNS Distribution of Members of the Two-Pore-Domain (KCNK) Potassium Channel Family. The Journal of Neuroscience, 21, 7491-7505.

Tamamaki, N. and Nojyo, Y. (1995). Preservation of topography in the connections between the subiculum, field, CA1, and the entorhinal cortex in rats. The Journal of Comparative Neurology 353, 379-390.

Tonello, F., Pellizzari, R., Pasqualato, S., Grandi, G., Peggion, E., and Montecucco, C. (1999). Recombinant and Truncated Tetanus Neurotoxin Light Chain: Cloning, Expression, Purification, and Proteolytic Activity. Protein Expression and Purification 15, 221–227.

Tsien, J.Z., Huerta, P.T., and Tonegawa, S. (1996). The essential role of hippocampal CA1 NMDA receptor-dependent synaptic plasticity in spatial memory. Cell 87, 1327-38.

Utomo, A.R., Nikitin, A.Y., and Lee, W.H. (1999). Temporal, spatial, and cell type-specific control of Cre-mediated DNA recombination in transgenic mice. Nature Biotechnology 17, 1091-1096.

van Strien, N.M., Cappaer, N.L.M., and Witter, M.P. (2009). The anatomy of memory: an interactive overview of the parahippocampal-hippocampal network. Nature Reviews Neuroscience 10, 272-282.

Vertes, R.P. (1992). PHA-L analysis of projections from the supramammillary nucleus in the rat. Journal of Comparative Neurology 326, 595–622.

Vertes, R.P., Fortin, W.J., and Crane, A.M. (1999). Projections of the median raphe nucleus in the rat. Journal of Comparative Neurology 407, 555–582.

Vorhees, C. V. and Williams, M. T. (2006). Morris water maze: procedures for assessing spatial and related forms of learning and memory. Nature Protocols 1, 848-58.

Wall, N. R., De La Parra, M., Callaway, E. M., and Kreitzer, A. C. (2013). Differential Innervation of Direct- and Indirect-Pathway Striatal Projection Neurons. Neuron 79, 347-60.

Wall, N.R., Wickersham, I.R., Cetin, A., De La Parra, M., and Callaway, E.M. (2010). Monosynaptic circuit tracing in vivo through Cre-dependent targeting and complementation of modified rabies virus. Proceedings of the National Academy of Sciences of the USA 107, 21848-21853.

Warming, S., Costantino, N., Court, D.L., Jenkins, N.A., and Copeland, N.G. (2005). Simple and highly efficient BAC recombineering using galK selection. Nucleic Acids Research 33, e36.

Watabe-Uchida, M., Zhu, L., Ogawa, S. K., Vamanrao, A., and Uchida, N. (2012). Whole-brain mapping of direct inputs to midbrain dopamine neurons. Neuron 74, 858-73.

Wersinger, S. R., Ginns, E. I., O'Carroll, A. M., Lolait, S. J., and Young, W.S. 3rd. (2002). Vasopressin V1b receptor knockout reduces aggressive behavior in male mice. Molecular Psychiatry 7, 975-84.

Wickersham, I. R., Sullivan, H. A. and Seung, H. S. (2010) Production of glycoprotein-deleted rabies viruses for monosynaptic tracing and high-level gene expression in neurons. Nature Protocols 5, 595-606.

Winters, B.D., Forwood, S.E., Cowell, R.A., Saksida, L.M., and Bussey, T.J. (2004). Double dissociation between the effects of peri-postrhinal cortex and hippocampal lesions on tests of object recognition and spatial memory: heterogeneity of function within the temporal lobe. Journal of Neuroscience 24, 5901-8.

Wittner, L., Huberfeld, G., Clémenceau, S., Erőss, L., Dezamis, E., Entz, L., Ulbert, I., Baulac, M., Freund, T.F., Maglóczky, Z., and Miles, R. (2009). The epileptic human hippocampal cornu ammonis 2 region generates spontaneous interictal-like activity in vitro. Brain 132, 3032-3046.

Wrenn, C.C. (2004). Social Transmission of Food Preference in Mice. Current Protocols in Neuroscience, 8.5G.1-8.5G.7.

Wyszynski, M., Kharazia, V., Shanghvi, R., Rao, A., Beggs, A.H., Craig, A.M., Weinberg, R., and Sheng, M. (1998). Differential regional expression and ultrastructural localization of alpha-actinin-2, a putative NMDA receptor-anchoring protein, in rat brain. The Journal of Neuroscience 18, 1383-1392.

Yamamoto, M., Wada, N., Kitabatake, Y., Watanabe, D., Anzai, M., Yokoyama, M., Teranishi, Y., and Nakanishi S. (2003) Reversible suppression of glutamatergic neurotransmission of cerebellar granule cells in vivo by genetically manipulated expression of tetanus neurotoxin light chain. Journal of Neuroscience 23, 6759-67.

Yang M. and Crawley J.N. (2009). Simple behavioral assessment of mouse olfaction. Current Protocols in Neuroscience 84, 8.24.1-8.24.12.

Young, W.S., Li, J., Wersinger, S.R., and Palkovits, M. (2006). The vasopressin 1b receptor is prominent in the hippocampal area CA2 where it is unaffected by restraint stress or adrenalectomy. Neuroscience 143, 1031-9.

Zaborszky, L., Pang, K., Somogyi, J., Nadasdy, Z., and Kallo, I. (1999). The basal forebrain corticopetal system revisited. Annals of the New York Academy of Sciences 877, 339-67.

Zhao, X., Lein, E.S., He, A., Smith, S.C., Aston, C., and Gage, F.H. (2001). Transcriptional profiling reveals strict boundaries between hippocampal subregions. The Journal of Comparative Neurology 441, 187-196.